University of Alberta

Dynamics and Control of Multibody Cable-Driven Mechanisms with Application in Rehabilitation Robotics

by

Siavash Rezazadeh

A thesis submitted to the Faculty of Graduate Studies and Research
in partial fulfillment of the requirements for the degree of

Doctor of Philosophy

Department of Mechanical Engineering

Fall 2012
Edmonton, Alberta

Abstract

With increasing demand for physical therapy in recent years, robotic systems have been proved to have great potential in improving the level of the delivered rehabilitation services both in quality and quantity and also providing huge savings in labor costs of. In this project a new cable-driven robotic cell for rehabilitation of human limbs is proposed and developed. This system has several advantages over the commercialized therapy robots, including reconfigurability and ability of handling redundancies. In this framework, the first challenge is to determine the number and configuration of the cables which guarantee the equilibrium of the system against an arbitrary force. The necessary and sufficient number of cables for single rigid body systems is well-known in the literature. However, since the human arm is a multibody system, a new theory was developed to determine the minimum total number of cables for a multibody as well as their possible distributions among the links of the multibody. In the second step, a method was proposed to obtain the boundaries of the workspace of the robot by Lagrangian formulation of dynamics of the multibody. Having the workspace, the final part of the thesis is on designing the control loop and its real-time implementation on a mechanical model of the human upper extremity. The control logic was designed in two levels: position control and compliance control. Position control is utilized for following a specified trajectory (representing an exercise for the patient's arm), while compliance control provides flexibility for deviating from that trajectory. The compliance control method used is impedance control in which the robot acts similar to a mass-spring-damper system. To achieve the exact stiffness required by impedance control, the inherent stiffness of the cable robot is formulated and taken into account by extending the theories proposed in the literature for stiffness of rigid-body cable robots for multibodies. Using

impedance control enables us to perform different scenarios for training including teaching/playback and assistive/resistive exercising. The experimental results prove the effectiveness of the theories developed for dynamics and control of the multibody cable-driven robots.

Acknowledgement

I am always grateful to the people who helped me in many different ways to complete this work. I can only mention a few names here, but thanks to all who supported and inspired me.

First of all, I thank my supervisor, Dr. Jin-Oh Hahn. Without his deep knowledge of control engineering and his great support I would not be able to finish this thesis. He was always insightful and enthusiastic, and I learned a lot from him about research and about persistence in research.

Also, I thank my first supervisor, Dr. Behzadipour, whose thoughts and ideas were the basis of this project. I regret that he had to leave the university and I had to finish the work that we had started together without him. However, during the years I worked under his supervision, I learned a great deal about how to address novel problems and how to develop new ideas and innovative research approaches.

My special appreciation goes to the department committee members, Dr. Roger Toogood, Dr. Don Raboud, and Dr. Farbod Fahimi, who helped me in different stages of this project. They always knew how to help me and challenge me at the same time. Many of the ideas developed and presented in this work were originally discussed and suggested in my committee meetings.

I am also grateful to all of the academic and non-academic staff and technicians of Department of Mechanical Engineering. Special thanks to Gail Dowler for all her supports, and to Roger Marchand and Andrew Campbell for all of their helps in fabrication and assembling of this robot.

These years also were a great opportunity for me to meet many great people and benefit from their friendship. I want to thank all of the members of Advanced Robotics and Control Lab, including Mojtaba, Mehdi, Chris, Sepehr, Touqeer, Omid, Reza, Mohammad, Ramin, and Nima, whom I had the pleasure of working with. Also, I am always thankful to my great friends, Mahdi Shahbakhti, Aydin Jafarnejad, Ahmad Ghazi, Saleh Nabi, Rasoul Milasi, and many others at University of Alberta who made these years one of the most memorable periods in my life.

And finally my warmest thanks and appreciation go to my family who always supported and encouraged me throughout my life, and to Parnian, whose smiles were the main inspiration for overcoming all the problems I encountered during these difficult yet memorable years.

Contents

List of Tables

List of Figures

List of Variables

Variable	Definition
$\mathbf{A}$	structure matrix
$\mathbf{A}^l$	structure matrix of the l'th link
$\mathbf{A}_\mathrm{L}$	Lagrangian structure matrix
$\mathbf{A}_\mathrm{t}$	Newtonian structure matrix
$\mathbf{b}$	vector of external force, inertia, and gravity
b_m	motor equivalent damping
$\mathbf{C}$	matrix of velocity and position depending forces of the robot
$\mathbf{C}^l$	constraints of the l'th joint
$\mathbf{C}_i^s$	redundant columns in joint i
$\mathbf{D}$	first dependency matrix
$\mathbf{d}_i$	i'th column of $\mathbf{A}_\mathrm{L}$
$\mathbf{E}_l$	matrix sweeping null space of l'th link
$\mathbf{f}_\mathrm{e}$	environment force
f_m	Motor equivalent Coulomb friction
$\mathbf{G}_l$	matrix of projection of extra cable wrenches on base cables of link l
$\mathbf{H}$	inertia matrix
$\mathbf{K}$	stiffness matrix
$\mathbf{K}_\mathrm{D}$	derivative gain
$\mathbf{K}_\mathrm{I}$	integral gain
k_{ij}	number of constraints between links i and j
$\mathbf{K}_\mathrm{p}$	proportional gain
L	Lagrangian
$\mathbf{l}$	vector of lengths of the cables
l_i	length of the i'th cable
M	number of links of a multibody
$\mathbf{M}_\eta$	moment in η direction
$\mathbf{M}_\theta$	moment in θ direction
$\mathbf{M}_\varphi$	moment in φ direction
$\mathbf{M}_\psi$	moment in ψ direction
m_i	number of cables on the i'th link
m_m	motor equivalent mass
$\overline{m}$	number of cables of a multibody or a multibody subsystem
n	space dimension
$\mathbf{n}_\mathbf{A}$	null space of structure matrix
$n_{A,i}$	i'th components of $\mathbf{n}_\mathbf{A}$
$\mathbf{n}_\mathrm{C}$	part of null space of the multibody pertaining to the constraints
$\mathbf{n}_i$	part of null space of the multibody pertaining to link i
$\mathbf{n}'_l$	part of null space of the l'th link pertaining to base cables
$\mathbf{n}''_l$	part of null space of the l'th link pertaining to extra cables
Q_i	Generalized force
q	constraint force magnitude
$\mathbf{R}_\eta$	rotation matrix for η
$\mathbf{R}_\theta$	rotation matrix for θ
$\mathbf{R}_\varphi$	rotation matrix for φ
$\mathbf{R}_\psi$	rotation matrix for ψ

$\mathbf{r}_i$	position of the i'th cable's connection point
r_l	number of extra cables on the l^{th} link
$\mathbf{S}$	Matrix formed by the first n_{DoF} columns of $\mathbf{A}_{\text{L}}$
s_i	degree of redundancy in joint i
t_i	tension of *i'th cable*
$\mathbf{u}$	Control input
$\mathbf{u}_i$	Unit vector in direction of i'th cable
$\mathbf{v}_i^j$	wrench of i'th base cable on the j'th link
$\mathbf{w}_i^j$	wrench of i'th extra cable on the j'th link
$\boldsymbol{\alpha}_{\text{d}}$	desired trajectory
α_i	Lagrange coordinate
$\bar{\boldsymbol{\alpha}}$	Equilibrium trajectory
$(\beta_i^{\,j})_l$	projection of the i^{th} extra cable wrench of the l^{th} link on the j^{th} constraint wrench (if $j \le k_{12}$), or on the $(j - k_{12})^{\text{th}}$ base cable wrench (if $j > k_{12}$)
$\boldsymbol{\Gamma}$	stiffness matrix of impedance control
$\boldsymbol{\Delta}_i$	basis for wrench space of the *i'th* link
κ	coefficient of antagonistic part of tension
$\boldsymbol{\Lambda}$	inertia matrix of impedance control
μ_i	linear combination coefficients
$\boldsymbol{\xi}$	feedback linearization intermediate variable
$\boldsymbol{\tau}$	vector of cable tensions
$\boldsymbol{\tau}_{\text{t}}$	vector of cable tensions and constraint forces
$\boldsymbol{\Psi}$	damping matrix of impedance control
$\boldsymbol{\Omega}$	diagonal matrix of stiffness along the cables

Chapter 1 Introduction

Technology-based solutions have become increasingly popular to assist the elderly population and the ones with disabilities. The increase of life expectancy in industrialized countries from one side, and decrease of birth rate from the other, will soon lead to a shortage of human specialists for assisting the aforementioned groups of people. In the demography provided in [1] (originally from [2]) in seven selected countries, the percentage of handicapped people ranges from 7.1 to 20 and of the elderly from 12.4 to 36.0. From these statistics one can conclude that new methods of rehabilitation aids are to be utilized for the rising number of people in need. The creation and growth of the field of rehabilitation robotics is a response to this rapidly increasing demand.

A class of robotic systems that has been a topic of interest in past years is cable-driven parallel mechanisms or cable robots. Cable robots have several advantages over the conventional robots. Higher payloads, reconfigurability, low-mass moving parts which in turn allows reaching higher speeds and accelerations, the possibility of working in large workspaces, and the ability for working in dangerous and hazardous environments have made them a thriving area of study in the field of robotics.

The goal of this thesis is to utilize the advantages of cable robots for development of a new robotic system for rehabilitation of the human limbs. The structure of the robot is a new form of cable robot and as a result, new problems in analysis of the robot have to be addressed and solved.

1.1 Problem Statement and Motivations

Due to the rising need for robotic therapy a lot of robotic systems have been proposed in past years. The majority of these systems can be categorized into two major groups: end-effector based systems and exoskeletons.

In end-effector based systems the contact of the robot with the patient is solely through its end-effector. However, since human limbs have more than six DoF (Degrees of Freedom), the end-effector based systems cannot control all DoF of the limbs, and as a result, redundant motions may occur during the exercise.

The other group of therapeutic robots are exoskeletons. In exoskeletons the problem of redundant motions has been solved; but in the cost of another problem: that the weight of the integrated actuators in the structure of the exoskeleton has to be compensated, which is often a not a simple task.

Another limitation from which both of these types of robots suffer from is their fixed configuration. In other words, they are designed for and restricted to performing a single task. Indeed, a robotic system that can be readily reconfigured for different tasks will be of considerable advantages in terms of cost, space, and usage simplicity.

Cable driven robots can be a good solution for the three problems stated above. They are parallel mechanisms and thus the DoF that they can control is unlimited. Furthermore, in cable robots the weight of the actuators does not cause any difficulty, as they are stationary and placed away from the driven object. Finally, one of the most important characteristics of cable robots is their ability to be easily reconfigured and reinstalled, making them an ideal candidate for applications such as physical therapy in which the ability of performing a variety of tasks is desirable.

From the characteristics of cable robots, they can be considered a good potential solution for the main limitations of the conventional therapeutic robots. In this thesis, the development of a cable-driven robotic system from concept to control is discussed and new theories necessary for this application are developed.

1.2 Challenges and Contributions

From dynamics point of view, human limbs are multibodies. Therefore, a cable robot for this application will be a "multibody cable-driven robot". In other words, the object being driven by the robot instead of a simple rigid body is itself a mechanism. The fact that almost all of the studies and analyses performed for cable robots have been on single rigid body cable-driven mechanisms[1] makes the proposed project not only a new system in the field of

[1]. For the sake of simplicity, hereafter "single rigid body cable-driven mechanisms" are referred to "rigid body cable-driven mechanisms".

rehabilitation robotics, but also a new type of cable robot. As a result, all of the theories developed for rigid body cable-driven robots have to be extended to the case of multibodies.

Since cables can only pull, in a cable robot it must always be guaranteed that the cables are in tension. The minimum necessary number of cables that can guarantee the existence of such a configuration has been studied widely in the case of rigid body cable-driven mechanisms. However, for multibodies this is a new problem and the number of cables that can guarantee positive tensions against an arbitrary external load, and the distribution of these cables among the links of the multibody have to be studied.

The number of cables and their possible distributions guarantee that at least in a manifold in the workspace, the system can maintain tensile forces in the cables. Since obviously this manifold is the part of the workspace that the system can work in, the next problem is finding the boundaries of this subspace. Again, this problem has been widely studied for rigid bodies, but it is required that these theories to be extended for the case of multibodies.

The last step of the thesis is to control the robot. The control of cable-driven robots is essentially similar to conventional robots. The only difference is that due to the nature of cable robots, the structural stiffness of the conventional robots is usually higher. This difference becomes important in impedance control which is a standard approach in applications involving interaction of the robot with humans. Therefore, the stiffness of multibody cable driven robots should be formulated and considered in the design of impedance control for the present application.

1.3 Structure of the Thesis

In chapter 2 of this thesis, rehabilitation robotic systems and their trends and challenges are reviewed and discussed. After that, the cable-driven mechanisms are introduced and the proposed concept is presented. In the last part of this chapter, the fabricated robot and the mechanical system developed for the control task are depicted and discussed.

Chapter 3 presents the developed theory for the necessary and sufficient number of cables and their possible distributions to guarantee positive tensions in the cables. In this way, first the necessary conditions for the number of cables for general multibodies is presented and then the sufficiency of these conditions are discussed for the case of two- and three-link multibodies. Finally, using the theories developed, the possible number of cables for the system developed is investigated and obtained.

In chapter 4 a method is suggested for the workspace analysis of multibody cable-driven robots. In this way, first the dynamics of cable robots is reformulated using Lagrange's method to obtain a framework for the workspace analysis. The boundaries of the workspace are obtained using two different (but equivalent) methods, namely null-space approach and separating/supporting hyperplane approach. Several case studies are presented for illustrating the method for simple multibodies. The final part is applying the developed theories for the workspace analysis of the developed system to determine the subspace in which the robot can work.

Chapter 5 presents the control design and the experiments performed. The robot is controlled using both position control and impedance control. For impedance control, as discussed before, the structural stiffness of the multibody cable-driven robots is formulated and incorporated in the control design. Having designed the control logic, in the last part of this chapter the controllers are implemented and the experimental results are presented and discussed.

Finally, chapter 6 summarizes the contributions and results of the present thesis and provides guidelines, ideas, and suggestions for extension and future continuation of this work.

Chapter 2 Basics of Rehabilitation Robotics and the System Proposed

In this chapter the system proposed and designed is presented and discussed. But before that, to establish the basics required for the proposed system, the rehabilitation robotic systems and the cable-driven mechanisms are introduced and reviewed.

2.1 Rehabilitation Robotics

In [1], rehabilitation robots are divided into two groups: assistance robots and therapy robots. The taxonomy provided by Tejima in [3] is somewhat different in that he divided these robots to four groups. However, three of these four groups, i.e. augmentative manipulation, augmentative mobility, and robots for helping care-givers fall in the first category of [1] taxonomy. These types of robots (assistive robots), although they have found many applications in recent years (wheelchairs, feeders, walking supports, etc.), are not the subject of this thesis. Therefore, we take a deeper look at the second category, i.e. therapy robots.

2.1.1 Commercialized Therapy Robots

Each year in the US, there are more than 300,000 individuals who need physical rehabilitation for motor recovery after stroke [4,5]. The direct cost of these services exceeds five billion dollars per year [5]. Due to the increasing number of disabilities caused by stroke and also spinal cord injuries in developed countries and the high cost and labor imposed on the health care sector, taking advantage of technological potentials for automation of the rehabilitation process is inevitable. Furthermore, there are numerous other advantages for the robotic systems; some of them which are listed in [1] are: 1) ability of working in long periods without becoming tired, 2) ability of measuring the patient's progress by robot's sensors, and 3) ability of working in different therapy modes with precision that cannot be provided by human therapists. To these benefits one can add the possibility of remote exercising of the patient by a therapist, mirroring the motion of the healthy limb of the patient by the injured limb, teaching the therapy students, and using computerized visual aids for more exciting exercises. All of these factors demonstrate the huge potential for research in the field of therapy robotics.

The advent of assistive robots almost returns to the early robotics times, 1950's and 1960's [1]. But therapy robots have a much younger history. The first therapy robot was probably BioDex [6] which was developed in mid 1980's. It was a single-axis force-controlled and programmable robot which could assist patients in performing simple exercises. The second attempt was made by Khalili and Zomlefer [7] at Santa Clara University where they introduced the first multi-axis concept for therapy automation. This was followed by the work of Erlandson and his group at the Wayne State University [8] who provided the first tested system [1] on a 6-DoF UMI RTX robotic arm with visual aids for upper extremity exercises.

In early 1990's the start of MIT-MANUS project by Hogan et al. [9] at MIT made a landmark in the history of therapy robots. As can be seen in Figure 2.1, MIT-MANUS has a planar module with 2 degrees of freedom (DoF) and a 1-DoF vertical module for arm therapy. A 3-DoF wrist module can be also added to provide the ability of hand therapy. MIT-MANUS has been the subject of many different studies to demonstrate the satisfactory performance of this robotic system compared to the conventional therapy and improve the exercises and control system of the robot.

Another important achievement in the field of therapy robotics was the Mirror Image Movement Enhancer (MIME) system which was developed at Stanford University [11]. This system uses a conventional Puma-560 robotic arm for providing upper limb therapy. Compared to MIT-MANUS, as a result of its 6 DoF, this system can provide more realistic movements. However, unlike MIT-MANUS force measurement is necessary for this robot [1].

A simple robot that gave interesting results in terms of improvement of movement ability compared to tabletop therapies is Bi-Manu-Track [12]. This system works on the basis of bilateral passive or active movement of the combination of forearm pronation/supination and wrist flexion/extension. As mentioned above, the comparison between tabletop therapy and robot exercises shows a significant improvement in mobility of the robot-trained group. In the 66-point range of Fugl-Meyer standard, robot-trained patients show 15 points superior motion improvement compared to the other group [12].

Gait training, due to its labor-intensive nature for the therapists [1] has been another target for development of robotic systems. Most of the efforts were based on body-weight supported treadmill (BWSTT) [1] because of the fact that automation is easier on a stationary setup. Some of the commercialized gait training systems are: GT-I [13], Lokomat [14], and AutoAmbulator [15].

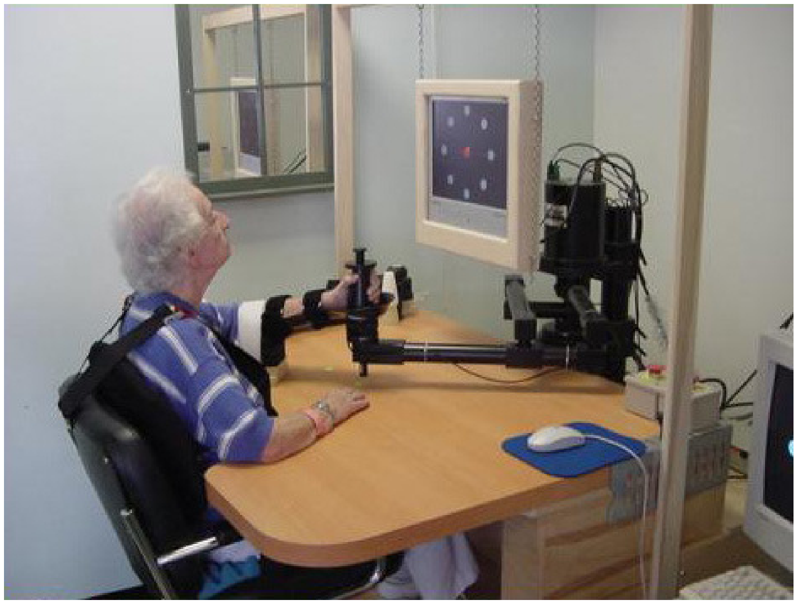

Figure 2-1 MIT-MANUS [10]

2.1.2 Examples of Therapy Robots under Development

The success of the abovementioned commercialized therapy robots has inspired a lot of research all around the world. A good example is ARMin family (ARMin I to IV) which has a semi-exoskeleton structure and provides 6 DoF's for natural movement of the upper limb [16] (Figure 2-2). The idea of this system is important in that it gives an alternative to the conventional end-effector-based systems and through that the ability of moving in more degrees of freedom than six (which is the limitation of end-effector-based systems) is provided. This is very useful, considering the fact that the human arm is usually modeled with more than six degrees of freedom.

HWARD [18] and RUPERT [19] are two other exoskeleton type systems which utilized pneumatic actuation. HWARD is a 3-DoF system which helps the patients in repetitive grasping and releasing tasks. RUPERT has 5 DoF and can help in therapy of the whole arm.

Two systems which took advantage of cables for driving motion are MACARM [5] (Figure 2-3) and MariBot [20] (Figure 2-4) and. As can be seen in Figure 2-4 Maribot has five DoF, two of which from the linkage part and three from the cable part. MACARM on the other hand has standard form of cable robots for driving rigid bodies. The rigid body here is the handle which can have spatial motion and help the patient's arm in following the specified path. Thus in fact the handle can be considered as the classic concept of end-effector therapy which in this case is manipulated by the cables.

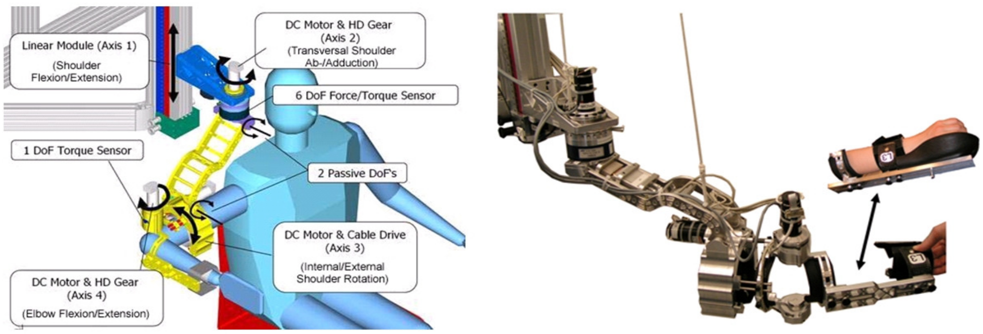

Figure 2-2. ARMin structure [17]

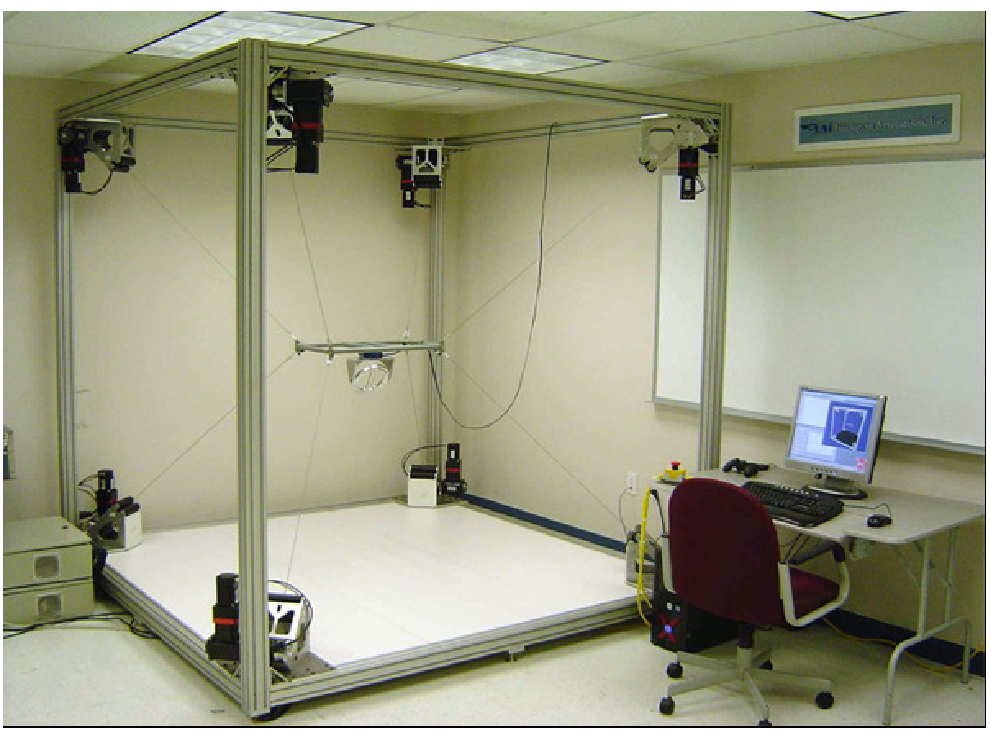

Figure 2-3. Structure of MACARM [21]

Figure 2-4. MariBot [20]

Another system proposed very recently is CAREX, developed at University of Delaware [22]. The structure of CAREX is very similar to MACARM in that it consists of the winches installed on a fixed supporting frame. But CAREX is basically an exoskeleton based robot and the cables move an exoskeleton worn by the patient. As a result of this, the design of CAREX eliminates the drawbacks of both end-effector based robots (redundancy) and exoskeletons (heavy actuators). However, although simplifying design and calibration, by positioning the spools around the shoulder the workspace of the cable robot becomes very small and to increase the size of the workspace additional actuators will be necessary.

2.2 Cable-Driven Robotic Systems

Since their popularity, right after Stewart's famous paper [23], parallel mechanisms have become a good alternative for the conventional serial robots. Their better precision and less inertia make them convenient for many different tasks such as accurate positioning, manipulating heavy loads, and/or reaching high speeds.

By Merlet's definition [24]: "A *parallel robot* is made up of an end-effector with *n* degrees of freedom, and of a fixed base, linked together by at least two independent kinematic chains. Actuation takes place through *n* simple actuators". Therefore cable driven mechanisms, in which the end-effector is connected to the fixed base by cables and the lengths of cables are controlled by the winches set up on the frame, are considered as a subset of parallel robots by this definition and thus they have the inherent advantages of the parallel mechanisms.

More than these advantages, cable driven mechanisms have other benefits, too. Since in this type of parallel mechanisms, the links are the cables, they are practically massless. This makes the mechanism convenient for reaching high speeds. Furthermore, the cables are much cheaper than link-joint systems and also are easily reconfigurable. Moreover, the possibility of using long cables makes them suitable for hazardous environment as well as large workspaces without imposing high costs or materials.

The difficulty of using cable-driven mechanisms arises from the fact that cables can only “pull”. Therefore for stability of the mechanism, the configuration of the cables must be designed such that all cables are in tension. The subspace of the workspace in which, with a selected configuration, all of the cables can be held in tension is called the tensionable workspace.

MACARM, which was introduced before, is an example of standard cable-driven robots in which the end-effector is manipulated by the motion of the cables generated from stationary winches installed on a frame. There are many other proposed cable robots with design variations and with other applications. Some examples are NIST ROBOCRANE [25], McDonnell Douglas Charlotte [26], FALCON [27], and DeltaBot [28].

2.3 Structure of the Proposed System

Figure 2-5 depicts a schematic of the proposed robotic system for rehabilitation of human limbs.

As can be seen from this figure, the structure of the robot is like MACARM in that the winches are installed on a fixed frame. The difference is that instead of a handle, the cables are directly connected to the patient’s limb through a special interface (which can be an exoskeleton similar to CAREX [22]).

A picture of the fabricated robot is shown in Figure 2-6. As can be seen from the photograph, beside the 12 edges of the cubic frame, there are 10 other members (two on each side face, one at the top face, and one at the bottom face of the cube) on which the winches can be set up. Since these members can move on the face that they have been installed on, the winches can be positioned anywhere on the six faces of the cube, depending on the optimal locations found for them for the specified task.

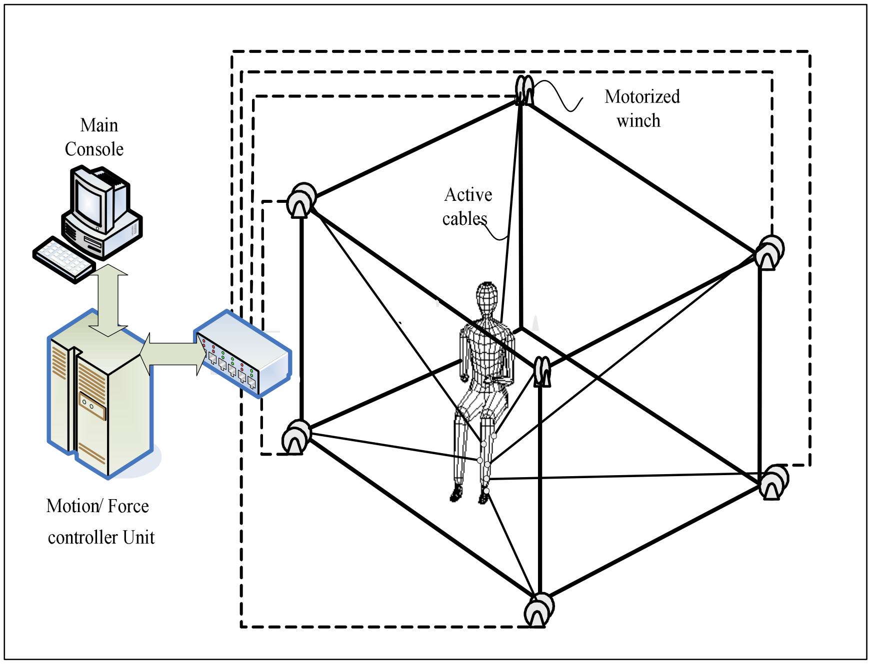

Figure 2-5. Schematic of the proposed robotic system

The winches, as can be seen in Figure 2-7, consist of an electromotor rotating a spool for pulling or releasing the cable. The cable passes around a small pulley so that its speed and force can be measured via an external encoder and load cell attached to the pulley. Hereby one can measure these variables more accurately compared to the ones obtained from the motor sensors which are subject to the errors of cables slippage and changes in effective spool diameter (due to winding of cable around it). After passing through a guide, which can freely rotate, the cable with a fitting is connected to the end-effector. The type of the fitting is varied according to the application.

The motors are driven by SERVOSTAR-CD drivers and the drivers are controlled from Labview® environment through PXI cards. The drivers can be set in different operation modes including torque mode, position mode and velocity mode.

Figure 2-6. The fabricated robot

For the scope of this thesis, the studies on dynamics, workspace analysis, and control of the proposed robotic system are performed on an anthropomorphic arm mechanism with four DoF (three for shoulder and one for flexion/extension of the elbow), as shown in Figure 2-8. The spherical joint connects the arm to a beam which has been fixed to the frame using bolts. The locations of the winches on the frame are selected according to the application and the required task. The placement and calibration of the winches and also details of the arm mechanism can be found in Ghasemalizadeh's thesis [29].

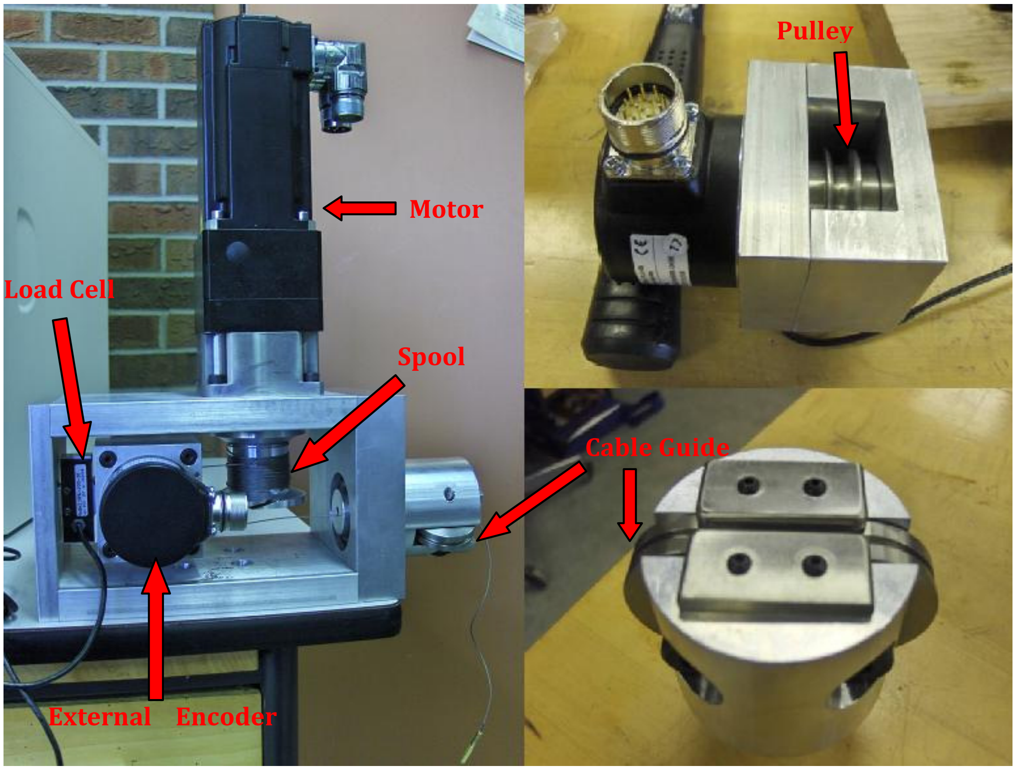

Figure 2-7. Winches

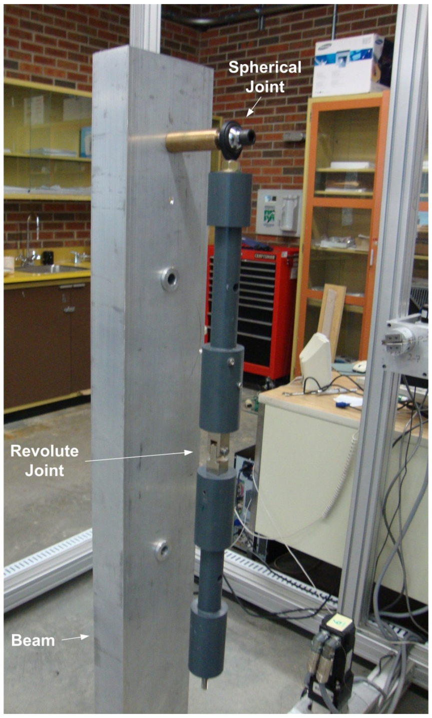

Figure 2-8. The mechanical arm mechanism used for analyses and experiments [29]

2.4 Summary

In this chapter the concept and design of the proposed system was presented and discussed. The concept of using cable robots for therapy has been proposed as a solution for the major drawbacks of the two groups of therapy robots, i.e. end-effector based robots and exoskeletons. The system was designed and fabricated in standard form of the cable-driven mechanisms and an anthropomorphic arm mechanism was used to simulate the patient's upper limb for the analysis and control design which will be presented in the next three chapters.

Chapter 3 Tensionability of Multibody Cable-Driven Mechanisms

The main challenge in cable-driven manipulators is ensuring their ability to develop tensile forces in all cables to maintain equilibrium against any arbitrary external load. For this aim, the number and configuration of the cables have to satisfy specific conditions. This area is well-investigated for rigid bodies, but very little studied for multibodies. Since in the present application the object driven by the cables (i.e. the human limb) is a multibody, in this chapter these conditions are studied and theorized for the multibodies.

3.1 Introduction and Literature Review

"Tensionability" of a cable-driven mechanism is defined as the ability of the mechanism to resist against an arbitrary external load with positive cable tensions. In the literature of cable-driven mechanisms, tensionability and terms such as "wrench closure" and "force closure" are equivalent. From the fact that tensionability has been defined for an arbitrary external load, it can be concluded that this property does not depend on the dynamics of the system and only depends on the kinematics and geometrical aspects of the mechanism.

It has been proven that for a rigid body cable-driven manipulator, i.e. a single moving platform suspended and driven by several cables, one redundant cable can guarantee the tensionability of the system [27]. The idea of the proof comes from Nguyen's works on grasping robots [30,31] which in turn is based on the mathematical concept of "vector closure" in convex cones theory [32]. However, in a multibody driven by cables, although the necessity of one redundant cable is almost obvious, there is no solid result reported in the literature for the sufficient number of the redundant cables guaranteeing tensionability. Knowing the minimum necessary and sufficient number of cables is important both for lowering the cost, and reducing the risk of cable interference.

The first endeavors to address the tensionability problem for multibodies returns to the research performed for controllability of tendon-driven manipulators, i.e. the multibodies whose joints were driven by cables [33]. The conditions derived in this work for the total number of cables and possible distributions have been a good basis for future studies. However this study is merely a special case of the general problem, limited to a serial multibody having only revolute joints with one link fixed to the ground and a particular arrangement of the cables on the links. Hence for addressing the general case of driving a multibody using cables, a more sophisticated approach is required. In a work by Kino et al. [34], the general case is tackled. However, their method which is based on transferring the effects of the cables of one link to the next one using a single force is incomplete and does not provide all the conditions affecting the tensionability of the system. As a result of this assumption, they concluded that for tensionability, each link of the multibody requires at least one cable, which (as will be shown and exemplified later in this chapter) is not necessary.

In a very recently published research [35] Mustafa and Agrawal used screw theory to formulate the tensionability of multibodies and through that they proved that for the conditions considered, the multibody will be tensionable with at least one redundant cable. However they did not address the problem of how to distribute these cables among the links of the multibody.

In this chapter, first the tensionability conditions of rigid bodies and two-link multibodies are completed by considering cable-wrench condition. Then the theory is extended to investigating the tensionability of three-link serial multibodies which are much more complicated due to possible dependencies among the constraints of the middle link. For all cases, the minimum number of cables and the corresponding conditions that are required to build a tensionable multibody cable-driven mechanism is determined through rigorous proofs.

As reviewed by Gouttefarde [36], there are three approaches proposed for tensionability analysis of rigid body cable-driven mechanisms: 1) Null space characterization, 2) separating/supporting planes, and 3) convex hull analysis. Although all of these approaches have been proved to be equivalent for a cable-driven rigid body [36] (and it is straightforward to extend this argument to serial multibodies), for deriving the conditions of tensionability of multibodies in this chapter, the first approach (i.e. null space characterization) is adopted. This is due to the closer relation between this characterization and the geometrical aspects of the system, together with simpler formulation of the constraints in this approach.

3.2 Tensionability of A Rigid Body Cable-Driven Mechanism

Figure 3-1 depicts a schematic of a rigid body driven by cables. Each cable is pulled by a motorized winch which is considered fixed to the ground in the present study.

One can write the equilibrium equations of this rigid body as:

$$\mathbf{A}\boldsymbol{\tau} = \mathbf{b} \tag{3.1}$$

where:

$$\mathbf{A}_{n\times m} = \begin{bmatrix} \mathbf{u}_1 & \mathbf{u}_2 & \cdots & \mathbf{u}_m \\ \mathbf{r}_1 \times \mathbf{u}_1 & \mathbf{r}_2 \times \mathbf{u}_2 & \cdots & \mathbf{r}_m \times \mathbf{u}_m \end{bmatrix} \tag{3.2}$$

is called *structure matrix*, $\mathbf{u}_i$ is the unit vector in the direction of the i^{th} cable pointing towards the corresponding winch, and $\mathbf{r}_i$ is the corresponding moment arm. n is the dimension of the motion space (3 for planar and 6 for spatial motions) and m is the number of cables. $\boldsymbol{\tau}$ is a column vector containing the tensions of the cables:

$$\boldsymbol{\tau}_{m\times 1} = \begin{bmatrix} t_1 & t_2 & \cdots & t_m \end{bmatrix}^T \tag{3.3}$$

where a positive t_i indicates a tensile force in the cable. The right hand side of Eq. (3.1), $\mathbf{b}$, is the summation of all external forces and moments including weight and inertial forces and moments.

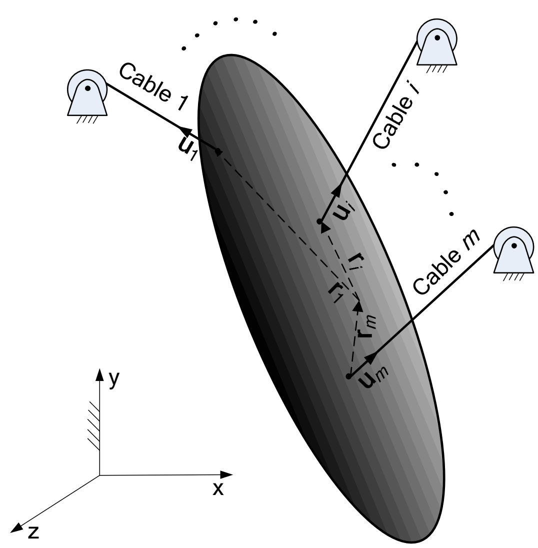

Figure 3-1. Schematic of a cable-driven rigid body

In general, for maintaining equilibrium, we need to have $m \geq n$ [37]. With this condition satisfied, one can write the general solution of Eq. (3.1) as:

$$\boldsymbol{\tau} = \mathbf{A}^{+}\mathbf{b} + \kappa\mathbf{n}_{\mathbf{A}} \tag{3.4}$$

Here $\mathbf{A}^{+}$ is the Moore-Penrose pseudo-inverse of matrix **A**. It is easy to perceive that if $m=n$ and **A** is full-rank, the pseudo-inverse will become the normal matrix inverse. Also it is clear that if **A** is rank-deficient it will have no inverse and hence Eq. (3.4) has no solution, implying that the equilibrium is impossible. $\mathbf{n}_{\mathbf{A}}$ is an arbitrary unit vector in the kernel of this matrix, and κ is an arbitrary real number.

The first term in the right hand side of Eq. (3.4) is fixed once the structure of the mechanism (i.e. **A**) and the external load (i.e. **b**) are determined. Therefore the resulting cable forces from $\mathbf{A}^{+}\mathbf{b}$ may be negative. However, the second term, $\kappa\mathbf{n}_{\mathbf{A}}$, may raise the cable tensions to positive values only if all components of $\mathbf{n}_{\mathbf{A}}$ ($n_{A,i}$'s) are nonzero and of the same sign. In such a case, one can take κ sufficiently large such that all components of $\boldsymbol{\tau}$ become positive [38]. Therefore the tensionability is guaranteed if and only if the following two conditions are satisfied:

1. **A** is full-rank (rank or equilibrium condition), and
2. There is a vector in the kernel of **A** with all components of the same sign (null space condition).

Hence the problem is to design the winch locations and cable connection points such that the two above conditions are satisfied. For this, throughout this chapter, we assume that there is no geometrical limitation on the positions of the winches or connecting the cables.

It can be shown that without geometrical limitations the null space condition can be simplified as: "There is a vector in the kernel of **A** without any zero components". To prove, one should note that by reversing the direction of a cable at a specific position, its corresponding column in **A** will switch sign. Using this, one can reverse those cable directions whose corresponding components in **n** are negative. This can be shown in the following equations:

$$\begin{gathered}\mathbf{A}\mathbf{n}_{\mathbf{A}} = \sum_{i=1}^{m} n_{A,i}\begin{bmatrix}\mathbf{u}_i \\ \mathbf{r}_i \times \mathbf{u}_i\end{bmatrix} = \mathbf{0} \\ \Rightarrow\ n_{A,i}\begin{bmatrix}\mathbf{u}_i \\ \mathbf{r}_i \times \mathbf{u}_i\end{bmatrix} = -n_{A,i}\begin{bmatrix}-\mathbf{u}_i \\ \mathbf{r}_i \times (-\mathbf{u}_i)\end{bmatrix}\end{gathered} \tag{3.5}$$

i.e. inversing the direction of the cable makes the corresponding null space component switch sign.

As it was mentioned before, the minimum necessary number of cables for a tensionable cable-driven mechanism is n+1. It can be shown that n+1 is sufficient, too; meaning that if there are no constraints on the direction and position of the cables, a tensionable configuration can be obtained by n+1 cables. To show the sufficiency, let $m = n+1$. Assuming there is no constraints on the directions and positions of the cables, one can select the configuration of the first n cables to obtain n linearly independent cable wrenches which fill the first n columns of **A**. The n+1[st] column of **A** is sufficient to be a complete linear combination of the other n columns:

$$\begin{bmatrix} \mathbf{u}_{n+1} \\ \mathbf{r}_{n+1} \times \mathbf{u}_{n+1} \end{bmatrix} = \sum_{i=1}^{n} \mu_i \begin{bmatrix} \mathbf{u}_i \\ \mathbf{r}_i \times \mathbf{u}_i \end{bmatrix}, \quad \mu_i \neq 0 \tag{3.6}$$

Then one can show that the kernel of **A** is spanned by:

$$\mathbf{n}_{\mathbf{A}} = \frac{1}{\mu_t} \begin{bmatrix} -\mu_1 & -\mu_2 & \dots & -\mu_n & 1 \end{bmatrix}^{\mathrm{T}} \tag{3.7}$$

where:

$$\mu_t = \left\| \begin{bmatrix} -\mu_1 & -\mu_2 & \dots & -\mu_n & 1 \end{bmatrix} \right\|$$

and all components of $\mathbf{n}_{\mathbf{A}}$ are nonzero. Note that if any component of $\mathbf{n}_{\mathbf{A}}$ in Eq. (3.7) is negative, the direction of the corresponding cable can be reversed as discussed above to change that component to a positive one. This method has been discussed in [32] under the title of vector closure and later used in [27] to obtain the tensionability conditions of cable-driven rigid bodies. However, an important point which seems to be overlooked in the above works is that the n+1[st] vector designed by Eq. (3.6) does not necessarily represent a cable wrench. For a cable wrench **w**, in spatial case, we have:

$$\mathbf{w} = \begin{bmatrix} w_1 \\ w_2 \\ w_3 \\ w_4 \\ w_5 \\ w_6 \end{bmatrix} = \begin{bmatrix} \mathbf{u} \\ \mathbf{r} \times \mathbf{u} \end{bmatrix} \tag{3.8}$$

Since $\mathbf{u} \perp (\mathbf{r} \times \mathbf{u})$, for $\mathbf{w}$ to be a cable wrench, it is required to have: $[w_1\ w_2\ w_3] \cdot [w_4\ w_5\ w_6] = 0$. Furthermore, the force part cannot be zero. Any 6-D vector satisfying these two conditions can be realized by a cable. In planar case, since the moment is reduced to a scalar, it is sufficient to have a nonzero force for a wrench to have an equivalent cable.

Applying these conditions to the n+1st wrench of Eq. (3.6), we have:

i. $$\mathbf{u}_{n+1} = \sum_{i=1}^{n} \mu_i \mathbf{u}_i \neq \mathbf{0}$$

ii. $$\mathbf{u}_{n+1}.(\mathbf{r}_{n+1} \times \mathbf{u}_{n+1}) = \mathbf{0}$$

The first condition is equivalent to:

$$\sum_{i=1}^{n} \mu_i \mathbf{u}_i^{(j)} \neq 0 \quad j = 1, \text{or } 2, \text{or } 3 \tag{3.9}$$

where $\mathbf{u}_i^{(j)}$ is the j^{th} component of $\mathbf{u}_i$. For this condition to be satisfied, Eq. (3.9) states that μ_i's can be anywhere in $\mathbb{R}^6$ except on the intersection of the three hyperplanes expressed in Eq. (3.9). This still leaves infinite possible selections for μ_i's that satisfy condition (i).

For the planar case, condition (ii) is automatically satisfied. This is because the moment part of the wrench is a scalar and already perpendicular to the plane of motion. In spatial systems, there are countless examples of tensionable spatial rigid bodies driven by seven cables which show that seven cables are indeed sufficient. However, the authors could not find a rigorous mathematical proof (such as what stated above) for this in the literature.

To summarize, for a rigid body driven by cables to be tensionable, it is necessary and sufficient to have n+1 cables. In other words, using one redundant cable: 1) **A** can be built to be full-rank, and 2) the null space can be formed to be spanned by a positive vector (i.e. all of its components are positive).

3.3 Tensionability of Two-Link Multibodies

In this section the procedure of obtaining tensionability conditions for a rigid body is extended to a two-link multibody. For this purpose, similar to the rigid body case, it will be shown that satisfying the same conditions (i.e. rank condition and null-space condition) ensures the tensionability for a two-link mechanism. Then the procedure to obtain a tensionable configuration is also presented.

We consider the following assumptions on the multibody cable-driven mechanisms:

1. The multibody has a serial kinematics and the constraints are holonomic;
2. Each cable is attached from one end to a link and pulled from the other end by a stationary winch;

3. There is no geometrical constraint on the directions and locations of the cables.

3.3.1 Formulation of the Equilibrium for a Two-Link Multibody

Figure 3-2 depicts a schematic of a two-link multibody in an n-dimensional motion space (n=3 for planar and n=6 for spatial motion). The kinematic joint between the two links has $n-k_{12}$ DoF.

Similar to a single link cable-driven mechanism, the free body diagram is considered for each link and the joint constraint is represented by k_{12} independent wrenches. Therefore, the equilibrium equations of link l can be written as:

$$\begin{bmatrix}\mathbf{A}^l & \mathbf{C}^l\end{bmatrix}\boldsymbol{\tau}^l = \mathbf{b}^l, \qquad l = 1,2 \tag{3.10}$$

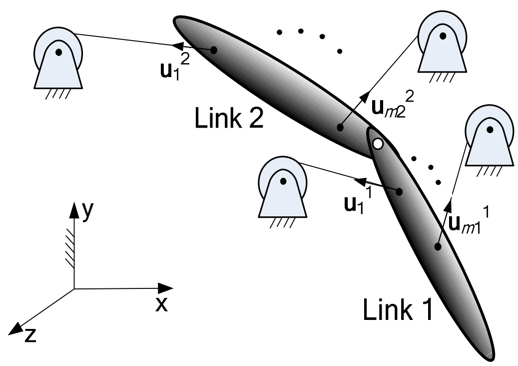

Figure 3-2. Schematic of a two-link cable-driven multibody

where $\mathbf{A}^l{}_{n\times m_l}$ represents[1] the configuration of the link with its attached cables and is found similar to Eq. (3.2) as:

$$\mathbf{A}^l{}_{n\times m_l} = \begin{bmatrix} \mathbf{u}_1{}^l & \mathbf{u}_2{}^l & \dots & \mathbf{u}_{m_l}{}^l \\ \mathbf{r}_1{}^l \times \mathbf{u}_1{}^l & \mathbf{r}_2{}^l \times \mathbf{u}_2{}^l & \dots & \mathbf{r}_{m_l}{}^l \times \mathbf{u}_{m_l}{}^l \end{bmatrix} \tag{3.11}$$

[1]. Throughout this chapter, superscripts are always used to show indexes and never represent power.

$\boldsymbol{\tau}^l$ contains the forces of the cables and constraint wrenches:

$$\boldsymbol{\tau}^l{}_{(m_l+k_{12})\times 1} = \begin{bmatrix} t_1{}^l & \dots & t_{m_l}{}^l & q_1 & \dots & q_{k_{12}} \end{bmatrix}^{\mathrm{T}} \tag{3.12}$$

where $t_i{}^l$'s are the cable forces (positive for tensile) and $q_1, \dots, q_{k_{12}}$ are such that $\mathbf{C}^l[q_1 \ \dots \ q_{k_{12}}]^{\mathrm{T}}$ gives the constraint wrenches on the l^{th} link. $\mathbf{C}^1 = -\mathbf{C}^2$ due to the Newton's third law of motion. Also note that $\mathbf{C}^1$ and $\mathbf{C}^2$ consist of k_{12} ($< n$) linearly independent columns.

By combining the two equations of Eq. (3.10) corresponding to the two links of the multibody, one can obtain:

$$\mathbf{A}_t \boldsymbol{\tau}_t = \mathbf{b}_t \tag{3.13}$$

in which:

$$(\mathbf{A}_t)_{2n\times(m_1+m_2+k_{12})} = \begin{bmatrix} \mathbf{A}^1{}_{n\times m_1} & \mathbf{C}_{n\times k_{12}} & \mathbf{0}_{n\times m_2} \\ \mathbf{0}_{n\times m_1} & -\mathbf{C}_{n\times k_{12}} & \mathbf{A}^2{}_{n\times m_2} \end{bmatrix} \tag{3.14}$$

and:

$$(\boldsymbol{\tau}_t)_{(m_1+m_2+k_{12})\times 1} = \begin{bmatrix} t_1{}^1 & \dots & t_{m_1}{}^1 & q_1 & \dots & q_{k_{12}} & t_1{}^2 & \dots & t_{m_2}{}^2 \end{bmatrix}^{\mathrm{T}} \tag{3.15}$$

$$\mathbf{b}_t = \begin{bmatrix} \mathbf{b}^1 \\ \mathbf{b}^2 \end{bmatrix} \tag{3.16}$$

and $\mathbf{C} = \mathbf{C}^1 = -\mathbf{C}^2$.

The solution of Eq. (3.13) is similar to Eq. (3.1). Thus for tensionability, one must satisfy the similar two conditions;

1. $\mathbf{A}_t$ should be full-rank (rank condition), and
2. There should be a vector in the kernel of $\mathbf{A}_t$ in which all of <u>the components corresponding to the cables</u> are nonzero (null-space condition).

The given formulation and conditions for tensionability are general and can be extended to any number of links. However, they do not indicate the minimum sufficient number of cables. In the following sections, we investigate these conditions in planar mechanisms to determine the necessary and sufficient number of cables for tensionability. This will be done by looking at the two abovementioned conditions (rank and null space conditions) separately.

3.3.2 Rank of the Structure Matrix for a Planar Two-Link Multibody

In this section we show that the minimum necessary number of cables is also sufficient, if used properly, to ensure the rank condition for any two-link planar[1] mechanism.

As mentioned before, in planar systems, an arbitrary wrench is a cable wrench if and only if its force component is not zero, i.e. a cable wrench cannot be a pure moment. Considering such wrenches as column vectors (as in our formulations) the first and second components should not be simultaneously zero. Therefore, as long as any moment arm is geometrically feasible and the above condition is satisfied, one can always design a cable for any arbitrary wrench.

In order for $\mathbf{A}_t$ in Eq. (3.13) to be full-rank, it is required that:

$$m_1 + m_2 + k_{12} \geq 2n \tag{3.17}$$

which states that the total number of wrenches (cables and constraints) restraining the multibody should be at least equal to the total dimension of the motion space. Therefore, on the total number of cables, we should have:

$$m_1 + m_2 \geq 2n - k_{12} \tag{3.18}$$

The same statement can be made for each link. Thus:

$$m_l \geq n - k_{12}, \qquad l = 1,2 \tag{3.19}$$

In other words, each link needs at least n–k_{12} cables that along with the constraint wrenches form a full-rank wrench set (otherwise equilibrium of that link becomes impossible). These cables are called *base cables* of that link. However, if we only assign base cables to the links, it is easily seen that the condition on the total number of cables (Eq. (3.18)) will not be satisfied. Therefore, there should be more cables on each link. These cables form second sets of cables which are called *extra cables*. From Eq. (3.18) the total number of these cables is equal or more than k_{12} for each link.

---

[1]. Although for planar motion n = 3, throughout this chapter the general case is addressed to provide a framework for extension to higher dimensions. In fact, the only condition that limits the analysis to the planar case is cable-wrench condition which, as mentioned before, has not been considered in the previous studies of cable robots.

Eq. (3.19) can also be obtained using the form of $\mathbf{A}_t$, expressed in Eq. (3.14). From the properties of rank of partitioned matrices, if $rank\{\mathbf{A}_t\}=2n$, then each of the two sets of rows in $\mathbf{A}_t$ must be of rank n. i.e. $rank\{[\mathbf{A}^1\ \mathbf{C}]\} = rank\{[-\mathbf{C}\ \mathbf{A}^2]\} = n$. This requires Eq. (3.19) to be satisfied; otherwise, the number of independent columns in $[\mathbf{A}^1\ \mathbf{C}]$ and $[-\mathbf{C}\ \mathbf{A}^2]$ will be less than n. Consequently, if r_l is the number of extra cables on the l^{th} link, then:

$$r_l = m_l - (n - k_{12}) \geq 0 \tag{3.20}$$

One can notice that r_1 and r_2 are also the dimensions of the null spaces pertaining to $[\mathbf{A}^1\ \mathbf{C}]$ and $[-\mathbf{C}\ \mathbf{A}^2]$, respectively.

Next, we need to show that as long as the conditions on the number of cables set out in Eq. (3.18) and Eq. (3.19) are satisfied, the base and extra cables can be designed to give a full-rank $\mathbf{A}_t$.

The existence of $n - k_{12}$ base cables for each link is almost obvious. For this purpose, one needs to form a basis using the k_{12} (predefined) constraint wrenches along with $n - k_{12}$ arbitrary wrenches as long as they are all linearly independent. Now if any of the wrenches does not satisfy the cable wrench condition (i.e. its force components are both zero), then it is sufficient to add arbitrary force components to that wrench. This will change that wrench to a cable wrench without violating the independency of the wrenches.

In order to find out how many extra cables are required and how they should be selected, we need to further investigate the structure matrix $\mathbf{A}_t$. Note that $\mathbf{A}_t$ is full-rank if and only if the only possible $\mathbf{n}_\mathbf{A}$ for equation:

$$\mathbf{A}_t \mathbf{n}_\mathbf{A} = \mathbf{0} \tag{3.21}$$

is $\mathbf{n}_\mathbf{A} = \mathbf{0}$. By breaking the $2n$ equations of Eq. (3.21) into two sets of n equations we will have:

$$\begin{cases} [\mathbf{A}^1 \quad \mathbf{C} \quad \mathbf{0}]\mathbf{n}_\mathbf{A} = 0 \\ [\mathbf{0} \quad -\mathbf{C} \quad \mathbf{A}^2]\mathbf{n}_\mathbf{A} = 0 \end{cases} \tag{3.22}$$

Since $k_{12} < n$, and because columns of $\mathbf{C}$ are assumed to be linearly independent, one can attach $n-k_{12}$ base cables to each link, with corresponding columns $\mathbf{v}_1^1, \dots, \mathbf{v}_{n-k_{12}}^1$ in $\mathbf{A}^1$ and $\mathbf{v}_1^2, \dots, \mathbf{v}_{n-k_{12}}^2$ in $\mathbf{A}^2$, such that, $[\mathbf{A}^1\ \mathbf{C}]$ is spanned by:

$$\mathbf{\Delta}_1 = [\mathbf{v}_1{}^1 \quad \dots \quad \mathbf{v}_{n-k_{12}}{}^1 \quad \mathbf{C}] \tag{3.23}$$

and $[-\mathbf{C}\ \mathbf{A}^2]$ by:

$$\mathbf{\Delta}_2 = [\mathbf{C} \quad \mathbf{v}_1{}^2 \quad \ldots \quad \mathbf{v}_{n-k_{12}}{}^2] \tag{3.24}$$

In other words $\mathbf{\Delta}_1$ and $\mathbf{\Delta}_2$ provide basis for wrench space of each link. These bases can be used to expand the wrenches of the extra cables. Hence, for the l^{th} link, the extra cable $\mathbf{w}_i$ (i=1, 2,..., r_l) can be expressed as:

$$\begin{aligned}
\mathbf{w}_i{}^l &= \mathbf{C}\begin{bmatrix} (\beta_i{}^1)_l \\ \vdots \\ (\beta_i{}^{k_{12}})_l \end{bmatrix} + \sum_{j=1}^{n-k_{12}} (\beta_i{}^{j+k_{12}})_l \mathbf{v}_j{}^l \\
&= \mathbf{C}\begin{bmatrix} (\beta_i{}^1)_l \\ \vdots \\ (\beta_i{}^{k_{12}})_l \end{bmatrix} + \begin{bmatrix} \mathbf{v}_1{}^l & \ldots & \mathbf{v}_{n-k_{12}}{}^l \end{bmatrix} \begin{bmatrix} (\beta_i{}^{k_{12}+1})_l \\ \vdots \\ (\beta_i{}^n)_l \end{bmatrix}
\end{aligned} \tag{3.25}$$

in which $(\beta_i{}^j)_l$ represents the projection of the i^{th} extra cable wrench of the l^{th} link on the j^{th} constraint wrench (if $j \leq k_{12}$), or on the $(j - k_{12})^{\text{th}}$ base cable wrench (if $j > k_{12}$).

An extra cable wrench is not feasible if its force component is zero. This happens only if the following two conditions hold true simultaneously:

$$\mathbf{C}^{(1)}\begin{bmatrix} (\beta_i{}^1)_l \\ \vdots \\ (\beta_i{}^{k_{12}})_l \end{bmatrix} + \sum_{j=1}^{n-k_{12}} (\beta_i{}^{j+k_{12}})_l [\mathbf{v}_j{}^l]^{(1)} = 0 \tag{3.26}$$

$$\mathbf{C}^{(2)}\begin{bmatrix} (\beta_i{}^1)_l \\ \vdots \\ (\beta_i{}^{k_{12}})_l \end{bmatrix} + \sum_{j=1}^{n-k_{12}} (\beta_i{}^{j+k_{12}})_l [\mathbf{v}_j{}^l]^{(2)} = 0 \tag{3.27}$$

where $\mathbf{C}^{(p)}$ and $[\mathbf{v}_j{}^l]^{(p)}$ represent the p^{th} row of the corresponding matrices. One can see that in the space of $(\beta_i{}^j)_l$'s, each of Eqs. (3.26) and (3.27) defines a plane that passes through the origin. The normal vectors corresponding to these planes for link l are defined by the first and second rows of the bases, i.e. $\mathbf{\Delta}_l{}^{(1)}$ and $\mathbf{\Delta}_l{}^{(1)}$. These planes cannot be identical; otherwise two rows of matrix $\mathbf{\Delta}_l$ will be identical and thus $\mathbf{\Delta}_l$ will not be a basis. Hence the intersection of these two planes is a line that passes through the origin in the 3-D wrench space of planar systems (n = 3). The points on this line (except the origin) represent unfeasible cable wrenches (zero force but nonzero moment). As a result, each point on this line corresponds to a set of β's that results in an unfeasible cable wrench. Let us represent the direction of these two lines by unit vector $\mathbf{p}_1$ and $\mathbf{p}_2$ for links 1 and 2, respectively. As a result, any arbitrary wrench for link l can be implemented by a cable through a unique set of β's in Eq. (3.25) as long as it is not a multiple of $\mathbf{p}_l$.

Let us arrange the columns of $\mathbf{A}^1$ and $\mathbf{A}^2$ as:

$$\mathbf{A}^l = \begin{bmatrix}\mathbf{v}_1^l & \dots & \mathbf{v}_{n-k_{12}}^l & \mathbf{w}_1^l & \dots & \mathbf{w}_{r_l}^l\end{bmatrix} \tag{3.28}$$

where the base cables are followed by the extra ones. Using Eq. (3.25), one can verify that the kernel of $[\mathbf{A}^l\ \mathbf{C}]$ is swept by linear combinations of the columns of the following matrix:

$$\mathbf{E}_l = \begin{bmatrix} (\beta_1^{k_{12}+1})_l & (\beta_2^{k_{12}+1})_l & \cdots & (\beta_{r_l}^{k_{12}+1})_l \\ \vdots & \vdots & \ddots & \vdots \\ (\beta_1^{n})_l & (\beta_2^{n})_l & & (\beta_{r_l}^{n})_l \\ \hline -1 & 0 & & 0 \\ 0 & -1 & & 0 \\ \vdots & \vdots & \ddots & \vdots \\ 0 & 0 & & -1 \\ \hline (\beta_1^{1})_l & (\beta_2^{1})_l & & (\beta_{r_l}^{1})_l \\ \vdots & \vdots & \ddots & \vdots \\ (\beta_1^{k_{12}})_l & (\beta_2^{k_{12}})_l & \cdots & (\beta_{r_l}^{k_{12}})_l \end{bmatrix}_{(n+r_l)\times r_l} \tag{3.29}$$

Next, let us divide the components of $\mathbf{n}_\mathbf{A}$ (in Eq. (3.22)) into three parts, corresponding to $\mathbf{A}^1$, $\mathbf{C}$, and $\mathbf{A}^2$, respectively:

$$(\mathbf{n}_\mathbf{A})_{(m_1+m_2+k_{12})\times 1} = \begin{bmatrix} (\mathbf{n}_1)_{m_1\times 1} \\ (\mathbf{n}_\mathbf{C})_{k_{12}\times 1} \\ (\mathbf{n}_2)_{m_2\times 1} \end{bmatrix} \tag{3.30}$$

It results from Eq. (3.22) that:

$$\begin{cases} \mathbf{A}^1\mathbf{n}_1 + \mathbf{C}\mathbf{n}_\mathbf{C} = \mathbf{0} \\ \mathbf{A}^2\mathbf{n}_2 + \mathbf{C}(-\mathbf{n}_\mathbf{C}) = \mathbf{0} \end{cases} \tag{3.31}$$

The first equation indicates that $[\mathbf{n}_1{}^T\ \ \mathbf{n}_\mathbf{C}{}^T]^T$ belongs to the null space of $[\mathbf{A}^1\ \mathbf{C}]$ and thus can be expanded in terms of the columns of $\mathbf{E}_1$ in Eq. (3.29):

$$\exists \mathbf{x}_1 \in \mathbb{R}^{n+r_1} \qquad \mathbf{E}_1\mathbf{x}_1 = \begin{bmatrix} \mathbf{n}_1 \\ \mathbf{n}_\mathbf{C} \end{bmatrix} \tag{3.32}$$

Similarly for l = 2 in Eq. (3.29):

$$\exists \mathbf{x}_2 \in \mathbb{R}^{n+r_2} \qquad \mathbf{E}_2\mathbf{x}_2 = \begin{bmatrix} \mathbf{n}_2 \\ -\mathbf{n}_\mathbf{C} \end{bmatrix} \tag{3.33}$$

Since $\mathbf{n}_\mathbf{C}$ is common between Eqs. (3.32) and (3.33), by using the corresponding parts in $\mathbf{E}_1$ and $\mathbf{E}_2$ one can write:

$$\begin{bmatrix} (\beta_1^{\ 1})_1 & (\beta_2^{\ 1})_1 & \cdots & (\beta_{r_1}^{\ 1})_1 \\ \vdots & \vdots & \ddots & \vdots \\ (\beta_1^{\ k_{12}})_2 & (\beta_2^{\ k_{12}})_1 & \cdots & (\beta_{r_1}^{\ k_{12}})_1 \end{bmatrix} \mathbf{x}_1 = -\begin{bmatrix} (\beta_1^{\ 1})_2 & (\beta_2^{\ 1})_2 & \cdots & (\beta_{r_2}^{\ 1})_2 \\ \vdots & \vdots & \ddots & \vdots \\ (\beta_1^{\ k_{12}})_2 & (\beta_2^{\ k_{12}})_2 & \cdots & (\beta_{r_2}^{\ k_{12}})_2 \end{bmatrix} \mathbf{x}_2 \tag{3.34}$$

Or:

$$\begin{bmatrix} (\beta_1^{\ 1})_1 & \cdots & (\beta_{r_1}^{\ 1})_1 & (\beta_1^{\ 1})_2 & \cdots & (\beta_{r_2}^{\ 1})_2 \\ \vdots & \ddots & \vdots & \vdots & \ddots & \vdots \\ (\beta_1^{\ k_{12}})_1 & \cdots & (\beta_{r_1}^{\ k_{12}})_1 & (\beta_1^{\ k_{12}})_2 & \cdots & (\beta_{r_2}^{\ k_{12}})_2 \end{bmatrix} \begin{bmatrix} \mathbf{x}_1 \\ \\ \mathbf{x}_2 \end{bmatrix} = \mathbf{D}_{k_{12}\times(r_1+r_2)}\mathbf{x} = \mathbf{0} \tag{3.35}$$

Matrix $\mathbf{D}$, as defined in Eq. (3.35), is named *First Dependency Matrix*. As can be seen from Eqs. (3.35) and (3.25), the columns of $\mathbf{D}$ are the projections of the extra cable wrenches on the constraints. Hence this matrix depends on the constraints and extra cables, but not on the base cables.

Theorem 3.1. In a two-link multibody, $\mathbf{A}_t$ is full-rank if and only if each link has a set of base cables and the first dependency matrix, $\mathbf{D}$, is full-rank.

Proof. If $\mathbf{D}$ is full-rank, then from Eq. (3.35), $\mathbf{x}_1= \mathbf{0}$ and $\mathbf{x}_2= \mathbf{0}$. Now, in Eqs. (3.32) and (3.33), independent from $\mathbf{E}_1$ and $\mathbf{E}_2$ which are found from the base cables, we will have $\mathbf{n}_\mathbf{C} = \mathbf{0}$, $\mathbf{n}_1 = \mathbf{0}$, and $\mathbf{n}_2 = \mathbf{0}$. This implies that $\mathbf{A}_t$ does not have any nonzero vector in its null space or in other words, it is full-rank.

To prove the other side of the theorem, assume $\mathbf{A}_t$ is full-rank. If $\mathbf{D}$ is not full-rank then there is some solution $\mathbf{x} \neq \mathbf{0}$ for Eq. (3.35). Thus, either $\mathbf{x}_1 \neq \mathbf{0}$ or $\mathbf{x}_2 \neq \mathbf{0}$. Without loss of generality, let us assume $\mathbf{x}_1 \neq \mathbf{0}$ which results $\mathbf{E}_1\mathbf{x}_1 \neq \mathbf{0}$ since the columns of $\mathbf{E}_1$ are linearly independent. Consequently and according to Eq. (3.32), $\mathbf{n}_1\neq \mathbf{0}$ and therefore $\mathbf{A}_t$ has a nonzero vector in its null space which indicates it is not full-rank.▲

Theorem 3.1 shows how the base and extra cables determine the rank of $\mathbf{A}_t$ through the first dependency matrix $\mathbf{D}$. The compact form of $\mathbf{D}$ can now be used to show that the minimum necessary number of cables is also sufficient to satisfy the rank condition, too.

Theorem 3.2. The structure matrix of a 2-link mechanism can be made full-rank if and only if the number of cables satisfies the conditions of Eqs. (3.18) and (3.19).

Proof. The necessity of these conditions is already shown. For the sufficiency, first note that Eq. (3.19) ensures that the base cables exist for each link. Now we show that **D** can be formed by the design of extra cables to be full-rank and then apply Theorem 3.1. For this purpose, one needs to notice that in fact any desired **D** can be obtained by the design of the extra cables (their directions and connection points on the links). This is due to the fact that the columns of **D** are projections of the extra cable wrenches onto the constraints.

For the design of **D** and the associated extra cables, one can start with an arbitrary full-rank **D**. For each column of **D**, an associated extra cable will be shown to exist. To determine an extra cable, one needs to find β_i^1 to β_i^n according to Eq. (3.25). Note that β_i^1 to $\beta_i^{k_{12}}$ are already determined by the columns of **D**. The remaining coefficients of the *i*th extra cable (i.e. $\beta_i^{k_{12}+1}$ to β_i^n) are determined by their projections on the base cables (remember that there is at least one base cable on each link in a 2-link mechanism). Now let us take arbitrary values for $\beta_i^{k_{12}+1}$ to β_i^{n-1}. The last coefficient, β_i^n, needs to be selected such that the resulting extra cable be a feasible cable wrench. However, it is easy to show that there is at most one value for β_i^n which satisfie both Eqs. (3.26) and (3.27). For this purpose, note that at least one of the parameters $[\mathbf{v}_{n-k_{12}}^l]^{(1)}$ or $[\mathbf{v}_{n-k_{12}}^l]^{(2)}$ in Eqs. (3.26) and (3.27) is nonzero; otherwise $\mathbf{v}_{n-k_{12}}^l$ is not a cable wrench. Thus, for the nonzero component of $\mathbf{v}_{n-k_{12}}^l$, there is a unique solution for β_i^n in the corresponding equation. As a result, there cannot be more than one solution for β_i^n to satisfy both Eqs. (3.26) and (3.27). Any other value for β_i^n results in a feasible cable wrench and consequently **D** and the structure matrix will be full-rank. ▲

To summarize, with the cable numbers obtained from Eqs. (3.18) and (3.19) and provided that there is no geometrical limitation on the cable directions and locations, for any configuration of the multibody, one can always find a configuration of the cables that results in a full-rank $\mathbf{A}_t$. This implies that the equilibrium of the system can be obtained under arbitrary external loading only if the cables could push as well as pull. However, we know that the cables cannot push and therefore redundant cables are necessary. In the next step, we show under what conditions one redundant cable can make the system tensionable. This requires us to show that the null space condition can also be satisfied with a number and distribution of cables that comply with Eqs. (3.18) and (3.19).

3.3.3 Null Space Condition for a Two-Link Multibody

For the null space condition to be satisfied, it was shown to be necessary that the number of cables be at least one more than the DoF:

$$m_1 + m_2 \geq 2n - k_{12} + 1 \tag{3.36}$$

and similarly, in each link, since there must be at least one cable attached, it is necessary to have:

$$m_j \geq n - k_{12} + 1, \qquad j = 1,2 \tag{3.37}$$

Now, we consider the minimum necessary cables, which is $n_{\mathrm{DoF}}+1$, or $r_1+r_2 = k_{12}+1$ for the whole mechanism and show this number is sufficient to satisfy the null space condition.

Theorem 3.3. In an arbitrary two-link mechanism, a tensionable configuration with minimum necessary cables is obtained if and only if $m_1+m_2 = 2n-k_{12}+1$, $m_1 \geq n-k_{12}+1$, and $m_2 \geq n-k_{12}+1$.

Proof. The theorem simply states that with the minimum necessary number of cables, there is at least one configuration of cables that satisfies both rank and null space conditions. Remember that when the null space is one dimensional, the null space condition requires the components of the null space spanning vector that correspond to the cables be all nonzero. Note that other components of the null space vector that correspond to the constraint wrenches can have any value. Using our notation in the previous section, this is equivalent to ensure that $\mathbf{n}_1$ and $\mathbf{n}_2$ of Eq. (3.30) are strictly nonzero (i.e. do not have any zero components).

For this purpose, let us partition $\mathbf{n}_1$ and $\mathbf{n}_2$ as:

$$\mathbf{n}_l = \begin{bmatrix} (\mathbf{n}'_l)_{(n-k_{12})\times 1} \\ (\mathbf{n}''_l)_{r_l \times 1} \end{bmatrix} \qquad l = 1,2 \tag{3.38}$$

where $\mathbf{n}'_l$ and $\mathbf{n}''_l$ correspond to the base and extra cables, respectively. We will show how the cables can be configured to have $\mathbf{n}'_l$ and $\mathbf{n}''_l$ strictly nonzero.

First, consider $\mathbf{n}''_1$ and $\mathbf{n}''_2$. It results from Eqs. (3.32) and (3.33) that:

$$\mathbf{n}''_l = -\mathbf{I}\mathbf{x}_l = \mathbf{x}_l \qquad l = 1, 2 \tag{3.39}$$

This is because the middle set of rows in $\mathbf{E}_1$ and $\mathbf{E}_2$ are in the form of identity matrices.

As a result of Eq. (3.39), $\mathbf{x}$ must be strictly nonzero to have $\mathbf{n}''_1$ and $\mathbf{n}''_2$ strictly nonzero. This can be ensured by the design of $\mathbf{D}$, remembering that $\mathbf{x}$ belongs to the null space of $\mathbf{D}$ (in Eq. (3.35)). Knowing that all columns of $\mathbf{D}$ (i.e. $(\beta_j)_l$'s) can be arbitrarily chosen by appropriate selection of the corresponding cable wrenches, we follow an approach similar to the rigid body case presented in Eq. (3.7). The first k_{12} columns of **D** are built to be linearly independent. This ensures that **D** is full-rank which in turn according to Theorem 3.1 guarantees that $\mathbf{A}_t$ is full-rank, and thus the equilibrium condition is satisfied. The last column in **D** (column k_{12}+1) is set as a nonzero linear combination of all other k_{12} columns. Similar to Eq. (3.7), this ensures that, there is a strictly nonzero solution **x** for Eq. (3.35). Consequently, $\mathbf{n}''_l$ will have nonzero components.

The remaining part is to ensure that $\mathbf{n}'_1$ and $\mathbf{n}'_2$ are strictly nonzero. According to Eqs. (3.32), (3.33), and (3.38), we have:

$$\mathbf{n}'_l = \begin{bmatrix} (\beta_1^{k_{12}+1})_l & (\beta_2^{k_{12}+1})_l & \dots & (\beta_{r_l}^{k_{12}+1})_l \\ \vdots & \vdots & \ddots & \vdots \\ (\beta_1^{\,n})_l & (\beta_2^{\,n})_l & \dots & (\beta_{r_l}^{\,n})_l \end{bmatrix} \mathbf{x}_l = \mathbf{G}_l \mathbf{x}_l \tag{3.40}$$

where $\mathbf{G}_l$ is the first set of rows in $\mathbf{E}_l$ and corresponds to the projections of extra cables on the base cables. Remember that $\mathbf{x}_l$ is determined and known from the first part of the proof. It remains to select the elements of $\mathbf{G}_l$ such that there is no zero in $\mathbf{n}'_l$ as well as ensuring that the resulting extra cable wrenches are feasible.

To obtain such $\mathbf{G}_l$'s, first it should be pointed out that according to Eq. (3.37), there is at least one extra cable on each link. Therefore, $\mathbf{G}_1$ and $\mathbf{G}_2$ will have at least one column. A procedure is suggested here for constructing the columns of $\mathbf{G}_l$'s. For this purpose, all columns but the last one are designed using the results of Theorem 3.2 and the last column is then found separately. Note that when **D** and $\mathbf{G}_l$'s are found, the extra cables can be determined using Eq. (3.25).

The first r_l–1 columns of $\mathbf{G}_l$ are found such that the corresponding extra cable wrenches will be feasible. In the proof of Theorem 3.2, it was shown that this is always possible. By this fact, any arbitrary selection for $\beta_i^{k_{12}+1}$ to β_i^{n-1} (the ith column of $\mathbf{G}_l$) results in at most one value for β_i^n that satisfies both Eqs. (3.26) and (3.27) and hence should be avoided.

Next, for the last column and to have the desired $\mathbf{n}'_l$, one needs to notice that having set columns 1 to (r_l – 1), the jth component of $\mathbf{n}'_l$ becomes zero according to Eq. (3.40) only if :

$$(\beta_{r_l}^{k_{12}+j})_l = -\frac{\sum_{i=1}^{r_l-1}(\beta_i^{k_{12}+j})_l x_l^i}{x_l^{r_l}} \tag{3.41}$$

where x_l^i is the ith component of $\mathbf{x}_l$.

From Eq. (3.41), it can be perceived that for each component of the last column of $\mathbf{G}_l$ there is a single value that must be avoided. Obviously, for the last component of the last column, β_{rl}^{n}, there is a second value to be avoided found from the cable wrench feasibility condition applied to this column (as applied to all other columns before). However, there are still infinite selections for the components of the last columns. This completes the proof.▲

From the above proof, one can summarize the steps towards finding a tensionable configuration for a two-link multibody in a given state as follows:

1. Select the base cables, i.e. $n-k_{12}$ cables for each link such that they form a full-rank wrench set along with the constraint wrenches.
2. Select matrix **D**, to be full-rank and have a one-dimensional null space spanned by a strictly nonzero vector.
3. Pick a possible distribution of cables according to Eqs. (3.36) and (3.37).
4. Obtain **x** from Eq. (3.35) and partition it into $\mathbf{x}_1$ and $\mathbf{x}_2$.
5. Select $\mathbf{G}_1$ and $\mathbf{G}_2$ according to the method explained in the proof of Theorem 3.3 using Eqs. (3.26), (3.27), and (3.41).
6. Obtain the extra cable wrenches from Eq. (3.25).

The following examples elaborate on the above steps.

3.3.4 Example of a Two-Link Mechanism

Example 3.1. Take n=3 (planar motion) and k_{12}=2. A realization of such mechanism is a two-link with a revolute joint. Let us consider a Cartesian coordinate frame and take constraint matrix **C** as:

$$\mathbf{C} = \begin{bmatrix} 1 & 0 \\ 0 & 1 \\ 0 & 0 \end{bmatrix}$$

which represents a revolute joint (1 DoF, two constraint forces, no constraint moment).

Step 1: The base cables can be taken as:

$$\mathbf{v}_1^{\,1} = \mathbf{v}_1^{\,2} = \begin{bmatrix} 1 \\ 0 \\ 1 \end{bmatrix}$$

which along with the constraint wrenches form a full-rank wrench set on each link. Obviously they satisfy cable wrench condition.

Step 2: Since **D** is 2×3, we take it as:

$$\mathbf{D} = \begin{bmatrix} 1 & 0 & -1 \\ 0 & 1 & -1 \end{bmatrix}$$

in which the first two columns are linearly independent and the last one is a nonzero combination of the first two.

Steps 3 and 4: From Eq. (3.35), one obtains:

$$\mathbf{x} = \begin{bmatrix} -1 \\ -1 \\ -1 \end{bmatrix}$$

in which, there is no zero component due to the way **D** was constructed.

We know that the minimum number of the extra cables is found from:

$$r_1 + r_2 = k_{12} + 1 = 3$$

Let us take $r_1 = 1$ and $r_2 = 2$. (Since $r_l \geq 1$, the only other distribution is $r_1 = 2$ and $r_2 = 1$). Then:

$$\mathbf{x}_1 = -1, \qquad \mathbf{x}_2 = \begin{bmatrix} -1 \\ -1 \end{bmatrix}$$

Step 5: Considering the size of $\mathbf{G}_1$ and $\mathbf{G}_2$, they can generally be considered as:

$$\mathbf{G}_1 = \beta_1, \qquad \mathbf{G}_2 = \begin{bmatrix} \beta_2 & \beta_3 \end{bmatrix}$$

Then, according to Eq. (3.25), the extra cables can be written as:

$$\mathbf{w}_1^{\ 1} = \begin{bmatrix} 1 & 0 \\ 0 & 1 \\ 0 & 0 \end{bmatrix} \begin{bmatrix} 1 \\ 0 \end{bmatrix} + (\beta_1) \begin{bmatrix} 1 \\ 0 \\ 1 \end{bmatrix} = \begin{bmatrix} 1 + \beta_1 \\ 0 \\ \beta_1 \end{bmatrix}$$

$$\mathbf{w}_1^{\ 2} = \begin{bmatrix} 1 & 0 \\ 0 & 1 \\ 0 & 0 \end{bmatrix} \begin{bmatrix} 0 \\ 1 \end{bmatrix} + (\beta_2) \begin{bmatrix} 1 \\ 0 \\ 1 \end{bmatrix} = \begin{bmatrix} \beta_2 \\ 1 \\ \beta_2 \end{bmatrix}$$

$$\mathbf{w}_2^{\ 2} = \begin{bmatrix} 1 & 0 \\ 0 & 1 \\ 0 & 0 \end{bmatrix} \begin{bmatrix} -1 \\ -1 \end{bmatrix} + (\beta_3) \begin{bmatrix} 1 \\ 0 \\ 1 \end{bmatrix} = \begin{bmatrix} -1+\beta_3 \\ -1 \\ \beta_3 \end{bmatrix}$$

Therefore, the two hyperplanes of Eqs. (3.26) and (3.27) for the first extra cable will be β_1+1=0 and 0=0. Thus for satisfying the cable wrench condition for this extra cable, the only situation that a wrench cannot be a cable occurs when $\beta_1 = -1$. For the second and third extra cables, because their second components are always nonzero, the intersection of the two hyperplanes is empty and all points of the space satisfy the wrench condition.

For having no zero component in $\mathbf{n'}_1$, since there is only one column pertaining to link 1:

$$\mathbf{G_1 x_1} = -\boldsymbol{\beta_1} \neq 0$$

And for $\mathbf{n'}_2$, according to Eq. (3.41):

$$\boldsymbol{\beta_3} \neq -\frac{(\boldsymbol{\beta_2})(-1)}{(-1)} = -\boldsymbol{\beta_2}$$

Having these conditions, we take:

$$\mathbf{G}_1 = -2, \qquad \mathbf{G}_2 = \begin{bmatrix} -1 & 0 \end{bmatrix}$$

by which Eq. (3.41) (the hyperplane) is not satisfied and therefore is an acceptable selection.

Step 6: Now by using Eq. (3.25) the wrench of the extra cables can be obtained:

$$\mathbf{w}_1^{\ 1} = \begin{bmatrix} 1 & 0 \\ 0 & 1 \\ 0 & 0 \end{bmatrix} \begin{bmatrix} 1 \\ 0 \end{bmatrix} + (-2) \begin{bmatrix} 1 \\ 0 \\ 1 \end{bmatrix} = \begin{bmatrix} -1 \\ 0 \\ -2 \end{bmatrix}$$

$$\mathbf{w}_1^{\ 2} = \begin{bmatrix} 1 & 0 \\ 0 & 1 \\ 0 & 0 \end{bmatrix} \begin{bmatrix} 0 \\ 1 \end{bmatrix} + (-1) \begin{bmatrix} 1 \\ 0 \\ 1 \end{bmatrix} = \begin{bmatrix} -1 \\ 1 \\ -1 \end{bmatrix}$$

$$\mathbf{w}_2^{\ 2} = \begin{bmatrix} 1 & 0 \\ 0 & 1 \\ 0 & 0 \end{bmatrix} \begin{bmatrix} -1 \\ -1 \end{bmatrix} + (0) \begin{bmatrix} 1 \\ 0 \\ 1 \end{bmatrix} = \begin{bmatrix} -1 \\ -1 \\ 0 \end{bmatrix}$$

And, $\mathbf{A}_t$ is obtained as:

$$\mathbf{A}_t = \begin{bmatrix} 1 & -1 & 1 & 0 & 0 & 0 & 0 \\ 0 & 0 & 0 & 1 & 0 & 0 & 0 \\ 1 & -2 & 0 & 0 & 0 & 0 & 0 \\ 0 & 0 & -1 & 0 & 1 & -1 & -1 \\ 0 & 0 & 0 & -1 & 0 & 1 & -1 \\ 0 & 0 & 0 & 0 & 1 & -1 & 0 \end{bmatrix}$$

which is full-rank and its null space is spanned by:

$$\mathbf{n}_{\mathbf{A}} = \begin{bmatrix} 2 & 1 & -1 & 0 & 1 & 1 & 1 \end{bmatrix}^{\mathrm{T}}$$

The only zero element in $\mathbf{n}_{\mathbf{A}}$ corresponds to a constraint wrench and does not violate tensionability. The negative element also corresponds to the other constraint and is not important in tensionability. However, as explained before, if there was a negative component pertaining to a cable, one could still switch the sign by reversing the cable direction (the associated winch was to be relocated). This verifies that for this example a tensionable configuration has been found. Figure 3-3 shows a schematic of the obtained arrangement. □

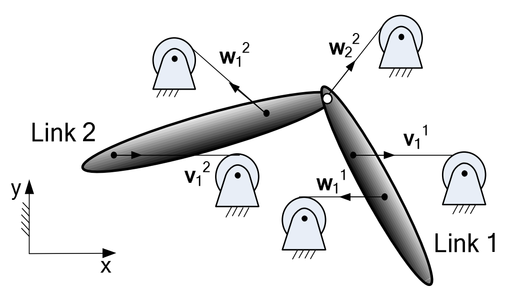

Figure 3-3. A schematic of a the cable arrangement obtained from Example 3.1

3.4 Tensionability of Three-Link Multibodies

Similar to two-link systems, it is assumed that the mechanism has a serial kinematics with holonomic constraints. Cables are attached from one end to one of the links and pulled from the other end by a stationary winch. Furthermore, there is no limitation on the directions and locations of the cables.

3.4.1 Formulation of the Equilibrium

Figure 3-4 depicts a typical three-link multibody driven by cables.

The equilibrium equations of the system can be written in the same format as in Eq. (3.13). However, for this case $\mathbf{A}_t$ has the following form:

$$\mathbf{A}_t = \begin{bmatrix} \mathbf{A}^1 & \mathbf{C}^{12} & \mathbf{0} & \mathbf{0} & \mathbf{0} \\ \mathbf{0} & -\mathbf{C}^{12} & \mathbf{A}^2 & \mathbf{C}^{23} & \mathbf{0} \\ \mathbf{0} & \mathbf{0} & \mathbf{0} & -\mathbf{C}^{23} & \mathbf{A}^3 \end{bmatrix}_{3n\times(m_1+k_{12}+m_2+k_{23}+m_3)} \tag{3.42}$$

where $(\mathbf{A}_j)_{n\times m_j}$, similar to the previous case, contains the cable wrenches on the j^{th} link and $\mathbf{C}^{ij}$ represents the constraints between links i and j. Also, k_{ij} is the number of constraint wrenches due to the joint between links i and j. Using the same logic as in the two previous cases, we convert the tensionability problem to satisfaction of rank condition and null space condition. The following sections detail the procedure for satisfying these conditions.

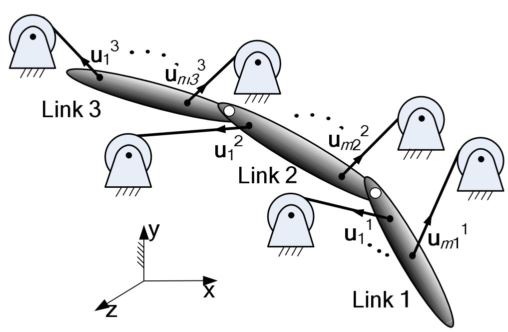

Figure 3-4. Schematic of a three-link cable-driven serial multibody

3.4.2 Rank of the Structure Matrix

For having $rank\{\mathbf{A}_t\}=3n$, we need the number of its columns to be at least equal to the number of the rows. Assuming this, the total number of the cables will be:

$$m_1 + m_2 + m_3 = 3n - k_{12} - k_{23} \tag{3.43}$$

For obtaining the dependency matrix, similar to the two-link case, the concept of base cables and extra cables are applied. The numbers of base cables for the first and third links are obviously $n-k_{12}$ and $n-k_{23}$, respectively. However, the number of base cables for the middle link is not as clear. Let us consider the equilibrium of the middle link:

$$\begin{bmatrix}\mathbf{0} & -\mathbf{C}^{12} & \mathbf{A}^2 & \mathbf{C}^{23} & \mathbf{0}\end{bmatrix}\boldsymbol{\tau}_t = \mathbf{b}^2 \tag{3.44}$$

or:

$$\begin{bmatrix}\mathbf{A}^2 & \mathbf{C}^2\end{bmatrix}\boldsymbol{\tau}^2 = \mathbf{b}^2 \tag{3.45}$$

where $\mathbf{C}^2$ = [$-\mathbf{C}^{12}$ $\mathbf{C}^{23}$] and $\boldsymbol{\tau}^2$ and $\mathbf{b}^2$ contain the components of cable forces and external loads applied on the middle link. Although each of matrices $\mathbf{C}^{12}$ and $\mathbf{C}^{23}$ consists of linearly independent columns, when combined in $\mathbf{C}^2$, there may exist linear dependency among the columns. Note that this is only true when the equilibrium equations of the middle link are considered (the other two links have only one set of constraints). Also note that even if $\mathbf{C}^2$ has dependent columns, the total constraint wrenches, i.e.:

$$\begin{bmatrix}\mathbf{C}^{12}\\ -\mathbf{C}^{12}\\ \mathbf{0}\end{bmatrix} \text{ and } \begin{bmatrix}\mathbf{0}\\ \mathbf{C}^{23}\\ -\mathbf{C}^{23}\end{bmatrix}$$

are still linearly independent due to the assumption and thus there is no redundancy in the columns of $\mathbf{A}_t$ pertaining to the constraints.

Let $rank\{\mathbf{C}^2\}= k_{12}+ k_{23}-s_2 \leq n$ where, $0 \leq s_2 \leq \min\{k_{12}, k_{23}\} < n$; s_2 represents the degree of redundancy when $\mathbf{C}^{12}$ and $\mathbf{C}^{23}$ are combined. As a result, the number of base cables on the middle link will be $n - k_{12} - k_{23}+s_2$ which can be zero (but not negative, since $rank\{\mathbf{C}^2\} \leq n$). Therefore in this case the total number of extra cables will be:

$$\begin{aligned} r_1+r_2+r_3 &= (m_1+m_2+m_3)-(n-k_{12})-(n-k_{23})-(n-k_{12}-k_{23}+s_2) \\ &= k_{12}+k_{23}-s_2 \end{aligned} \tag{3.46}$$

Similar to Eq. (3.22), we can break the $3n$ equilibrium equations of the whole mechanism down to three sets of n equations:

$$\begin{cases} \begin{bmatrix}\mathbf{A}^1 & \mathbf{C}^{12} & \mathbf{0} & \mathbf{0} & \mathbf{0}\end{bmatrix}\mathbf{n}_\mathbf{A} = \mathbf{0} \\ \begin{bmatrix}\mathbf{0} & -\mathbf{C}^{12} & \mathbf{A}^2 & \mathbf{C}^{23} & \mathbf{0}\end{bmatrix}\mathbf{n}_\mathbf{A} = \mathbf{0} \\ \begin{bmatrix}\mathbf{0} & \mathbf{0} & \mathbf{0} & -\mathbf{C}^{23} & \mathbf{A}^3\end{bmatrix}\mathbf{n}_\mathbf{A} = \mathbf{0} \end{cases} \tag{3.47}$$

Also, the null space vector, $\mathbf{n_A}$, can be partitioned as:

$$\mathbf{n_A} = \begin{bmatrix} (\mathbf{n}_1)_{m_1 \times 1} \\ (\mathbf{n}_{\mathbf{C}^{12}})_{k_{12} \times 1} \\ (\mathbf{n}_2)_{m_2 \times 1} \\ (\mathbf{n}_{\mathbf{C}^{23}})_{k_{23} \times 1} \\ (\mathbf{n}_3)_{m_3 \times 1} \end{bmatrix} \tag{3.48}$$

One can perceive that since the first and third links have the same conditions as the links of a two-link multibody (being connected to only one other link), $\mathbf{E}_1$ and $\mathbf{E}_3$ will be similar to the two-link case given by Eq. (3.29) ($\mathbf{E}_l$ is a matrix whose columns form a base for the null space of $[\mathbf{A}^l \ \ \mathbf{C}^l]$) :

$$\mathbf{E}_l = \begin{bmatrix} (\mathbf{G}_l)_{(n-k_l) \times r_l} \\ \hline -\mathbf{I}_{r_l \times r_l} \\ \hline (\mathbf{R}_l)_{k_l \times r_l} \end{bmatrix} \qquad l = 1,3 \tag{3.49}$$

where k_l is the total number of constraints on link l,

$$(\mathbf{G}_l)_{ij} = (\beta_j^{k_{12}+i})_l, \quad i = 1,\ldots,n-k_l, \;\; j = 1,\ldots,r_l$$

which in general contains the projections of the extra cables on the base cable wrenches, and,

$$(\mathbf{R}_l)_{ij} = (\beta_j^{i})_l, \quad i = 1,\ldots,k_l, \;\; j = 1,\ldots,r_l$$

includes the projections of the extra cables on the constraint wrenches.

For detailed definitions of β_j^i refer to Eq. (3.25).

For $\mathbf{E}_2$, first remember that $\mathbf{E}_2$ is different from $\mathbf{E}_1$ and $\mathbf{E}_3$ in that its columns do not totally come from the extra cables. Instead, due to the possible redundancy among the constraint wrenches in $\mathbf{C}^2$ (as discussed before, this redundancy is of order s_2) there will be s_2 columns in $\mathbf{E}_2$, originating from the constraints, $\mathbf{C}^{12}$ and $\mathbf{C}^{23}$. To simplify the formulation, assume that the s_2 dependent constraint wrenches of $\mathbf{C}^2$ merely belong to $\mathbf{C}^{12}$. For this aim, it is sufficient to take $\mathbf{C}^{12}$ and $\mathbf{C}^{23}$ such that the columns (constraint wrenches) of each matrix are orthogonal <u>and</u> all of the $k_{12} - s_2 + k_{23}$ remaining linearly independent vectors are orthogonal as well. Noting that $s_2 \leq k_{12}$, it is straightforward to show that the kernel of the middle link is swept by the columns of a matrix of the following form:

$$
\mathbf{E}_2 = \begin{bmatrix} \mathbf{0} & (\mathbf{F}_2)_{(k_{12}-s_2)\times r_2} \\ -\mathbf{I}_{s_2\times s_2} & \mathbf{0} \\ \mathbf{0} & (\mathbf{G}_2)_{(n-k_{12}-k_{23}+s_2)\times r_2} \\ \mathbf{0} & -\mathbf{I}_{r_2\times r_2} \\ (\mathbf{H}_2)_{k_{23}\times s_2} & (\mathbf{R}_2)_{k_{23}\times r_2} \end{bmatrix}_{(n+s_2+r_2)\times(s_2+r_2)} \tag{3.50}
$$

As can be seen in Eq. (3.50), $\mathbf{E}_2$ is partitioned into two sets of s_2 and r_2 columns. The left s_2 columns correspond to the dimensions of the null space coming from the linear dependency among the constraints, and the right ones correspond to the dimensions resulted from adding the extra cables. Similarly, the rows of $\mathbf{E}_2$ are partitioned into five sets corresponding to k_{12}–s_2 independent constraints between links 1 and 2, s_2 dependent constraints (between links 1 and 2), the base cables, the extra cables, and the constraints between links 2 and 3, respectively. Thereby, $\mathbf{H}_2$ will be the projection of s_2 dependent constraint wrenches coming from $\mathbf{C}^{12}$ on the k_{23} constraint wrenches of the $\mathbf{C}^{23}$. $\mathbf{F}_2$, $\mathbf{G}_2$, and $\mathbf{R}_2$ are the projections of the extra cable wrenches on the k_{12}–s_2 independent constraint wrenches between links 1 and 2, on the base cable wrenches, and on the wrenches of the constraints between links 2 and 3, respectively. $\mathbf{I}$ represents the identity matrix.

Now, similar to Eqs. (3.32) and (3.33):

$$
\exists \mathbf{x}_1, \mathbf{x}_2, \mathbf{x}_3 \qquad \begin{cases} \mathbf{E}_1\mathbf{x}_1 = \begin{bmatrix} \mathbf{n}_1 \\ \mathbf{n}_{\mathbf{C}^{12}} \end{bmatrix} \\ \mathbf{E}_2\mathbf{x}_2 = \begin{bmatrix} -\mathbf{n}_{\mathbf{C}^{12}} \\ \mathbf{n}_2 \\ \mathbf{n}_{\mathbf{C}^{23}} \end{bmatrix} \\ \mathbf{E}_3\mathbf{x}_3 = \begin{bmatrix} \mathbf{n}_3 \\ -\mathbf{n}_{\mathbf{C}^{23}} \end{bmatrix} \end{cases} \tag{3.51}
$$

Next, by enforcing the third Newton's law on the constraints working between the two links, Eqs. (3.49) and (3.50) result:

$$
\begin{cases} \mathbf{R}_1\mathbf{x}_1 + \begin{bmatrix} \mathbf{0} & \mathbf{F}_2 \\ -\mathbf{I}_{s_2\times s_2} & \mathbf{0} \end{bmatrix}\mathbf{x}_2 = \mathbf{0} \\ \begin{bmatrix} \mathbf{H}_2 & \mathbf{R}_2 \end{bmatrix}\mathbf{x}_2 + \mathbf{R}_3\mathbf{x}_3 = \mathbf{0} \end{cases} \tag{3.52}
$$

Rewriting these equations in matrix form, the first dependency matrix is obtained:

$$\begin{bmatrix} \mathbf{R}_1 & \begin{bmatrix} \mathbf{0} \\ -\mathbf{I} \end{bmatrix} & \begin{bmatrix} \mathbf{F}_2 \\ \mathbf{0} \end{bmatrix} & \mathbf{0} \\ \mathbf{0} & \mathbf{H}_2 & \mathbf{R}_2 & \mathbf{R}_3 \end{bmatrix} \begin{bmatrix} \mathbf{x}_1 \\ \mathbf{x}_2 \\ \mathbf{x}_3 \end{bmatrix} = \mathbf{D}_{(k_{12}+k_{23})\times(k_{12}+k_{23})}\mathbf{x} = \mathbf{0} \tag{3.53}$$

Theorem 3.4. In a three-link multibody, $\mathbf{A}_t$ is full-rank if and only if each link has a set of base cables and the first dependency matrix, **D**, is full-rank.

Proof. The proof is almost identical to Theorem 3.1 and hence is not repeated.▲

Now, to further simplify the dependency matrix, we introduce another matrix named *Second Dependency Matrix* which has a similar property; i.e. it is full-rank if and only if the first dependency matrix is full-rank or equivalently $\mathbf{A}_t$ is full-rank. To obtain this equivalent matrix, first we partition $\mathbf{R}_1$ as:

$$\mathbf{R}_1 = \begin{bmatrix} (\mathbf{R}_1{}^1)_{(k_{12}-s_2)\times r_1} \\ (\mathbf{R}_1{}^2)_{s_2\times r_1} \end{bmatrix} \tag{3.54}$$

Then, by a corresponding change of variables:

$$\begin{cases} \mathbf{x}_1 = \mathbf{y}_1 \\ \mathbf{x}_2 = \begin{bmatrix} (\mathbf{z}_2)_{s_2\times 1} \\ (\mathbf{y}_2)_{r_2\times 1} \end{bmatrix} \\ \mathbf{x}_3 = \mathbf{y}_3 \end{cases} \tag{3.55}$$

From Eq. (3.53) one can derive:

$$\mathbf{z}_2 = \mathbf{R}_1{}^2\mathbf{x}_1 = \mathbf{R}_1{}^2\mathbf{y}_1 \tag{3.56}$$

Now, using Eqs. (3.55) and (3.56), and substituting them in Eq. (3.53), one can obtain:

$$\begin{bmatrix} \mathbf{R}_1{}^1 & \mathbf{F}_2 & \mathbf{0} \\ \mathbf{H}_2\mathbf{R}_1{}^2 & \mathbf{R}_2 & \mathbf{R}_3 \end{bmatrix} \begin{bmatrix} \mathbf{y}_1 \\ \mathbf{y}_2 \\ \mathbf{y}_3 \end{bmatrix} = \mathbf{D}'\mathbf{y} = \mathbf{0} \tag{3.57}$$

$\mathbf{D}'$ is the second dependency matrix.

Theorem 3.5. The second dependency matrix, $\mathbf{D}'$, is full-rank, if and only if the dependency matrix, **D**, is full-rank.

Proof. It is easily resulted from Eqs. (3.53) to (3.57).▲

As a result of Theorem 3.5, if the cables are designed such that each link has the minimum required base cables and $\mathbf{D}'$ is full-rank, then $\mathbf{A}_t$ will be full-rank, too.

Looking back at Eq. (3.57), one can see that:

1) The only matrix which is set by the inherent characteristics of the multibody is $\mathbf{H}_2$. The elements of all other matrices in $\mathbf{D}'$ are determined by design of the cable wrenches.
2) $\mathbf{D}'$ becomes structurally rank-deficient[1] if one of the following happens:

$$r_3 > k_{23} \tag{3.58}$$

$$r_1 > k_{12} \tag{3.59}$$

If the condition of Eq. (3.58) is satisfied, then $(\mathbf{R}_3)_{k_{23}\times r_3}$ will have more columns than rows and hence $\mathbf{D}'$ will have redundant columns. If Eq. (3.59) is not satisfied, one can see from $\mathbf{D}$ in Eq. (3.53) that $(\mathbf{R_1})_{k_{12}\times r_1}$ will have more columns than rows and therefore $\mathbf{D}$ will have redundant columns. In both cases, according to Theorems 3.4 and 3.5, $\mathbf{A}_t$ will not be full-rank.

In order to show how the rank condition on $\mathbf{A}_t$ can be satisfied by the minimum necessary cables, the following two Lemmas are required.

Lemma 3.1. A matrix of the form:

$$\begin{bmatrix} (\mathbf{M}_1)_{p\times t} & \mathbf{0} \\ \mathbf{Q}_{q\times t} & (\mathbf{M}_2)_{q\times(p+q-t)} \end{bmatrix}_{(p+q)\times(p+q)}$$

can be made full-rank by appropriate selection of $\mathbf{M}_1$ and $\mathbf{M}_2$, provided that $rank\{\mathbf{Q}\} \geq t-p$ and the matrix is not structurally rank-deficient.

Proof. It is easy to see that the matrix is structurally rank-deficient if and only if $p > t$. Therefore and due to the assumption of the Lemma we must have $p \leq t$ which will be used later in the proof. Let us assume that the matrix is rank deficient, i.e. for some vectors $\mathbf{f}_1$ and $\mathbf{f}_2$:

$$\begin{bmatrix} (\mathbf{M}_1)_{p\times t} & \mathbf{0} \\ \mathbf{Q}_{q\times t} & (\mathbf{M}_2)_{q\times(p+q-t)} \end{bmatrix}_{(p+q)\times(p+q)} \begin{bmatrix} \mathbf{f}_1 \\ \mathbf{f}_2 \end{bmatrix} = \mathbf{0} \tag{3.60}$$

[1]. By "structurally rank-deficient" we mean the structure of matrix is such that by any choice of its entries it remains rank-deficient.

which implies:

$$\mathbf{M}_1\mathbf{f}_1 = \mathbf{0}$$

Suppose that the kernel of $\mathbf{M}_1$ is swept by the linearly independent columns of some matrix **N**. Then, there will be vector **d** such that:

$$\mathbf{f}_1 = \mathbf{N}_{t\times(t-p)}\mathbf{d}_{(t-p)\times 1} \tag{3.61}$$

Thereby, Eq. (3.60) is simplified to:

$$\begin{bmatrix}\mathbf{QN} & \mathbf{M}_2\end{bmatrix}_{q\times q}\begin{bmatrix}\mathbf{d}\\ \mathbf{f}_2\end{bmatrix} = \mathbf{0} \tag{3.62}$$

Since $\mathbf{M}_2$ is arbitrary and the number of its columns is less than or equal to the number of its rows ($p \le t$), it can be designed to have independent columns. Now it is sufficient to design **N** such that **QN** provides (t–p) linearly independent columns. If this can be done, then the only solution of Eq. (3.62) is a zero vector and the proof will be complete.

By assumption, $rank\{\mathbf{Q}\} \ge t\text{–}p$, and since **N** is arbitrary (because $\mathbf{M}_1$ is arbitrary) with t–p columns, **N** can always be chosen such that $rank\{\mathbf{QN}\}= t\text{–}p$. ▲

Lemma 3.2. Columns of $\mathbf{H_2}$ as defined in Eq. (3.50) are linearly independent.

Proof. Let $\mathbf{C}_1{}^s$ be the s_2 redundant columns of $\mathbf{C}^{12}$ in the wrench set of $\begin{bmatrix}\mathbf{C}^{12} & \mathbf{C}^{23}\end{bmatrix}$, as explained before. Then, from Eqs. (3.50) and (3.51), and by the definition of $\mathbf{H}_2$ (see Eq. (3.50)) we have:

$$\mathbf{C}^{23}\mathbf{H}_2 = \mathbf{C}_1{}^s \tag{3.63}$$

If columns of $\mathbf{H}_2$ are not linearly independent, there is some vector **g** such that $\mathbf{H}_2\mathbf{g} = \mathbf{0}$. Then from Eq. (3.63), $\mathbf{C}_1{}^s\mathbf{g} = \mathbf{0}$. This is contradictory, since the columns of $\mathbf{C}^{12}$ are assumed to be linearly independent. Thus columns of $\mathbf{H}_2$ are linearly independent as well.▲

Theorem 3.6. In a three-link multibody, if each link has the minimum required number of base cables and the number of the extra cables satisfy the distribution conditions which are:

$$\begin{cases} r_1 + r_2 + r_3 = k_{12} + k_{23} - s_2 \\ r_1 \le k_{12} \\ r_3 \le k_{23} \end{cases}$$

then there is a configuration of the cables that makes $\mathbf{D}'$ full-rank and consequently $\mathbf{D}$, and $\mathbf{A}_t$ will be full-rank as well.

Proof. Using Lemmas 3.1 and 3.2, one can easily conclude that $\mathbf{R}_1{}^1$, $\mathbf{R}_1{}^2$, and $\mathbf{R}_3$ can be selected such that the matrix:

$$\begin{bmatrix} \mathbf{R}_1{}^1 & \mathbf{0} \\ \mathbf{H}_2\mathbf{R}_1{}^2 & \mathbf{R}_3 \end{bmatrix}$$

has linearly independent columns. Note that since $\mathbf{G}_1$ and $\mathbf{G}_3$ are nonempty (since there is at least one extra cables for links 1 and 3) the wrench condition can be satisfied by these matrices, and thereby $\mathbf{R}_1{}^1$, $\mathbf{R}_1{}^2$, and $\mathbf{R}_3$ remain arbitrary.

Next, if $\mathbf{G}_2$ is nonempty, similarly the elements of the matrix $\begin{bmatrix} \mathbf{F}_2 \\ \mathbf{R}_2 \end{bmatrix}$ are entirely arbitrary and they can be chosen such that the whole matrix $\mathbf{D}'$ becomes full-rank. Consequently $\mathbf{D}$ and $\mathbf{A}_t$ are full-rank as well.

If $\mathbf{G}_2$ is empty (i.e. there is no extra cable on link 2), $\mathbf{F}_2$ and $\mathbf{R}_2$ must be selected such that the wrench condition for link 2 is met. For this aim, the elements of these matrices are not entirely arbitrary and for each column (i.e. each extra cable of link 2) the wrench must not be on the intersection of two hyperplanes similar to Eqs. (3.26) and (3.27). ▲

As a summary, it was proved for a three-link serial multibody with total number of cables equal to the number of degrees of freedom of multibody, and with a distribution of cables satisfying Eqs. (3.58) and (3.59), one can always find a configuration that makes $\mathbf{A}_t$ full-rank.

3.4.3 Forming the Null Space of the Structure Matrix

After proving that the structure matrix with given conditions can be made full-rank, it remains to prove that the null space condition can be also met and hence the mechanism is tensionable. This, as discussed before, is equivalent to the fact that the vector spanning the one dimensional null space has no zero components corresponding to the cables.

For this purpose, first, the system needs multiple solutions for the equilibrium equations which is equivalent to at least one redundant cable:

$$r_1 + r_2 + r_3 \geq k_{12} + k_{23} - s_2 + 1$$

In addition, similar to rigid body and two-link systems, it will be shown that null-space can be designed through the proper selection of the cables such that in the spanning vector of the kernel, the components that correspond to the cable tensions be nonzero. In other words, there should be no zero in $\mathbf{n}_1$, $\mathbf{n}_2$, and $\mathbf{n}_3$ (as in Eq. (3.48)).

As mentioned before, the first link and the third link are similar to the links of a two-link system, meaning that they are subjected to independent constraint wrenches. Therefore, similar to the two-link multibody case, we partition $\mathbf{n}_1$ and $\mathbf{n}_3$ as:

$$\mathbf{n}_l = \begin{bmatrix} (\mathbf{n}'_l)_{(n-k_l)\times 1} \\ (\mathbf{n}''_l)_{r_l\times 1} \end{bmatrix} \qquad l=1,3 \tag{3.64}$$

For the middle link, from Eqs. (3.48), (3.50), and (3.51), $\mathbf{n}_2$ is found as:

$$\mathbf{n}_2 = \begin{bmatrix} (\mathbf{n}'_2)_{(n-k_{12}-k_{23}+s_2)\times 1} \\ (\mathbf{n}''_2)_{r_2\times 1} \end{bmatrix} \tag{3.65}$$

Since links 1 and 3 need at least one extra cable, conditions of Eqs. (3.58) and (3.59) change as follows:

$$1 \le r_3 \le k_{23} \tag{3.66}$$

$$1 \le r_1 \le k_{12} \tag{3.67}$$

As for the middle link, if the number of base cables is nonzero then, similar to the other links, we need to have $r_2 \ge 1$. Otherwise, i.e. if the number of base cables is zero, then we should have $r_2 \ge 0$ since there is no cable force to be made positive.

Theorem 3.7. In a three-link serial multibody, if the necessary conditions on r_l's mentioned above are satisfied (the cable distribution conditions), and if $m_1 + m_2 + m_3 \ge 3n - k_{12} - k_{23} + 1$ (i.e. the total number of cables must be at least one more than DoF) or equivalently $r_1 + r_2 + r_3 \ge k_{12} + k_{23} - s_2 + 1$, then there exist a configuration of cables to make the system tensionable.

Proof. First we assume the base cables are selected as explained in the previous section to satisfy the rank condition. Next, we show how the extra cables should be designed to both satisfy the rank and null space conditions.

Let us partition $\mathbf{n}_1$, $\mathbf{n}_2$, and $\mathbf{n}_3$, as in Eqs. (3.64) and (3.65). Now we show separately how $\mathbf{n}''_l$ and $\mathbf{n}'_l$ can be determined through designing cable wrenches to have no zero components.

For $\mathbf{n}''_l$, using Eqs. (3.53) and (3.55), and similar to Eq. (3.39), one can write:

$$\mathbf{n}''_l = -\mathbf{y}_l, \quad l = 1,2,3 \tag{3.68}$$

Therefore for $\mathbf{n}''_l$ to have no zero components, we need to have all elements of $\mathbf{y}_l$'s to be nonzero. For this, $\mathbf{D}'$ in Eq. (3.57) should be designed such that the result for $\mathbf{y}_l$'s has the desired form (i.e. having no zero component) while satisfying the wrench condition for the resulted extra cables. Due to the assumption of the theorem, the number of cables is at least one more than the number that is necessary to make $\mathbf{D}'$ full-rank, and due to Eq. (3.66) $r_3 \geq 1$. Therefore, by excluding one extra cable from link three, the conditions of Theorem 3.6 are still held. As a result, $\mathbf{D}'$ can still be designed to be full-rank. Now remember that $r_3 \leq k_{23}$ and thus $r_1+r_2 \geq k_{12}-s_2+1$. Hence, matrix $[\mathbf{R}_1^1 \ \mathbf{F}_2]_{(k_{12}-s_2)\times(r_1+r_2)}$ has a null space. In selection of $\mathbf{R}_1{}^1$ and $\mathbf{F}_2$ in Theorem 3.6, one needs to choose them such that there is a vector in kernel of $[\mathbf{R}_1{}^1 \ \mathbf{F}_2]$ with all of its elements being nonzero. Let us call this vector $\begin{bmatrix} \hat{\mathbf{y}}_1 \\ \hat{\mathbf{y}}_2 \end{bmatrix}$. Then if we take the eliminated column of $\mathbf{R}_3$ as:

$$\boldsymbol{\rho}_3 = -(\mathbf{H}_2\mathbf{R}_1{}^2\hat{\mathbf{y}}_1 + \mathbf{R}_2\hat{\mathbf{y}}_2 + \hat{\mathbf{R}}_3\hat{\mathbf{y}}_3) \tag{3.69}$$

where $\hat{\mathbf{R}}_3$ is obtained by removing the column corresponding the last extra cable from $\mathbf{R}_3$:

$$(\mathbf{R}_3)_{k_{23}\times r_3} = [\hat{\mathbf{R}}_3 \quad \boldsymbol{\rho}_3]$$

and $\hat{\mathbf{y}}_3$ consists of arbitrary nonzero numbers, adding the vector of Eq. (3.69) ensures that all $\mathbf{y}_l$'s (which are equal to $\hat{\mathbf{y}}_l$'s) have nonzero elements. Consequently $\mathbf{n}''_l$'s consist of nonzero components.

For the other part of $\mathbf{n}_l$, i.e. $\mathbf{n}'_l$, the only remaining matrices, $\mathbf{G}_l$'s, are to be selected. Similar to Eq. (3.40) we have:

$$\mathbf{n}'_l = \mathbf{G}_l\mathbf{y}_l \tag{3.70}$$

Since $\mathbf{G}_1$ and $\mathbf{G}_3$ are always nonempty, the procedure of Theorem 3.3 can be applied to obtain $\mathbf{G}$'s for this case as well. Note that the case in which $\mathbf{G}_2$ is empty (i.e. there is no extra cable for the second link) has been addressed in Theorem 3.6.

Following the procedure above, $\mathbf{n}_l$ will not have any zero component.▲

Theorem 3.7 guarantees a tensionable configuration, if the conditions of the theorem are satisfied. However, note that unlike the two-link multibody, it does not state that by only one redundant cable, the tensionability can be reached. It is due to the fact that there might be simply no distribution to satisfy the conditions of the theorem. This is further elaborated in the following examples; but before that, let us summarize the steps to design a tensionable configuration for a three-link serial mechanism:

1. Pick a possible distribution of the cables to satisfy necessary conditions of Theorem 3.7. Since there is no guarantee that with one cable more than DoF all of the inequalities are satisfied, it might be necessary to increase the total number of cables.
2. Investigate the dependency of constraints on the middle link, and obtain $\mathbf{H}_2$.
3. Select the base cables.
4. Exclude one of the extra cables from link 3 and, select matrix $\mathbf{D}'$ for the remaining system to be full-rank and satisfying the conditions mentioned in Theorem 3.6 and Theorem 3.7.
5. Obtain $\mathbf{x}$ from Eq. (3.53) and partition it according to Eq. (3.55).
6. Obtain $\boldsymbol{\rho}_3$ from Eq. (3.69).
7. Select $\mathbf{G}_1$, $\mathbf{G}_2$, and $\mathbf{G}_3$ similar to the two-link case, to satisfy the cable wrench conditions and nonzero null space components.
8. Obtain the extra cable wrenches.

3.4.4. Examples of Three-Link Mechanisms

Example 3.2. Let n = 3 (planar) and k_{12}=k_{23}=s_2=1. An example of such mechanism is a three-link serial mechanism with planar joints, i.e. allowing motion in x and y directions but constraining the rotation. This can be realized by two prismatic joints with perpendicular axes. For this mechanism, using one redundant cable, we will have:

$$r_1 + r_2 + r_3 = k_{12} + k_{23} - s_2 + 1 = 2$$

However, from Eqs. (3.66) and (3.67) we must have $r_1 \geq 1$ and $r_3 \geq 1$, and since the number of base cables on the second link is 2>0, we must have $r_2 \geq 1$ as well (every link that has a base cable needs at least one extra cable). Thus, $r_1 + r_2 + r_3 \geq 3$, which contradicts the above equation. Hence it is not possible to satisfy the necessary conditions of Theorem 3.7 by having only one redundant cable. In other words, there is no feasible distribution to satisfy the necessary conditions of Theorem 3.7. However, with two redundant cables (i.e. the total number of cables will be 9), $r_1 + r_2 + r_3 = 3$ and [m_1, m_2, m_3] = [3, 3, 3] is a distribution (and the only distribution) which satisfies the necessary conditions of cable distribution. This demonstrates that unlike rigid bodies, one redundant cable does not guarantee the existence of a tensionable configuration and one may require increasing the number of cables in order to achieve tensionability. Note that the procedure for obtaining the cable wrenches with two redundant cables is very similar to one redundant cable (expressed in the previous section), except that matrix $\mathbf{D}'$ in step 4 instead of being a square matrix, will have one column more than its rows. This gives more freedom in the selection of extra cables. □

Example 3.2 proves the importance of the distribution of the cables. As a result of not considering this, study of Mustafa and Agrawal [35] and stating that a cable-driven mechanism can be made tensionable by $n_{\mathrm{DoF}}+1$ cables is incomplete.

Example 3.3. Consider a three-link multibody with planar motion and k_{12}=k_{23}=2 and s_2=1. A possible realization is a three-link with revolute joints between the successive links. The number of base cables on links one, two and three are 1, 0, and 1, respectively. With conditions expressed in Theorem 3.7:

$$r_1 + r_2 + r_3 = k_{12} + k_{23} - s_2 + 1 = 4$$

there are several possible distributions satisfying conditions of Theorem 3.7 and thus making the system tensionable. An interesting one is:

$$[r_1, r_2, r_3] = [2, 0, 2]$$

in which no cable (neither base cable nor extra cable) is connected to the second link, but according to Theorem 3.7, it satisfies the tensionability conditions.

Suppose that the constraints are shown by the following matrices:

$$\mathbf{C}^{\mathbf{12}} = \begin{bmatrix} -1 & 0 \\ 0 & 1 \\ 1 & 0 \end{bmatrix} \quad \text{and} \quad \mathbf{C}^{\mathbf{23}} = \begin{bmatrix} -1 & 1 \\ 2 & 1 \\ -1 & 1 \end{bmatrix}$$

Note that although each of $\mathbf{C}^{12}$ and $\mathbf{C}^{23}$ are full-rank, there will be one dependent column when they are combined in $\mathbf{C}^2$=[$\mathbf{C}^{12}$ $\mathbf{C}^{23}$]. As mentioned before, we assume the dependent columns to be presented by $\mathbf{C}_1^s$ which should come from $\mathbf{C}^{\mathbf{12}}$. In this example, $\mathbf{C}_1^s$ is the second column of $\mathbf{C}^{12}$. One can see that the columns in each matrix are orthogonal and the columns of the linearly independent vectors remaining after removing $\mathbf{C}_1^s$ are orthogonal as well. Thus from Eq. (3.50):

$$\mathbf{H_2} = \begin{bmatrix} 1/3 \\ 1/3 \end{bmatrix}$$

The first step towards the design of a tensionable configuration is to select the base cables for links 1 and 3. Let us choose the base cable wrenches as:

$$\mathbf{v}_1{}^1 = \begin{bmatrix} 1 \\ 5 \\ 1 \end{bmatrix}, \qquad \mathbf{v}_1{}^3 = \begin{bmatrix} 2 \\ 2 \\ 1 \end{bmatrix}$$

Now according to Theorem 3.7, the next step is to design the second dependency matrix to be full-rank without using the last extra cable of the third link.

Since there is no cable attached to link 2, matrices $\mathbf{F}_2$ and $\mathbf{R}_2$ vanish. Thus the form of the second dependency matrix (without the last extra cable) will be:

$$\hat{\mathbf{D}}' = \begin{bmatrix} \mathbf{R}_1{}^1 & \mathbf{0} \\ \mathbf{H}_2\mathbf{R}_1{}^2 & \hat{\mathbf{R}}_3 \end{bmatrix}$$

Let us take:

$$\mathbf{R}_1 = \begin{bmatrix} 1 & -1 \\ 3 & 3 \end{bmatrix}$$

$$\Longrightarrow \quad \mathbf{R}_1^1 = [1 \quad -1], \;\; \mathbf{R}_1^2 = [3 \quad 3]$$

Then the null space of $\mathbf{R}_1{}^1$ (as in Eq. (3.61)) will be:

$$\mathbf{N} = \begin{bmatrix} 1 \\ 1 \end{bmatrix}$$

in which there is no zero and thus satisfies the condition mentioned in the proof of Theorem 3.7. From Eq. (3.62):

$$\mathbf{QN} = \mathbf{H_2 R_1^2 N} = \begin{bmatrix} 2 \\ 2 \end{bmatrix}$$

Thus taking:

$$\hat{\mathbf{R}}_3 = \begin{bmatrix} 1 \\ -1 \end{bmatrix}$$

makes matrix $[\mathbf{QN} \quad \hat{\mathbf{R}}_3]$ full-rank. The second dependency matrix will become:

$$\hat{\mathbf{D}}' = \begin{bmatrix} 1 & -1 & 0 \\ 1 & 1 & 1 \\ 1 & 1 & -1 \end{bmatrix}$$

Adding the last cable using Eq. (3.69), and noting that $\hat{\mathbf{y}}_1 = \mathbf{N}$ and $\hat{\mathbf{y}}_2$ is empty, and taking $\hat{\mathbf{y}}_3 = 1$:

$$\boldsymbol{\rho}_3 = -\left(\begin{bmatrix} 1/3 \\ 1/3 \end{bmatrix} [3 \quad 3] \begin{bmatrix} 1 \\ 1 \end{bmatrix} + \mathbf{0} + \begin{bmatrix} 1 \\ -1 \end{bmatrix} (1)\right) = \begin{bmatrix} -3 \\ -1 \end{bmatrix}$$

Thereby:

$$\mathbf{D}' = \begin{bmatrix} 1 & -1 & 0 & 0 \\ 1 & 1 & 1 & -3 \\ 1 & 1 & -1 & -1 \end{bmatrix}$$

Then the null space of $\mathbf{D}'$ in Eq. (3.57) will be:

$$\mathbf{y} = \begin{bmatrix} 1 \\ 1 \\ 1 \\ 1 \end{bmatrix} \implies \mathbf{y}_1 = \mathbf{y}_3 = \begin{bmatrix} 1 \\ 1 \end{bmatrix}$$

Now, considering the sizes of $\mathbf{G}_1$ and $\mathbf{G}_3$, they can be parametrically considered as:

$$\mathbf{G}_1 = [\beta_1 \quad \beta_2] \quad \text{and} \quad \mathbf{G}_3 = [\beta_3 \quad \beta_4]$$

Thereby the extra cable wrenches will become:

$$\mathbf{w}_1^1 = \begin{bmatrix} -1 & 0 \\ 0 & 1 \\ 1 & 0 \end{bmatrix} \begin{bmatrix} 1 \\ 3 \end{bmatrix} + \beta_1 \begin{bmatrix} 1 \\ 5 \\ 1 \end{bmatrix} = \begin{bmatrix} \beta_1 - 1 \\ 5\beta_1 + 3 \\ \beta_1 + 1 \end{bmatrix}$$

$$\mathbf{w}_2^1 = \begin{bmatrix} -1 & 0 \\ 0 & 1 \\ 1 & 0 \end{bmatrix} \begin{bmatrix} -1 \\ 3 \end{bmatrix} + \beta_2 \begin{bmatrix} 1 \\ 5 \\ 1 \end{bmatrix} = \begin{bmatrix} \beta_2 + 1 \\ 5\beta_2 + 3 \\ \beta_2 - 1 \end{bmatrix}$$

$$\mathbf{w}_1^3 = \begin{bmatrix} -1 & 1 \\ 2 & 1 \\ -1 & 1 \end{bmatrix} \begin{bmatrix} 1 \\ -1 \end{bmatrix} + \beta_3 \begin{bmatrix} 2 \\ 2 \\ 1 \end{bmatrix} = \begin{bmatrix} 2\beta_3 - 2 \\ 2\beta_3 + 1 \\ \beta_3 - 2 \end{bmatrix}$$

$$\mathbf{w}_2^3 = \begin{bmatrix} -1 & 1 \\ 2 & 1 \\ -1 & 1 \end{bmatrix} \begin{bmatrix} -3 \\ -1 \end{bmatrix} + \beta_4 \begin{bmatrix} 2 \\ 2 \\ 1 \end{bmatrix} = \begin{bmatrix} 2\beta_4 + 2 \\ 2\beta_4 - 7 \\ \beta_4 + 2 \end{bmatrix}$$

The hyperplane conditions (for ensuring the force part of the wrench is nonzero and thus the wrench can be a cable wrench) are obtained as follows:

$$\begin{cases} \mathbf{w}_1^1\!: \ \beta_1 = 1 \ \ and \ \ \beta_1 = -3/5 \quad \implies \quad \beta_1 = \emptyset \qquad \textbf{(i)} \\ \mathbf{w}_2^1\!: \ \beta_2 = -1 \ and \ \ \beta_2 = -3/5 \quad \implies \quad \beta_2 = \emptyset \qquad \textbf{(ii)} \\ \mathbf{w}_1^3\!: \ \beta_3 = 1 \ \ and \ \ \beta_3 = -1/2 \quad \implies \quad \beta_3 = \emptyset \qquad \textbf{(iii)} \\ \mathbf{w}_2^3\!: \ \beta_4 = -1 \ \ and \ \ \beta_4 = 7/2 \quad \implies \quad \beta_4 = \emptyset \qquad \textbf{(iv)} \end{cases}$$

The other two conditions come from the fact that $\mathbf{n'}_1$ and $\mathbf{n'}_3$ should have nonzero components:

$$\begin{cases} \mathbf{n'}_1 = \mathbf{G}_1\mathbf{y}_1 = \beta_1 + \beta_2 \quad \implies \quad \beta_1 + \beta_2 = 0 \quad \textbf{(v)} \\ \\ \mathbf{n'}_3 = \mathbf{G}_3\mathbf{y}_3 = \beta_3 + \beta_4 \quad \implies \quad \beta_3 + \beta_4 = 0 \quad \textbf{(vi)} \end{cases}$$

Considering conditions (i) to (vi) (all of which must be avoided to obtain a tensionable configuration of cables) we take:

$$\beta_1 = 0,\ \beta_2 = -1,\ \beta_3 = -1,\ \beta_4 = 0$$

Then the extra cable wrenches will be:

$$\mathbf{w}_1^1 = \begin{bmatrix} -1 \\ 3 \\ 1 \end{bmatrix}, \qquad \mathbf{w}_2^1 = \begin{bmatrix} 0 \\ -2 \\ -2 \end{bmatrix}, \qquad \mathbf{w}_1^3 = \begin{bmatrix} -4 \\ -1 \\ -3 \end{bmatrix}, \qquad \mathbf{w}_2^3 = \begin{bmatrix} 2 \\ -7 \\ 2 \end{bmatrix}$$

And finally the structure matrix and its null space become:

$$\mathbf{A}_\mathrm{t} = \begin{bmatrix} 2 & -1 & -1 & -1 & 0 & 0 & 0 & 0 & 0 & 0 \\ 2 & 3 & 1 & 0 & 1 & 0 & 0 & 0 & 0 & 0 \\ 1 & 1 & -2 & 1 & 0 & 0 & 0 & 0 & 0 & 0 \\ 0 & 0 & 0 & 1 & 0 & -1 & 1 & 0 & 0 & 0 \\ 0 & 0 & 0 & 0 & -1 & 2 & 1 & 0 & 0 & 0 \\ 0 & 0 & 0 & -1 & 0 & -1 & 1 & 0 & 0 & 0 \\ 0 & 0 & 0 & 0 & 0 & 1 & -1 & 2 & -4 & 2 \\ 0 & 0 & 0 & 0 & 0 & -2 & -1 & 2 & -1 & -7 \\ 0 & 0 & 0 & 0 & 0 & 1 & -1 & 1 & -3 & 2 \end{bmatrix}$$

and:

$$\mathbf{n}_\mathbf{A} = [1 \quad 1 \quad 1 \quad -7 \quad 0 \quad -2 \quad -2 \quad 1 \quad 1 \quad 1]^\mathrm{T}$$

As can be seen, the components of the null space vector corresponding to the cables are all positive (and equal) and satisfy the conditions for tensionability of the system. The resulted mechanism is depicted in Figure 3-5. □

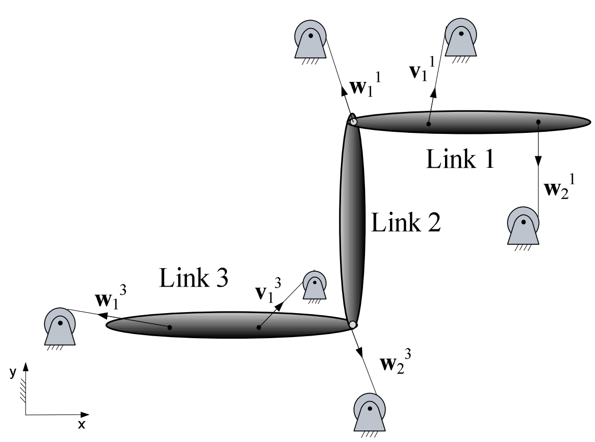

Figure 3-5. A schematic of a the cable arrangement obtained from Example 3.3

Example 3.3 proves that a tensionable configuration can be obtained even if the middle link has no cable attached. Thus the assumption made by Kino et al. [34] in that each link of the multibody have to have at least one cable attached to it is not correct.

3.5 Higher Number of Links

The complete study of extending the method developed for two- and three-link multibodies (based on using dependency matrices) to higher number of links and obtaining the necessary and sufficient conditions of tensionability is outside the scope of this thesis. However, in this section a brief study of necessary conditions on the cable numbers and their distribution is presented. For more complete discussion of the subject see [39].

Through dynamic formulation (similar to Eqs. (3.14) and (3.42)) the structure matrix for an arbitrary multibody can be obtained[1]. Since the number of the rows of the structure matrix is $n\bar{m}$, and because for tensionability a necessary condition is that the structure matrix must have null space (i.e. more columns than rows), the condition on the total number of the cables will be:

$$\sum m_i \geq nM - k + 1 = n_{\mathrm{DoF}} + 1 \tag{3.71}$$

which is not a surprising result.

For a multibody to be in equilibrium against some arbitrary load, all of the subsystems of it must be in equilibrium, as well. By "subsystems" of a multibody we mean all single and connected sets of links (which are rigid bodies) of the multibody. Therefore, since for having equilibrium by using of cables we always need at least one cable more than DoF, each subsystem which has at least one cable must satisfy:

$$\sum m_i \geq nM' - k' + 1 \tag{3.72}$$

where M' is the number of links of the subsystem and k' is the total number of constraints on the subsystem. Note that Eq. (3.72) for the special case of a 3-link multibody is equivalent to Eqs. (3.66) and (3.67). If $nM' = k'$, then the subsystem can be in equilibrium without any cable, provided that the other necessary conditions (cable numbers for other subsystems) are satisfied.

[1]. Also look at chapter 4 of this thesis.

Note that these necessary conditions are not limited to serial multibodies and are applicable to any multibody. For proof of the above statements (based the dynamic equations of the system and form of the structure matrix) see [39].

3.6 Tensionability of the Fabricated Arm Mechanism

The arm mechanism explained in chapter 2 for simulating a human arm is a 4-DoF two-link multibody. The difference with the systems discussed in this chapter is that a spherical joint connects the arm to the ground, whereas the two- and three-link systems studied are not connected to the ground and are float in the space.

This problem can be resolved by considering the system as three-link mechanism where the first link is the ground. Thereby, the conditions of the tensionability of the 3-link mechanisms obtained in section 3.4 can be applied here as well. The only difference is that the arm mechanism is a spatial mechanism whereas the considered two- and three-link mechanisms have been assumed to be planar. However, as mentioned before, the only part of the methods suggested in sections 3.3 and 3.4 which limits the analysis to the planar case is the condition of cable wrenches discussed in section 3.2, i.e. $[w_1\ w_2\ w_3] \cdot [w_4\ w_5\ w_6] = 0$. As shown before, in case of planar mechanisms this condition is simplified to equations of hyperplanes (Eqs. (3.26) and (3.27)), whereas for spatial mechanisms it leads to nonlinear equations of hypersurfaces. However, since these hypersurfaces exclude only lower-dimension manifolds of the space, it is always possible to design the system without considering them, and then check for the conditions. In fact, as mentioned earlier in this chapter, before the present work, this condition had not been considered for rigid bodies and the well-known proof of tensionability for rigid body cable-driven mechanisms has been without considering the cable wrench condition.

Since the arm mechanism is a 4-DoF multibody, at least 5 cables are required for tensionability. On the first link (upper arm) there are 3+5=8 total constraints, out of which only 6 constraints can be independent. On the second link (forearm) there are only 5 constraints of the revolute elbow joint. Hence there are four possible distributions of the five cables: {0,5}, {1,4}, {2,3}, and {3,2}. The distribution selected is {3,2} due to the fact that it minimizes the forces of the elbow constraints. In a distribution such as {0,5} the control of the first link is merely done using the constraint forces of the elbow and therefore it maximizes the force on the joint. For the synthesis and placement of the winches see [29]. In the next chapter we show that the synthesized system of [29] is indeed tensionable.

3.7 Summary

In this chapter conditions on the tensionability of cable-driven mechanisms were studied. The study started with the review of rigid body systems from the literature. It has been shown that although the study of tensionability of the rigid bodies is a classic subject, the cable wrench condition has not been considered in the previous researches and the existence of a set of wrenches that satisfy the condition of being a cable wrench has been assumed trivial. Although it is not difficult for rigid bodies to obtain wrenches satisfying cable wrench conditions, it has been shown that for multibodies it is not an easy task. As a result and for this study, the cable wrench condition was considered merely for planar cases.

Based on this, the conditions of tensionability were investigated for two- and three-link multibodies. It was proved that in 2-link mechanisms, the minimum necessary number of cables (one redundant cable) is also sufficient to build a tensionable configuration as long as there is no constraint on the location of the winches.

In the case of 3-link mechanisms, it was shown that in some cases one redundant cable is not sufficient since there is no acceptable distribution of cables. As a result, more than one redundant cable may be required. It was proved that with the minimum cable number and a valid distribution, there is always a configuration of cables which provides a tensionable mechanism.

The proposed method is algorithmic in the sense that it provides an algorithm to design the cable configurations to ensure the tensionability. The algorithm is based on transferring the structure matrix of the multibody, $\mathbf{A}_t$, to simpler forms, named the dependency matrices, and utilizing these matrices to find equivalent conditions on the cable wrenches for equilibrium and tensionability of the multibody. Using the dependency matrices is easier than the structure matrix due to their compact forms and clear connection to the wrenches of the cables and constraints.

The study of multibodies was applied to the fabricated arm mechanism to obtain the number and distribution of the cables guaranteeing the tensionability. In the next chapter it is shown that the system with this configuration is indeed tensionable and the boundaries of the tensionable workspace are obtained.

Chapter 4 Workspace Analysis[1]

As it is renowned in the literature of cable-driven mechanisms, having a sufficient number of cables attached to the mechanism does not guarantee the tensionability of the system at all points of the reachable workspace of the robot. In other words, the system will merely be tensionable in certain poses of the mechanism. Hence, it is required to determine the regions in the workspace in which the cable-driven mechanism is tensionable. In this thesis, the subspace of the reachable workspace in which the system is tensionable is named *tensionable workspace*, and the procedure leading to obtaining these regions is referred to as *workspace analysis*.

It is noteworthy that in some other researches, other definitions and terminologies have been used. Verhoeven and Hiller [40] used "controllable workspace" and defined it as "the set of poses in which the robot can maintain equilibrium against all external wrenches". Some other works contributed to analyzing the set of all poses that the robot can attain static equilibrium (i.e. in the absence of motions and external loads) [41,42]. This workspace was referred to as *static equilibrium workspace* (SEW) in [43]. Accordingly, "dynamic workspace" was defined as the set of all attainable poses with a specific acceleration, by positive cable tensions [44]. A more practical workspace definition is wrench feasible workspace (WFW) which is the set of all poses in which a specified range of external wrenches can be generated using a limited range of cable tensions [43,45,46]. Wrench closure workspace (WCW) is a special case of WFW when both cable tension and the wrench sets are unbounded [45,46]. One can see that WCW, tensionable workspace, and controllable workspace are equivalent. They are merely dependent on the kinematics of the manipulator rather than the external loading, static or dynamic equilibrium or cable properties.

Due to the complexity of the workspace analysis problem, most of the works in the literature are based on numerical methods [47,48]. The basic method for numerical estimation of the workspace consists of point-to-point examination of the workspace. This examination can be done in several different ways (as reviewed by Gouttefarde [36]). However, especially when the number of the redundant cables is more than one, most of these methods encounter

[1]. A version of this chapter has been published in ASME Journal of Mechanisms and Robotics, **3**(2), Art. No. 021005, 2011

computational difficulties. In [49,50], other more efficient methods for checking the workspace are proposed.

Another approach to workspace analysis which has become a topic of interest in the recent years is using interval analysis [51,52]. The main advantage of interval analysis over the point-to-point search is that the search is continuous and the information at the "intermediate" points is not lost.

There are also a few studies that tackled the workspace problem analytically. Properties of the constant-orientation workspace of planar cable robots with one redundant cable are discussed in [45]. Later, in [46], the authors extended their method to more than one redundant cable. In [43] and [53], similar problem is addressed with different viewpoints. In both researches, the analytical descriptions for the boundaries of the tensionable workspace were found. The main difference in the two approaches is that in [43] the focus has been on obtaining WFW, whereas in [53] the method which was based on methods of checking positive tensions of the cables at a particular point of the workspace. Some other examples of analytical studies on the workspace exist on robots with particular geometries. In [54], it was shown that the tensionable workspace for a particular cable-driven robot is the same as the reachable workspace. Their geometrical procedure has been adopted in [55] for obtaining the workspace of a similar robot.

The aim of this chapter is to develop a framework to: 1) extend the concept of tensionable workspace (defined so far for a single rigid body) to multibody systems; 2) obtain the tensionable workspace analytically by finding its boundaries; 3) analyze the obtained workspace and compare the inherent differences with a similar single rigid body cable-driven robot; and 4) obtain the workspace of the robotic system designed and fabricated.

4.1 Formulation of Dynamics of Cable-Driven Multibodies – General Case

4.1.1 General Formulation

Figure 4-1 depicts a schematic of a serial multibody system. Similar to the previous chapter, the cables are connected to one and only one of the links from one end and pulled from the other end by a stationary motorized winch. Also, (again as in the previous chapter) the joints connecting the links are binary with holonomic constraints.

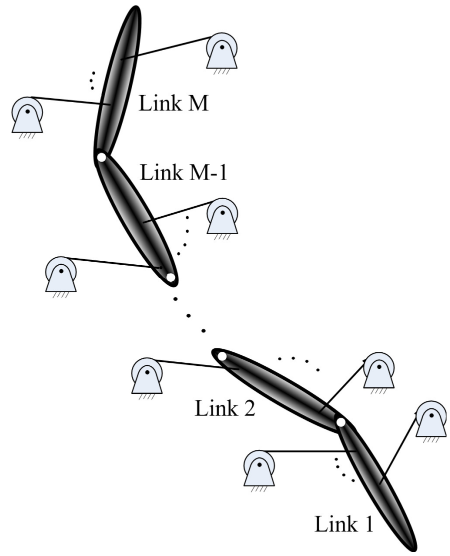

Figure 4-1. A typical cable-driven serial multibody system

Similar to rigid bodies and the simple multibodies studied in the previous chapter, the equilibrium equations of a serial multibody system with M links, $\overline{m}$ cables and $\bar{k}$ constraints in Cartesian space leads to an equation of the following form:

$$(\mathbf{A}_t)_{(nM)\times(\bar{m}+\bar{k})}(\boldsymbol{\tau}_t)_{(\bar{m}+\bar{k})\times 1} = (\mathbf{b}_t)_{(nM)\times 1} \tag{4.1}$$

Using the same approach of the previous chapter, for a general M-link serial multibody system these matrices take the following form:

$$(\mathbf{A}_t)_{nM\times(\bar{m}+\bar{k})} = \begin{bmatrix} (\mathbf{A}_1)_{n\times m_1} & (\mathbf{C}_1)_{n\times k_1} & \mathbf{0} & \mathbf{0} & \mathbf{0} & \mathbf{0} & & \mathbf{0} & \mathbf{0} \\ \mathbf{0} & -(\mathbf{C}_1)_{n\times k_1} & (\mathbf{A}_2)_{n\times m_2} & (\mathbf{C}_2)_{n\times k_2} & \mathbf{0} & \mathbf{0} & & \mathbf{0} & \mathbf{0} \\ \mathbf{0} & \mathbf{0} & \mathbf{0} & -(\mathbf{C}_2)_{n\times k_2} & (\mathbf{A}_3)_{n\times m_3} & (\mathbf{C}_3)_{n\times k_3} & & \mathbf{0} & \mathbf{0} \\ \vdots & & & & & \vdots & \ddots & \vdots & \\ \mathbf{0} & \mathbf{0} & \mathbf{0} & \mathbf{0} & \mathbf{0} & \mathbf{0} & \cdots & -(\mathbf{C}_{M-1})_{n\times k_{M-1}} & (\mathbf{A}_M)_{n\times m_M} \end{bmatrix} \tag{4.2}$$

$$(\boldsymbol{\tau}_t)_{(\bar{m}+\bar{k})\times 1} = \begin{bmatrix} t_{1,1} & \dots & t_{m_1,1} & q_{1,1} & \dots & q_{k_1,1} & t_{1,2} & \dots & t_{m_2,2} & q_{1,2} & \dots & q_{k_2,2} \cdots & t_{1,M} & \dots & t_{m_M,M} \end{bmatrix}^T \tag{4.3}$$

$$\mathbf{b}_t = \begin{bmatrix} \mathbf{b}_1 \\ \vdots \\ \mathbf{b}_M \end{bmatrix} \tag{4.4}$$

where $\bar{m}$ and $\bar{k}$ are the total number of cables and total number of constraints for the multibody system, respectively, m_i is the total number of cables on the i'th link, and k_i is the number of constraints between links i and i+1.

Evaluation of tensionability in a cable-driven multibody system requires the analysis of the rank and null space of matrix $\mathbf{A}_t$ which is also called structure matrix of the multibody. From Eq. (4.1), it is seen that the size of this matrix grows rapidly with the number of links and cables. For instance, in a 3-link spatial mechanism, $\mathbf{A}_t$ has 18 rows and at least 19 columns. Analysis of such matrices can easily lead to numerical complexities. In the next section, we apply Lagrange's method to minimize the size of the structure matrix.

4.1.2 Tensionability Formulation Using Generalized Forces

The large size of $\mathbf{A}_t$ is mostly due to the Newtonian formulation of the dynamics which leads to the presence of internal reaction forces/moments. As long as the multibody system is a serial kinematic chain, using Lagrange's approach and the notion of generalized forces eliminates all the internal unknown forces/moments from the dynamic equations. Thereby, one can reduce the number of the equilibrium equations and simplify the tensionability analysis.

The general form of Lagrange's equation -if the Lagrangian can be expressed in terms of a minimal set of generalized coordinates- is:

$$\frac{d}{dt}\left(\frac{\partial L}{\partial \dot{\alpha}_i}\right) - \frac{\partial L}{\partial \alpha_i} = Q_i \ , \ i = 1,\ldots, n_{\mathrm{DoF}} \tag{4.5}$$

where L is the Lagrangian, n_{DoF} is the degrees of freedom of the multibody system, and α_i`s and $Q_i$`s are the generalized coordinates and generalized forces, respectively.

In a cable-driven mechanism, the contribution of cables to the dynamics is modeled as point forces applied to the links (i.e. the inertia and elastic stiffness of the cables are neglected). Therefore, Q_i`s in Eq. (4.5) are divided into two parts: $Q_i = Q_i^c + Q_i^r$, where Q_i^c is the part pertaining to the cable forces, and Q_i^r includes all other generalized external forces/moments. The latter part together with the terms in the left hand side of Lagrange's equation can be incorporated in a vector named $\mathbf{b}_{\mathrm{L}}$:

$$\mathbf{b}_{\mathrm{L}} = \begin{bmatrix} \frac{d}{dt}\left(\frac{\partial L}{\partial \dot{\alpha}_1}\right) - \frac{\partial L}{\partial \alpha_1} - Q_1^r \\ \vdots \\ \frac{d}{dt}\left(\frac{\partial L}{\partial \dot{\alpha}_{n_{\mathrm{DoF}}}}\right) - \frac{\partial L}{\partial \alpha_{n_{\mathrm{DoF}}}} - Q_{n_{\mathrm{DoF}}}^r \end{bmatrix} \tag{4.6}$$

In order to use the Lagrange's formulation, the cable forces need to be presented in generalized coordinates. Suppose that $t_j\mathbf{u}_j$ is a cable force and $\mathbf{r}_j$ is the position vector of the connection point of the cable to the multibody, both expressed in the fixed Cartesian frame. According to Lagrange's method, one can express Q_i^c in terms of the cables forces as:

$$Q_i^c = \sum_{j=1}^{\overline{m}} \left(t_j \mathbf{u}_j \cdot \frac{\partial \mathbf{r}_j}{\partial \alpha_i} \right) \tag{4.7}$$

which can be then arranged in matrix form as:

$$Q_i^c = \sum_{j=1}^{\overline{m}} \left(\mathbf{u}_j \cdot \frac{\partial \mathbf{r}_j}{\partial \alpha_i} \right) t_j = \begin{bmatrix} \mathbf{u}_1 \cdot \left(\frac{\partial \mathbf{r}_1}{\partial \alpha_i} \right) & \cdots & \mathbf{u}_{\overline{m}} \cdot \left(\frac{\partial \mathbf{r}_{\overline{m}}}{\partial \alpha_i} \right) \end{bmatrix} \begin{bmatrix} t_1 \\ \vdots \\ t_{\overline{m}} \end{bmatrix} \tag{4.8}$$

or:

$$\begin{bmatrix} Q_1^c \\ \vdots \\ Q_{n_{\mathrm{DoF}}}^c \end{bmatrix} = \begin{bmatrix} \mathbf{u}_1 \cdot \left(\frac{\partial \mathbf{r}_1}{\partial \alpha_1} \right) & \cdots & \mathbf{u}_{\overline{m}} \cdot \left(\frac{\partial \mathbf{r}_{\overline{m}}}{\partial \alpha_1} \right) \\ \vdots & \ddots & \vdots \\ \mathbf{u}_1 \cdot \left(\frac{\partial \mathbf{r}_1}{\partial \alpha_{n_{\mathrm{DoF}}}} \right) & \cdots & \mathbf{u}_{\overline{m}} \cdot \left(\frac{\partial \mathbf{r}_{\overline{m}}}{\partial \alpha_{n_{\mathrm{DoF}}}} \right) \end{bmatrix} \begin{bmatrix} t_1 \\ \vdots \\ t_{\overline{m}} \end{bmatrix} \tag{4.9}$$

Now, $\mathbf{A}_{\mathrm{L}}$ and $\boldsymbol{\tau}_{\mathrm{L}}$ are defined according to Eq. (4.9) as:

$$\mathbf{A}_{\mathrm{L}} = \begin{bmatrix} \mathbf{u}_1 \cdot \left(\frac{\partial \mathbf{r}_1}{\partial \alpha_1} \right) & \cdots & \mathbf{u}_{\overline{m}} \cdot \left(\frac{\partial \mathbf{r}_{\overline{m}}}{\partial \alpha_1} \right) \\ \vdots & \ddots & \vdots \\ \mathbf{u}_1 \cdot \left(\frac{\partial \mathbf{r}_1}{\partial \alpha_{n_{\mathrm{DoF}}}} \right) & \cdots & \mathbf{u}_{\overline{m}} \cdot \left(\frac{\partial \mathbf{r}_{\overline{m}}}{\partial \alpha_{n_{\mathrm{DoF}}}} \right) \end{bmatrix}_{n_{DoF} \times \overline{m}} \tag{4.10}$$

and:

$$\boldsymbol{\tau}_{\mathrm{L}} = \begin{bmatrix} t_1 & \ldots & t_{\overline{m}} \end{bmatrix}^T \tag{4.11}$$

Consequently, the dynamic equations of the system given in Eq. (4.9), can be written in the following form:

$$\mathbf{A}_{\mathrm{L}}\boldsymbol{\tau}_{\mathrm{L}} = \mathbf{b}_{\mathrm{L}} \tag{4.12}$$

where $\mathbf{b}_{\mathrm{L}}$ was defined in Eq. (4.6) and includes all the external forces (other than cable forces) as well as the inertia effects. Note that the left side of Eq. (4.12) is a linear combination of the columns of $\mathbf{A}_{\mathrm{L}}$ by the cable tensions. The columns of $\mathbf{A}_{\mathrm{L}}$, according to Eq. (4.10), can be perceived as the cable wrenches expressed in the space of generalized coordinates.

Note that due to the omission of the internal forces, the dimension of the problem has been significantly reduced. For instance in a planar double pendulum ($n_{\mathrm{DoF}} = 2$) driven by 3 cables, $\mathbf{A}_{\mathrm{t}}$ will be 6×7, whereas $\mathbf{A}_{\mathrm{L}}$ is a 2×3 which is much preferred for computational purposes.

4.2 Boundaries of the Tensionable Workspace

4.2.1 Methods for Checking Tensionability

As discussed in the previous chapter, a rigid body cable-driven mechanism is tensionable if and only if the following conditions are satisfied:

1. The structure matrix is full-rank, <u>and</u>
2. There is a vector in the null space of the structure matrix such that all of its components are of the same sign.

The second condition requires the null space of **A** to be analyzed which may become cumbersome, especially when the number of redundant cables is more than one (multi-dimensional null space). An alternative approach which has attracted a lot of attention is using the concept of supporting and separating hyperplanes [36,53]. Let us consider a matrix such as $\mathbf{\Pi}$ with its columns $\boldsymbol{\pi}_i$:

$$\mathbf{\Pi}_{n\times m} = \begin{bmatrix}\boldsymbol{\pi}_1 & \boldsymbol{\pi}_2 & \dots & \boldsymbol{\pi}_m\end{bmatrix} \tag{4.13}$$

A *separating hyperplane H* for $\mathbf{\Pi}$ is a hyperplane in the n-dimensional span of $\mathbf{\Pi}$ passing through the origin and having at least one of vectors $\boldsymbol{\pi}_i$ (i=1,2,…, m) on each side. Mathematically, for a separating hyperplane with normal vector $\mathbf{h}$, there exists two vectors $\boldsymbol{\pi}_j$ and $\boldsymbol{\pi}_k$ where $\boldsymbol{\pi}_j.\mathbf{h} > 0$ and $\boldsymbol{\pi}_k.\mathbf{h} < 0$. A hyperplane which passes through the origin and is not a separating hyperplane is a *supporting hyperplane*.

For analysis of tensionability, the following theorem provides the conditions in terms of separating and supporting hyperplanes [36]:

Theorem 4.1. A cable-driven rigid body system is tensionable if and only if all hyperplanes passing through the origin are separating hyperplanes for the structure matrix **A**.

For tensionability investigation using Theorem 1, an infinite number of hyperplanes are required to be assessed. Since this is not practical, a refinement of Theorem 1 has been proposed as follows [36]:

Theorem 4.2. A cable-driven rigid body system is tensionable if and only if all of the hyperplanes passing through the origin and spanned by $n - 1$ linearly independent columns of **A** are separating hyperplanes.

Using Theorem 4.2, one can analyze the tensionability of a system by investigating a limited number of hyperplanes. Each of these hyperplanes is generated by a selection of $n-1$ linearly independent columns from matrix **A**. As a result, there are $\binom{m}{n-1}$ such hyperplanes to check. If (and only if) they are all separating planes, then the mechanism is tensionable.

In the previous chapter the study of the tensionability of the multibodies was based on a Newtonian structure matrix. This was due to the fact that the constraints would affect the analysis of cable numbers. However, for checking tensionability at a given pose of the mechanism, there is no need for the constraint wrenches, and as a result of the above discussions, using Lagrange's formulation is preferred. Note that by use of this approach all of the constraint wrenches are eliminated from the formulation and only the cable wrenches will be present. Thus the analysis of the system will become essentially the same as an unconstrained rigid body; i.e. a rigid body in the space of the generalized coordinates [56].

Now, using Eqs. (4.10) to (4.12), one can determine whether a given configuration of a cable-driven multibody system is tensionable. This can be performed either using the concept of null space or supporting/separating hyperplanes. However, it is usually desired to obtain a description of the whole tensionable workspace. For instance, in design or operation of such systems, knowing the boundaries of the tensionable workspace is critical to make sure the task requirements can be met. The most available solution would be to search the whole configuration space for tensionable points. This can be done by either discretization of the space which compromises the accuracy or using the interval analysis method which is computationally intensive.

Another method is to determine the boundaries of the tensionable workspace and investigate the regions surrounded by these boundaries. In the followings, the boundaries of the tensionable workspace are found based on the formulation given in section 4.1.

4.2.2 One Redundant Cable – Null Space Approach

The solution of Eq. (4.12), similar to rigid body case, is:

$$\boldsymbol{\tau}_{\mathrm{L}} = \mathbf{A}_{\mathrm{L}}^{+}\mathbf{b}_{\mathrm{L}} + \mathbf{n}_{\mathrm{A}} \tag{4.14}$$

where $\mathbf{A}_{\mathrm{L}}^{+}$ is the pseudo-inverse of $\mathbf{A}_{\mathrm{L}}$ and $\mathbf{n}_{\mathrm{A}}$ is a vector in the kernel of $\mathbf{A}_{\mathrm{L}}$.

By a similar argument as the one discussed in the previous chapter, one can conclude that the multibody is tensionable if and only if:

1. $\mathbf{A}_{\mathrm{L}}$ is full rank (rank condition),
2. There is a vector in the null space of $\mathbf{A}_{\mathrm{L}}$ with all of its components of the same sign (null space condition).

Note that for a full rank $\mathbf{A}_{\mathrm{L}}$, the dimension of the null space is $\overline{m} - n_{\mathrm{DoF}}$ which is the number of the redundant cables. In case of one redundant cable ($\overline{m} - n_{\mathrm{DoF}} = 1$), the null space of $\mathbf{A}_{\mathrm{L}}$ is one-dimensional and spanned by a single vector such as $\mathbf{n}_{\mathbf{A}}$. This vector can be analytically found and used to determine the boundaries of the tensionable workspace. In order to find $\mathbf{n}_{\mathrm{A}}$, first let $\mathbf{d}_i$ be the i^{th} column of $\mathbf{A}_{\mathrm{L}}$ which is the column that pertains to the i^{th} cable. As a result, we have:

$$\mathbf{A}_{\mathrm{L}} = \begin{bmatrix} \mathbf{d}_1 & \ldots & \mathbf{d}_{n_{\mathrm{DoF}}+1} \end{bmatrix} \tag{4.15}$$

Now let matrix $\mathbf{S}$ be formed by the first n_{DoF} columns of $\mathbf{A}_{\mathrm{L}}$:

$$\mathbf{S} = \begin{bmatrix} \mathbf{d}_1 & \ldots & \mathbf{d}_{n_{\mathrm{DoF}}} \end{bmatrix} \tag{4.16}$$

For a full rank $\mathbf{A}_{\mathrm{L}}$, one can assume $\mathbf{S}$ to be full rank too (it may only require changing the orders of columns in $\mathbf{A}_{\mathrm{L}}$). Therefore, it will be easy to show that $\mathbf{n}_{\mathrm{L}}$, as defined below, spans the null space of $\mathbf{A}_{\mathrm{L}}$:

$$\mathbf{n}_{\mathrm{L}} = \begin{bmatrix} -\mathbf{S}^{-1}\mathbf{d}_{n_{DoF}+1} \\ 1 \end{bmatrix} = \begin{bmatrix} -\dfrac{1}{|\mathbf{S}|}\mathbf{S}^{*}\mathbf{d}_{n_{DoF}+1} \\ 1 \end{bmatrix} \tag{4.17}$$

where $\mathbf{S}^{*}$ is the adjoint matrix of $\mathbf{S}$.

In case of a singular $\mathbf{S}$ (i.e. $\mathbf{A}_{\mathrm{L}}$ is not full-rank), the definition of $\mathbf{n}_{\mathrm{L}}$ given in Eq. (4.17) will involve a division-by-zero. In order to avoid this, one can consider a scaled version of $\mathbf{n}_{\mathrm{L}}$, named $\mathbf{n}_{\mathbf{A}}$, as:

$$\mathbf{n}_{\mathbf{A}} = \begin{bmatrix} -\mathbf{S}^{*}\mathbf{d}_{n_{DoF}+1} \\ |\mathbf{S}| \end{bmatrix} \tag{4.18}$$

in which, as long as the elements of **S** are finite, there will be no chance of singularity.

In order to find the boundaries of the tensionable workspace, the two conditions (rank and null space) are revisited here. The null space condition states that all components of the spanning vector of the null space, as given in Eq. (4.18), should be of the same sign. Since the components of $\mathbf{n}_{\mathbf{A}}$ are continuous functions of the generalized coordinates, a sign change occurs if and only if one of the components becomes zero. Therefore, the boundaries of the regions that satisfy the null space condition is determined by solving for the roots of each component of $\mathbf{n}_{\mathbf{A}}$:

$$n_{A,i} = 0\,,\ i = 1,\ldots,n_{\mathrm{DoF}} + 1 \tag{4.19}$$

where $n_{A,i}$ is the i^{th} component of $\mathbf{n}_{\mathbf{A}}$ and a function of the generalized coordinates. Therefore, Eq. (4.19) results in a set of hypersurfaces in the generalized coordinate space. Each hypersurface divides the space into two regions with different signs for a particular component of $\mathbf{n}_{\mathbf{A}}$. On each hypersurface, the corresponding component of the null space vector is zero. This is an extension of the method proposed in [45], [46], and [53] for finding workspace of constant-orientation rigid bodies driven by cables.

For the first condition of tensionability, note that if $\mathbf{A}_{\mathrm{L}}$ is rank deficient, then $|\mathbf{S}|= 0$. From Eq. (4.18) since $|\mathbf{S}|$ is the last component of $\mathbf{n}_{\mathbf{A}}$, one can notice that in such a case, at least one component of $\mathbf{n}_{\mathbf{A}}$ must be zero. Therefore, the first condition of tensionability may be violated only on the boundaries of the regions found for the null space condition in Eq. (4.19). As a result, the inside of the regions -where all the components of $\mathbf{n}_{\mathbf{A}}$ are nonzero- satisfy the first condition as well. Therefore, if in a region surrounded by the abovementioned hypersurfaces the components of the null space vector are all of the same sign, the region will be a region of tensionability. This is, as mentioned before, due to the fact that the first tensionability condition can only be violated on the boundaries of a region and not inside of it. Furthermore, note that since the signs of the components of the null space vector do not change inside a region, it is sufficient to check the sign of only one of the points in a region; all of the other points in that region will have the same sign.

4.2.3 Multiple Redundant Cables

With more than one redundant cable, the null space of $\mathbf{A}_{\mathrm{L}}$ will be multi-dimensional. This complicates the assessment of the null space condition. Alternatively, the method of supporting/separating planes can be used as detailed here.

As mentioned in Theorem 2, the necessary and sufficient condition for tensionability is that all of the hyperplanes formed by $n_{\mathrm{DoF}} - 1$ columns of $\mathbf{A}_{\mathrm{L}}$ be separating hyperplanes. This can be easily applied to determine whether a given configuration of a multibody cable-driven mechanism is tensionable. However, it is much preferred to have a description of the tensionable workspace boundaries. This is detailed in the following.

In the notion of separating/supporting hyperplanes, a configuration of the mechanism is on the boundary of the tensionable workspace if and only if a separating hyperplane is on the verge of becoming a supporting one. Remember that as long as there is at least one column of $\mathbf{A}_{\mathrm{L}}$ on each side of a hyperplane, it is still a separating one. Therefore, in view of Theorem 2, at a boundary configuration, there will be a hyperplane with at least n columns of $\mathbf{A}_{\mathrm{L}}$ on it ($n_{\mathrm{DoF}}-1$ columns that form the hyperplane plus at least one extra column lying on it) and all other columns on one side. This can be used to detect the configurations of the mechanism that are on the boundary of the tensionable workspace. Such configurations will satisfy the following two conditions:

1. There is a set of n_{DoF} columns in $\mathbf{A}_{\mathrm{L}}$ with a rank of $n_{\mathrm{DoF}} - 1$, <u>and</u>
2. The hyperplane formed by these columns is a supporting hyperplane.

Note that each of the two above items is a necessary condition for a boundary configuration. Therefore, one way to identify these boundaries is to determine all hypersurfaces in the generalized coordinate space that satisfy the first condition and then identify those that satisfy the second one too. Let us consider $\mathbf{A}_{\mathrm{L}}$ with its columns:

$$\mathbf{A}_{\mathrm{L}} = \begin{bmatrix} \mathbf{d}_1 & \mathbf{d}_2 & \dots & \mathbf{d}_{\overline{m}} \end{bmatrix} \tag{4.20}$$

and let

$$\{c_{i,1},\dots,c_{i,n_{\mathrm{DoF}}}\},\ i = 1,\dots,\binom{\overline{m}}{n_{\mathrm{DoF}}} \tag{4.21}$$

be an n_{DoF}-combination of $\{1,2,\dots,\overline{m}\}$. Now the following hypersurfaces indicate the configurations where there is a set of n_{DoF} linearly dependent columns in $\mathbf{A}_{\mathrm{L}}$:

$$\det\left(\begin{bmatrix}\mathbf{d}_{c_{i,1}} & \dots & \mathbf{d}_{c_{i,n_{\mathrm{DoF}}}}\end{bmatrix}\right)=0\ ,\ \ i=1,\dots,\binom{\overline{m}}{n_{\mathrm{DoF}}} \tag{4.22}$$

From these hypersurfaces, only those that pertain to a supporting hyperplane determine the boundaries of the tensionable regions. Note that in some of the hypersurfaces of Eq. (4.22), the corresponding columns of $\mathbf{A}_{\mathrm{L}}$ may not be of rank $n_{\mathrm{DoF}}-1$ and hence do not form any hyperplane. Also, in some cases, the hyperplane may still be a separating one. Therefore, from the hypersurfaces obtained from Eq. (4.22), only the ones that satisfy both conditions of the boundary configurations should be identified which form the tensionable regions of the workspace. Also note that for a particular hypersurface, the conditions mentioned above must be examined for every single point on that hypersurface. In other words, only some sections of a hypersurface might be part of the boundary of the tensionable workspace.

The approach of separating/supporting hyperplanes is also applicable to the special case of one redundant cable. Note than in such case ($\overline{m}=n_{\mathrm{DoF}}+1$), the number of equations that should be solved from Eq. (4.22) is:

$$\binom{\overline{m}}{n_{\mathrm{DoF}}}=\binom{n_{\mathrm{DoF}}+1}{n_{\mathrm{DoF}}}=n_{\mathrm{DoF}}+1 \tag{4.23}$$

This corresponds to $n_{\mathrm{DoF}}+1$ equations for the roots of the null space vector components discussed in the previous section (Eq. (4.19)). However, in the hyperplane method the number of determinants to be evaluated (in Eq. (4.22)) is $\binom{\overline{m}}{n_{\mathrm{DoF}}}=n_{\mathrm{DoF}}+1$; whereas in the null space method there is only one determinant ($|\mathbf{S}|$ in Eq. (4.18)) for evaluation and the other equations are obtained by matrix multiplication (i.e. $-\mathbf{S}^{*}\mathbf{d}_{n_{\mathrm{DoF}}+1}$). This shows that the null space method is advantageous in terms of the cost of computation. Hence for the one redundant cable case this method has been selected in this work.

In the followings case studies, the tensionable workspaces of one- and two-DoF multibody systems driven by cables with different arrangements of cables are analyzed. The boundaries of the tensionable workspace are determined by analyzing the null space vector for one redundant cable and hyperplanes for two redundant cables, and some design guidelines are obtained. We start with a 1-DoF planar system and then extend to a 2-DoF mechanism. Note that in multibody cable-driven mechanisms, both the number of cables and their distribution among the links of the mechanism affect the boundaries of the tensionable workspace. Therefore, we have examined two possible cable distributions for the 2-DoF mechanism with one redundant cable. Moreover, the method is applied to a two-redundant-cable mechanism and its tensionable workspace is compared with one-redundant-cable mechanisms.

4.3 Case Studies

4.3.1 Tensionable Workspace of a 1-DoF Cable-Driven System

We start with a simple mechanism shown in Figure 4-2, which is a 1-DoF planar mechanism. In this mechanism, a rigid body is connected to the ground by a revolute joint and is being driven by two cables. For simplicity and reducing the number of parameters, the cables are assumed to be attached along the central line of the rigid body (the line connecting the joint and the center of mass). Note that the extension to general case can be done by adding a constant parameter indicating the connection position of each cable with respect to the central line and it does not affect the concepts discussed in the following.

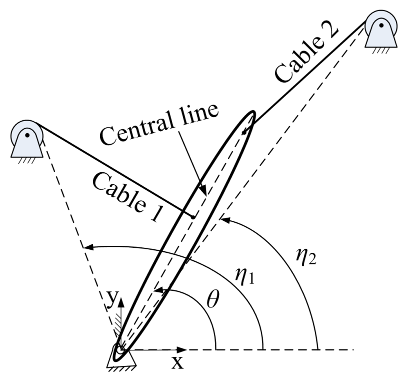

Figure 4-2. A schematic of a 1-DoF rigid body driven by two cables

According to Eq. (4.10) $\mathbf{A}_{\mathrm{L}}$ is 1×2:

$$\mathbf{A}_{\mathrm{L}} = \begin{bmatrix} -(x_1 - d_1\cos\theta)d_1\sin\theta + (y_1 - d_1\sin\theta)d_1\cos\theta \\ -(x_2 - d_2\cos\theta)d_2\sin\theta + (y_2 - d_2\sin\theta)d_2\cos\theta \end{bmatrix}^T \qquad (4.24)$$

where x_i, and y_i are the coordinates of the i^{th} winch, and d_i is the distance of the point of connection of the i^{th} cable to the body from the joint (origin). Then the null space spanning vector will be found from Eq. (4.18):

$$\mathbf{n}_{\mathbf{A}} = \begin{bmatrix} (x_2 - d_2\cos\theta)d_2\sin\theta - (y_2 - d_2\sin\theta)d_2\cos\theta \\ -(x_1 - d_1\cos\theta)d_1\sin\theta + (y_1 - d_1\sin\theta)d_1\cos\theta \end{bmatrix} \tag{4.25}$$

And by setting the components of $\mathbf{n}_A$ equal to zero, one obtains the following curves:

$$\begin{cases} (x_2 - d_2\cos\theta)d_2\sin\theta - (y_2 - d_2\sin\theta)d_2\cos\theta = 0 \\ -(x_1 - d_1\cos\theta)d_1\sin\theta + (y_1 - d_1\sin\theta)d_1\cos\theta = 0 \end{cases} \tag{4.26}$$

The mechanism is tensionable if and only if the left-hand-side of both equations are nonzero and of the same sign. From this, it is easy to conclude that this will be satisfied either if:

$$y_1\cos\theta - x_1\sin\theta > 0 \;\text{ and }\; y_2\cos\theta - x_2\sin\theta < 0 \tag{4.27}$$

or

$$y_1\cos\theta - x_1\sin\theta < 0 \;\text{ and }\; y_2\cos\theta - x_2\sin\theta > 0 \tag{4.28}$$

The geometrical interpretation of the above inequalities is that the cables are required to be in two different sides of the link, which was intuitively known due to the simplicity of the mechanism. The boundaries of the tensionable workspace can be also expressed from Eqs. (4.27) and (4.28) as $\tan\theta = y_1/x_1 = \tan\eta_1$ and $\tan\theta = y_2/x_2 = \tan\eta_2$, which indicate the points at which one of the cables and the link are aligned.

4.3.2 Tensionable Workspace of a 2-DoF Planar Multibody System with {1,2} Cable Distribution

Figures 4.3 and 4.4 depict a schematic of a two-link multibody system. It is a planar double pendulum driven by three cables as shown in the figure. It can be shown that there are two possible distributions for the cables in such a multibody system: {1,2} and {0,3}. The first one is shown in Figures 4.3 and 4.4, and is considered here.

Since the mechanism has 2 DoF and three cables, $\mathbf{A}_L$ will be 2×3. The null space of $\mathbf{A}_L$ is spanned by the vector $(\mathbf{n}_A)_{3\times1}$ which can be found symbolically using Eq. (4.18) in terms of the joint variables, θ_1 and θ_2:

$$(\mathbf{n}_{\mathbf{A}})_{3\times1} = \begin{bmatrix} n_{A,1}(\theta_1,\theta_2) & n_{A,2}(\theta_1,\theta_2) & n_{A,3}(\theta_1,\theta_2) \end{bmatrix}^T \tag{4.29}$$

Finding the roots of each component of the null space vector provides three equations:

$$n_{A,i}(\theta_1,\theta_2) = 0,\; i = 1,2,3 \tag{4.30}$$

Note that the equations presented in Eq. (4.30) are nonlinear and therefore may have multiple solutions. For instance, in the present case, the three equations of Eq. (4.30) result in four curves in the plane of θ_1 and θ_2. The first one can be expressed as:

$$\theta_2 = \tan^{-1}\left(\frac{y_3 - l_1 \sin\theta_1}{x_3 - l_1 \cos\theta_1}\right) \pm k\pi = \eta_3 \pm k\pi \tag{4.31}$$

where l_1 is the length of link 1. Note that Eq. (4.31) is a set of curves separated by a multiple of π. On each of these curves the second component of the null space, $n_2(\theta_1,\theta_2)$, becomes zero. Also, the sign of this component changes as one crosses these curves. Similarly, the first and third sets of curves can be expressed as:

$$\theta_2 = \tan^{-1}\left(\frac{y_2 - l_1 \sin\theta_1}{x_2 - l_1 \cos\theta_1}\right) \pm k\pi = \eta_2 \pm k\pi \tag{4.32}$$

and:

$$\theta_2 = \tan^{-1}\left(\frac{y_1}{x_1}\right) \pm k\pi = \eta_1 \pm k\pi \tag{4.33}$$

The fourth set of curves is also periodic (as the other three ones). However, its symbolic expression is too long and hence is not presented here[1].

The third set of curves (Eq. (4.33)) occurs when cable 1 becomes aligned with link 1. Similar to the 1-DoF mechanism, at such configurations, the cable cannot apply any moment to link 1 (generally cable 1 can only apply moment to link 1) and as a result, the first column of $\mathbf{A}_L$ becomes zero. Thus in this case: $n_{A,2}(\theta_1,\theta_2) = n_{A,3}(\theta_1,\theta_2) = 0$.

The first two sets of curves given by Eqs. (4.31) and (4.32) represent conditions where one of the cables 1 or 2 becomes aligned with link 2. Therefore they will not be able to apply moment to link 2. Hence they become linearly dependent with column 1. Mathematically, in these cases, the second component of column 2 or 3 (for Eq. (4.32) or (4.31), respectively) becomes zero. Thus: $n_{A,3}(\theta_1,\theta_2) = 0$ or $n_{A,2}(\theta_1,\theta_2) = 0$.

Finally, the fourth set of curves comes from the dependency between columns 2 and 3 which corresponds to $n_{A,1}(\theta_1,\theta_2) = 0$.

All curves are shown in Figure 4-5. For this purpose, some typical values were used for the parameters of the mechanisms as shown in Table 4-1.

[1]. The expression can be provided upon request.

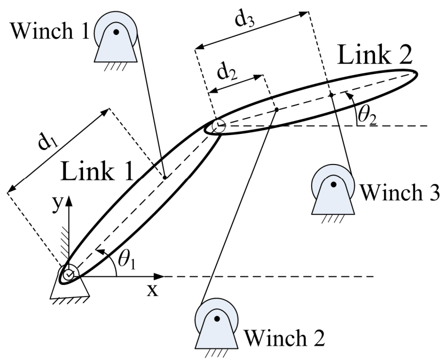

Figure 4-3. Schematic of a 2-DoF 2-link multibody system driven by three cables having {1,2} distribution

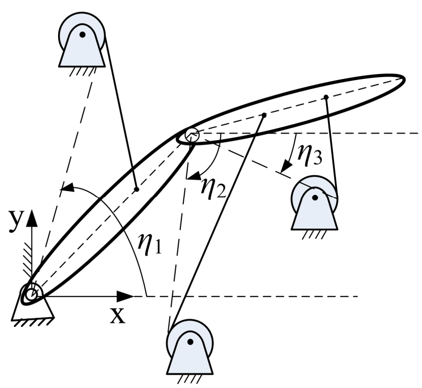

Figure 4-4. The angular positions of the winches of the system of Figure 4-3

Table 4-1. Parameter values for the 2-link mechanism (all in meters)

Length of link 1	d_1	d_2	d_3	Location of winch 1	Location of winch 2	Location of winch 3
1	0.6	0.3	0.8	[1.2,5.6]	[3.2,–0.8]	[5.1,4.3]

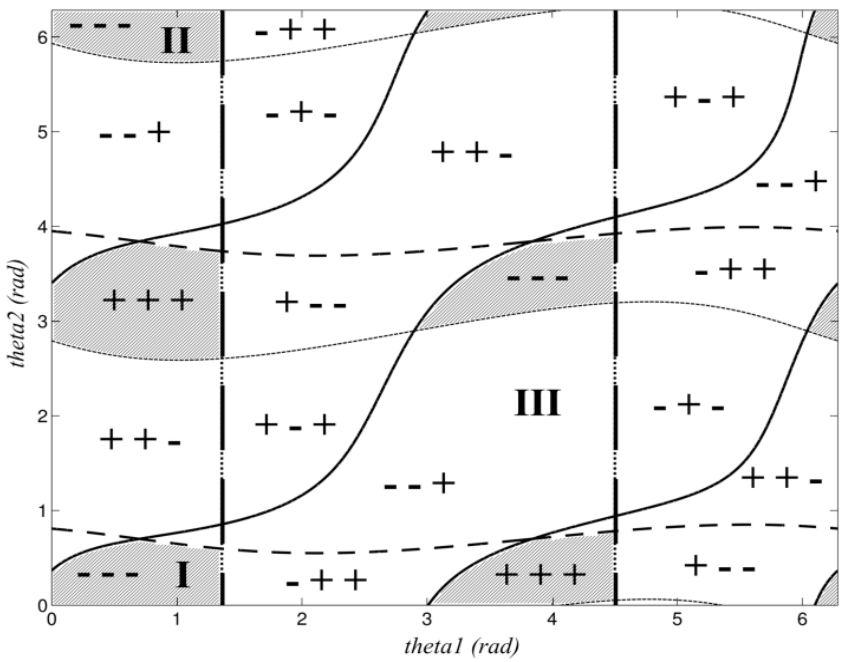

Figure 4-5. Regions of configuration space for a two-link mechanism with {1,2} cable distribution:

Curve set 1: - - - - - - - Curve set 2: ....

Curve set 3: —··—··— Curve set 4: ————

These curves have partitioned the configuration space into several regions. As shown before, as long as the configuration of the robot falls inside any of these regions, $\mathbf{A}_L$ is full rank which satisfies the first condition of tensionability. The signs of the components of $\mathbf{n}_A$ are also shown for each region in Figure 4-5 by a string of pluses and minuses, respectively. For instance, + – + indicates that the first and the last components of $\mathbf{n}_A$ are positive while the second one is negative.

From this figure one can distinguish nine separate regions in which the components of the null space vector have the same sign and the system is tensionable. However, since the angular coordinates are periodic, some of these regions are in fact connected. For example, regions I and II are two parts of the same region. From this argument, the nine abovementioned regions will form four continuous regions which are shown by a darker pattern in the same figure. It is noteworthy that the tensionable workspace of such mechanism is not connected. As a result, one cannot move the mechanism from one tensionable configuration to any other one along a tensionable path. Also it is seen from Figure 4-5 that the tensionable regions are not necessarily convex. Therefore, if two configurations are tensionable, one cannot expect that any configuration in between the two will be tensionable as well.

4.3.3 Improving the Tensionable Workspace

In section 3.2 it was shown that changing the sign of a null space component (say $n_{A,i}$) is possible by changing the sign of the corresponding column of the structure matrix via relocating the winches. As a result of this, any point in the workspace can be changed into a tensionable one as long as the cable directions can be reversed. In other words, one can choose a region of interest from Figure 4-5 and change it to a tensionable region by relocating the appropriate winches.

As an example, suppose that region III from Figure 4-5 is the range in which the system is required to be tensionable. Since the components of the null space are of different signs, currently the system is not tensionable in this region. From the above discussion one can notice that the third cable can be reversed in order to make this region tensionable. Note that the method for relocating winches and changing the sign of the corresponding null space component is valid only for one point in the workspace. As Figure 4-6 shows, as mechanism moves from (θ_1,θ_2) to (θ'_1,θ'_2), the relocated winch is not at the exact symmetrically inverted point along cable 3, and as a result, the boundaries of the tensionable workspace change. However, since normally the cable lengths (i.e. the distance of winches from the multibody) are much larger than the size of the multibody, one can expect that the changes are not significant. Thereby, it is reasonable to relocate the winch at a point in the middle of this region to have minimum change in the boundaries.

From the above argument we relocate winch 3 at $(\theta_1, \theta_2) = (\pi, \pi/2)$, which is a point in the middle of this region. This results in the new location of (-7.1,-2.7) for winch 3. The new tensionable workspace plot is depicted in Figure 4-7. Compared with Figure 4-5, it is observed that although the boundaries are different, the change is not considerable and still the similarity of the two workspaces is easily noticed. Note that this relocation makes five other regions tensionable as well, and the currently tensionable regions change to untensionable regions. The new tensionable regions are hatched.

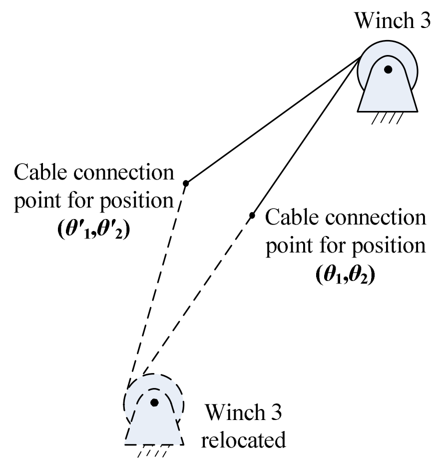

Figure 4-6. Cable 3 at positions (θ_1,θ_2) and (θ'_1,θ'_2), as winch 3 is relocated with respect to the connection point at (θ_1,θ_2)

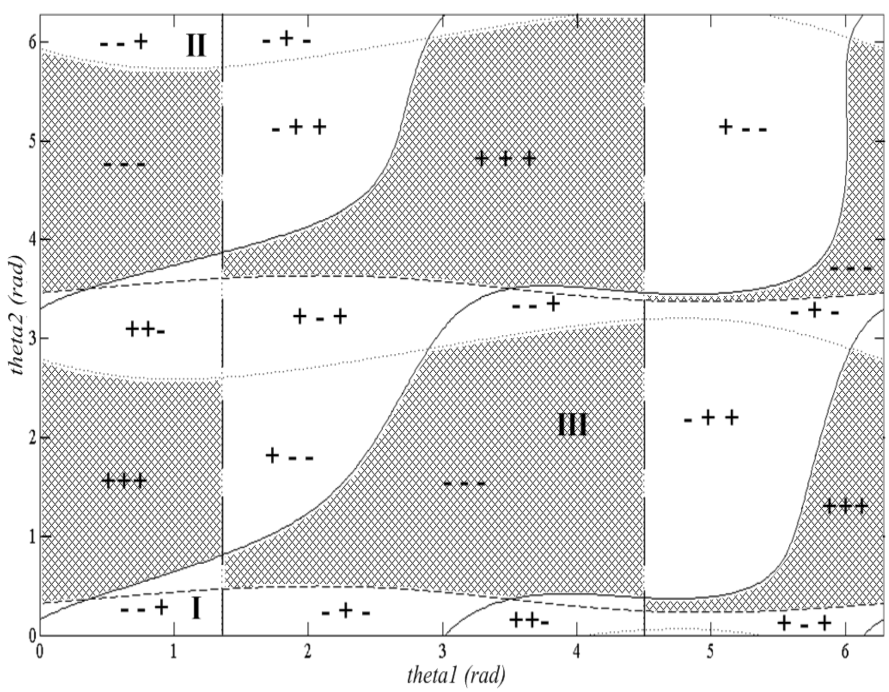

Figure 4-7. Regions of configuration space for the {1,2} cable distribution and relocated winch 3

Curve set 1: ‒ ‒ ‒ ‒ ‒ ‒ ‒ ‒ Curve set 2: ....
Curve set 3: ‒ · · ‒ · · ‒ · Curve set 4: ————————

4.3.4 Tensionable Workspace of a Two-Link Planar Multibody System with {0,3} Cable Distribution

As mentioned before, multiple distributions of cables may exist for driving a multibody system. For instance, the two-link mechanism of the previous section can be also driven by all three cables attached to the second link as shown in Figure 4-8. Figure 4-9 depicts the configuration space and the regions for this mechanism which is obtained by following the null space method similar to the previous section. However, the main difference here is that there are only three sets of curves (instead of four) to determine the boundaries of the regions.

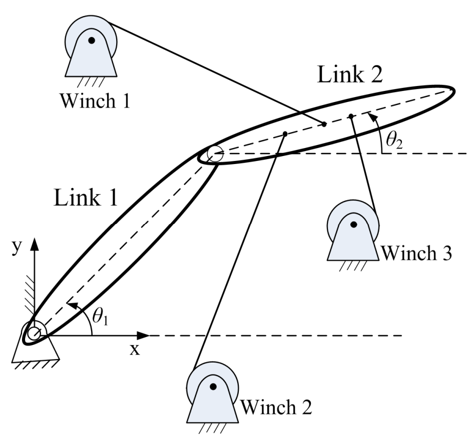

Figure 4-8. Schematic of a 2-DoF 2-link multibody system driven by three cables having the distribution {0,3}

According to Figure 4-9, for these particular numeric values (Table 4-1), most of the boundary curves correspond to the situations where two links are more or less inline. In other words, when the two links are far from being inline, none of the curves is crossed. This has left relatively larger empty regions in between the curves (as numbered I, II, III and IV) which are not tensionable in the current configuration. However, as discussed before, note that one can still change the signs of the null space components by relocating the winches. For example, by reversing the direction of the 3rd cable, one can make regions I, II, III, and IV tensionable. The resultant mechanism is shown in Figure 4-10. It is interesting to note that this significant improvement of the tensionable workspace is not intuitively apparent from Figure 4-8; i.e. the configuration of the cables (unlike rigid bodies) do not easily show whether the system is tensionable.

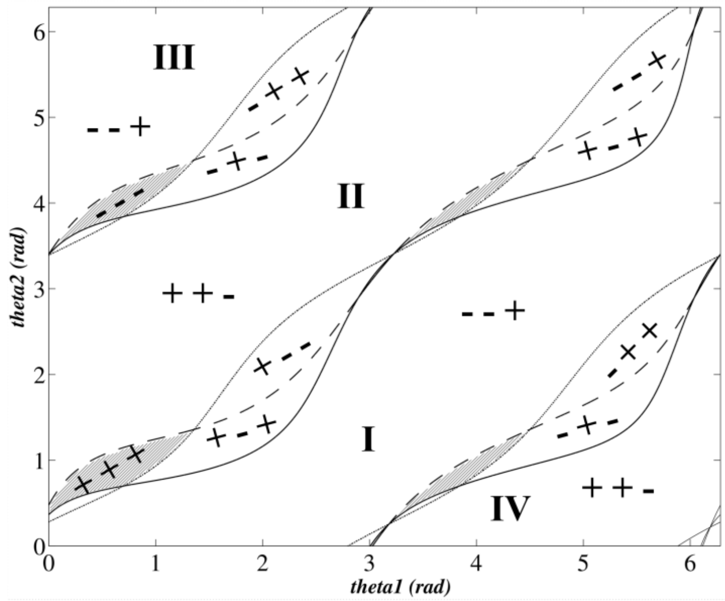

Figure 4-9. Workspace analysis of a two-link mechanism driven by three cables attached to the second link
Curve set 1: ———— Curve set 2: - - - - - -
Curve set 3: ·····················

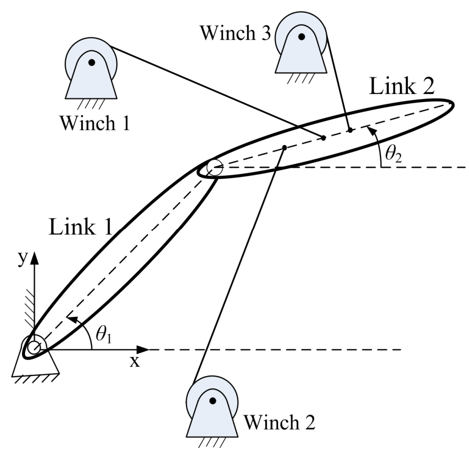

Figure 4-10. The modified design for {0,3} cable distribution

4.3.5 Tensionable Workspace of a Two-Link Planar Multibody System with Multiple Redundant Cables

The same mechanism is considered again using two redundant cables (total of 4 cables). Figure 4-11 shows a schematic for this example.

The fourth winch is located at [–2,–9], and $d_4 = 0.5$.

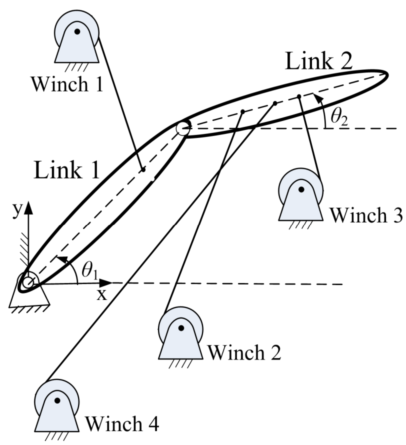

Figure 4-11. Schematic of a 2-DoF 2-link multibody system driven by four cables having the distribution {1,3}

In this case, there are two redundant cables. Thus the null space is two-dimensional and, as mentioned before, the use of the hyperplane method is preferred. The number of the equations required to be solved for this system (Eq. (4.22)) is $\binom{4}{2} = 6$. Solving these equations, the candidate hypersurfaces (which are curves in this 2-D system) are obtained. Since there will be too many curves in this case, for the sake of clarity, the curves which are not the boundary of the tensionable workspace are eliminated. For this purpose, the second condition of the separating/supporting hyperplanes method, explained in section 4.2.3 is applied. According to this condition, when a set of n_{DoF} columns of $\mathbf{A}_{\mathrm{L}}$ becomes linearly dependent, the hyperplane defined by those columns can be separating or supporting. Thus, in the next step the points where the abovementioned hyperplane is a supporting hyperplane (and not a separating one) are detected. Such points are on the boundary of the tensionable workspace.

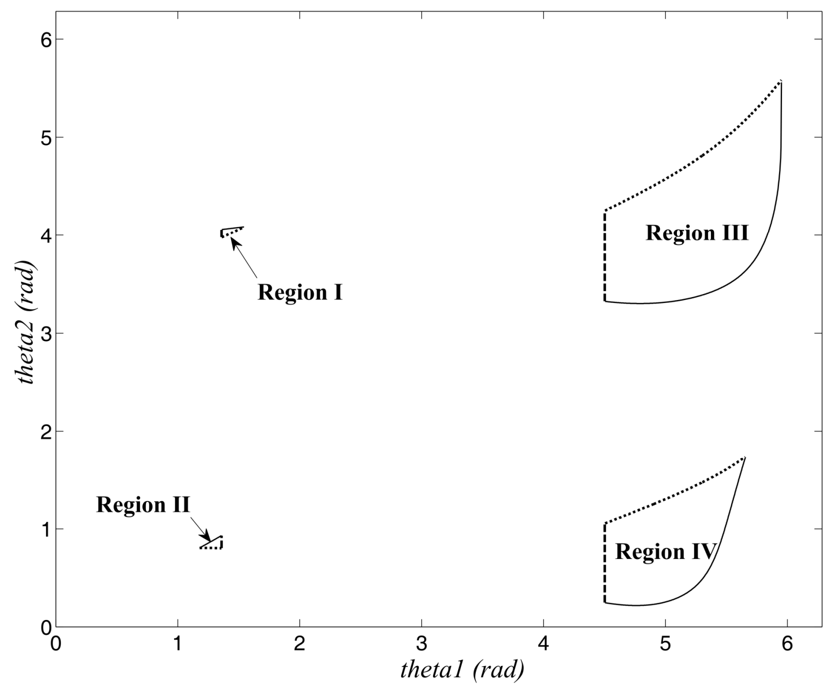

Figure 4-12. Workspace analysis of a two-link mechanism driven by the distribution {1,3}

Curve set 1: ——— Curve set 2: – – – –

Curve set 3: ············

The results of the tensionable workspace analysis are shown in Figure 4-12, which can be compared with Figures 4-5, 4-7, and 4-9 which are primarily the same mechanisms but with one less cable[1]. It is interesting to observe that by adding one cable, the majority of the reachable workspace has become tensionable. Only four relatively small regions (named as regions I-IV) are not tensionable, which compared to the previous mechanism demonstrates a significant improvement.

Although the given formulation for the boundaries of the tensionable workspace obtained using this formulation are valid for any DoF, the examples are limited to two-DoF multibody systems. The reason is that for such systems the two-dimensional tensionable space can be conveniently presented graphically. For systems of higher DoF, either some degrees of freedom of the system should be fixed (for example a "constant orientation" planar rigid

[1]. Compared with the {1,2} design, the extra cable of this case has been attached to link 2, and compared with {0,3} design, the extra cables has been attached to link 1.

body as in [45]), or numeric analyses should be used to determine the subsections of the tensionable workspace formed by the obtained boundaries.

4.4 Workspace Analysis of the Designed Arm Mechanism

Figure 4-13 depicts a schematic of the designed arm, which was discussed in section 2.3.

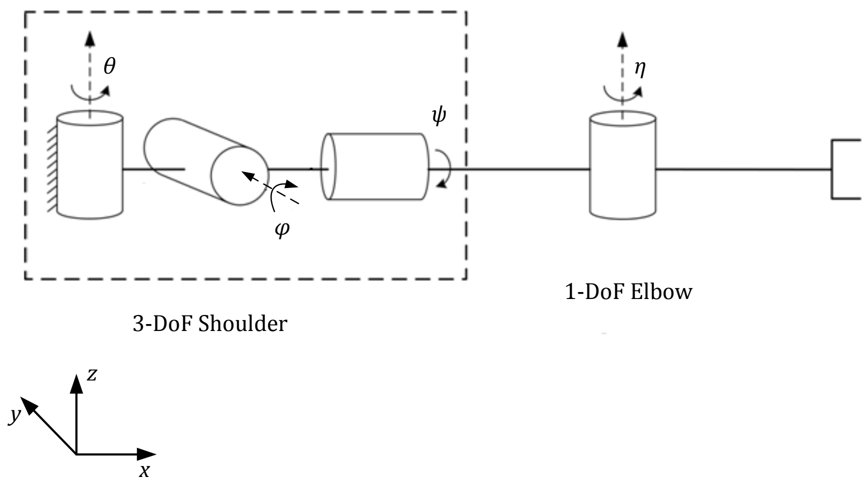

Figure 4-13. Schematic of the designed arm

As can be seen in the figure, θ, φ, ψ, and η are the four generalized coordinates considered for this system. For the first link, taking θ, φ, and ψ as Euler angles, one can write the corresponding rotation matrices as:

$$\mathbf{R}_\theta = \begin{bmatrix} \cos\theta & -\sin\theta & 0 \\ \sin\theta & \cos\theta & 0 \\ 0 & 0 & 1 \end{bmatrix} \tag{4.34}$$

$$\mathbf{R}_\varphi = \begin{bmatrix} \cos\varphi & 0 & \sin\varphi \\ 0 & 1 & 0 \\ -\sin\varphi & 0 & \cos\varphi \end{bmatrix} \tag{4.35}$$

$$\mathbf{R}_\psi = \begin{bmatrix} 1 & 0 & 0 \\ 0 & \cos\psi & -\sin\psi \\ 0 & \sin\psi & \cos\psi \end{bmatrix} \tag{4.36}$$

Thus for a point on the arm initially at:

$$\mathbf{r}_{0,1} = [d_{a,1} \quad p_a \cos\sigma \quad p_a \sin\sigma]^{\mathrm{T}} \tag{4.37}$$

where $d_{a,1}$ is the distance of the point from yz plane and p_a and σ are polar coordinates of the point at that section of the arm. Subscript ",1" means that the point belongs to link 1, i.e. the upper arm. The coordinates of the point with respect to the fixed frame (with origin at the center of the spherical joint) after these three rotations will be:

$$\mathbf{r}_{j,1} = \mathbf{R}_\theta \mathbf{R}_\varphi \mathbf{R}_\psi \mathbf{r}_{0,1} \tag{4.38}$$

This is the general description of a point on link 1, subject to the three rotations by Euler angles. Since this point can also be a connection point of a cable, it can be used for calculation of the Lagrangian structure matrix of Eq. (4.10).

For the second link, one can write the rotation of elbow joint as:

$$\mathbf{R}_\eta = \begin{bmatrix} \cos\eta & -\sin\eta & 0 \\ \sin\eta & \cos\eta & 0 \\ 0 & 0 & 1 \end{bmatrix} \tag{4.39}$$

Then for a point initially at:

$$\mathbf{r}_{0,2} = [d_{a,2} \quad p_a \cos\sigma \quad p_a \sin\sigma]^{\mathrm{T}} \tag{4.40}$$

where $d_{a,2}$ is the normal distance of the center of the section of the arm containing the point from the elbow joint, the final position is obtained as:

$$\mathbf{r}_{j,2} = \mathbf{R}_\theta \mathbf{R}_\varphi \mathbf{R}_\psi \left(\mathbf{R}_\eta \mathbf{r}_{0,2} + \begin{bmatrix} l_{a,1} \\ 0 \\ 0 \end{bmatrix} \right) \tag{4.41}$$

where $l_{a,1}$ is the length of the first link.

Using Eqs. (4.38), (4.41), and (4.10) one can obtain the Lagrangian structure matrix of the multibody cable-driven robot. The numeric values of the parameters required for numerically obtaining the structure matrix have been listed in Table 4-2. The length of the first link, $l_{a,1}$ is 372.4 mm. As mentioned before, the distribution considered is $\{3,2\}$. For the procedure of selecting the locations of the winches and the cable connection points see [29].

Using these parameters, $\mathbf{A}_{\mathrm{L}}$ can be obtained as a function of the generalized coordinates. Next, using the methods suggested for workspace analysis of the multibody cable-driven robots, one can obtain the analytical expressions of the boundaries of the tensionable workspace. Due to complexity of the expressions, the boundaries were obtained using Maple®.

For representation of the tensionable workspace, since the system is 4-D, it is impossible to depict it in all of the system's DoF at once. Therefore, the two dimensional plots of the workspace were generated by assuming the other two generalized coordinates (angles) are fixed at zero. Thereby six workspace plots are obtained, which have been depicted in Figures 4-14 to 4-19, in which the tensionable regions have been highlighted by numbers. The method used is separating/supporting hyperplanes, and similar to Figure 4-12, the curves which were not the boundaries were not shown. The figures prove that with the given configuration, the system is indeed tensionable around its starting point (i.e. around [0,0,0,0]).

Table 4-2. Parameters of the designed robot

Winch No.	Winch Location (mm)	$d_{a,1}$ (mm)	$d_{a,2}$ (mm)	p_a (mm)	σ (deg.)
1	[-595.6, -325.0, -1.2]	284.5	_	28.4	-90
2	[389.9, -918.5, 127.6]	254.0	_	28.4	90
3	[-105.9, 596.5, -799.7]	254.0	_	28.4	-60
4	[-481.9, 895.6, 111.5]	_	79.9	28.4	90
5	[1277.2, -438.0, 63.7]	_	260.9	28.4	180

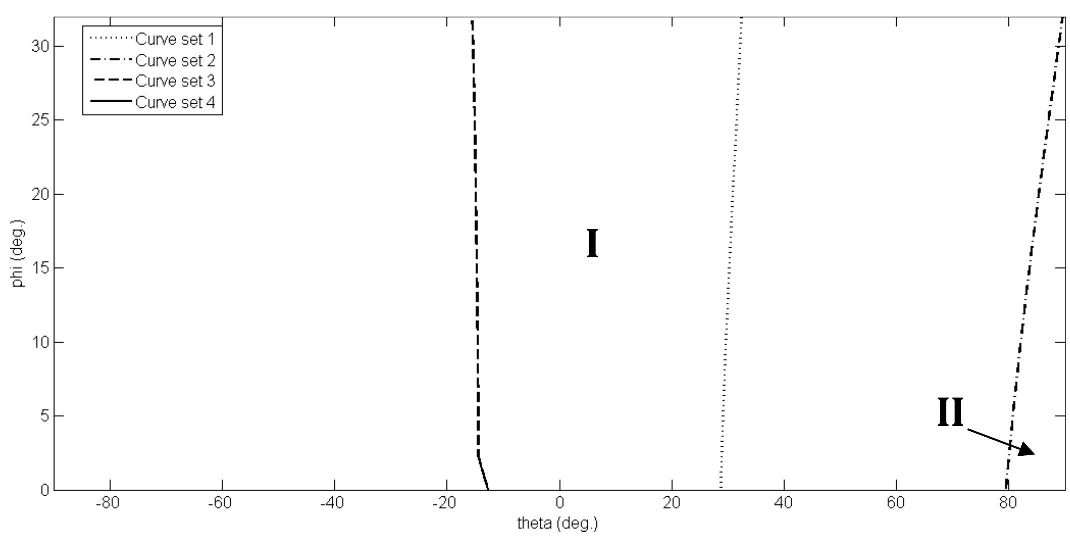

Figure 4-14. Tensionable workspace in θ-φ plane

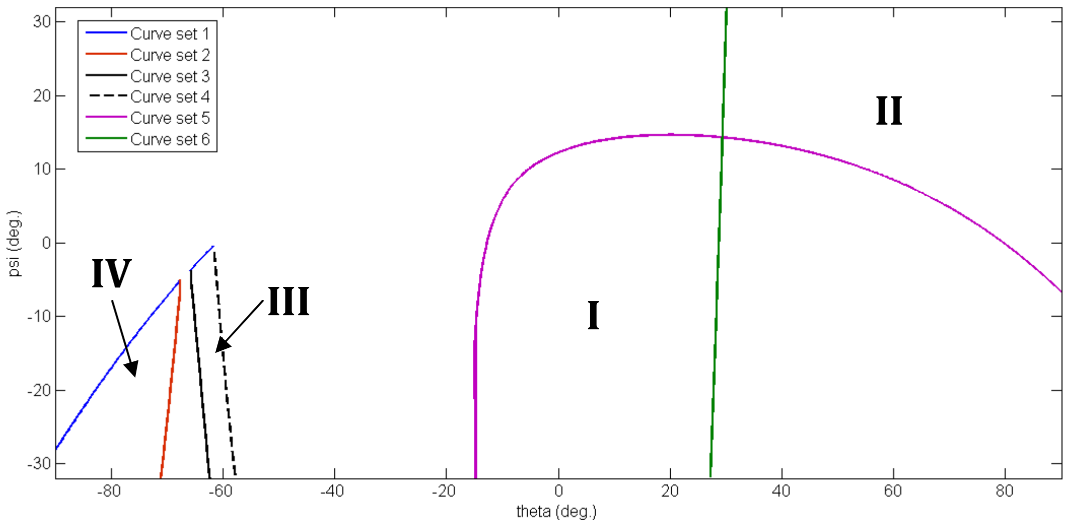

Figure 4-15. Tensionable workspace in θ-ψ plane

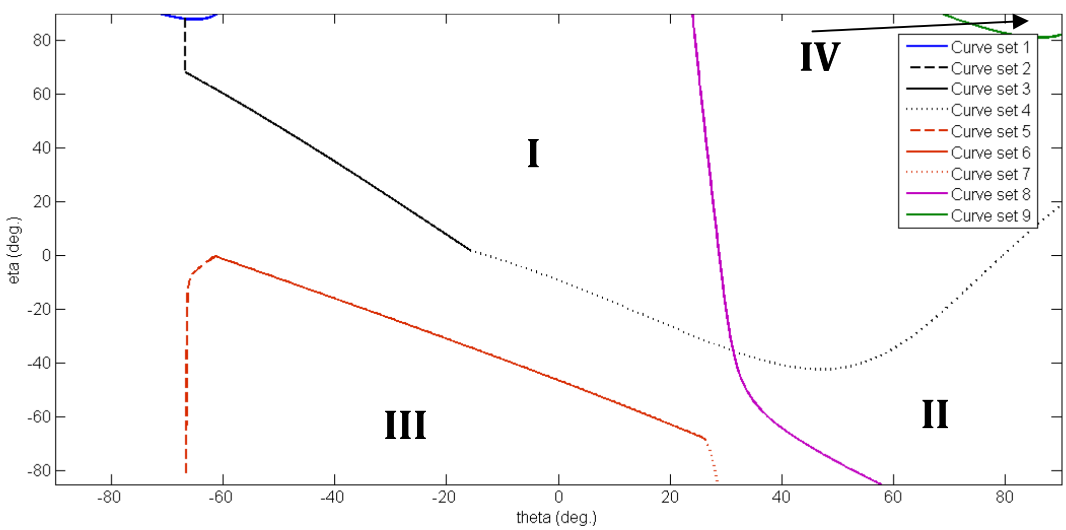

Figure 4-16. Tensionable workspace in θ-η plane

Note that in this analysis the physical limitations of the mechanism have been considered, too. For example because of the presence of the beam connecting the arm to the ground, φ cannot be negative; or the spherical joint maximum angle of 33° limits φ and ψ. The spherical joint limitation is especially notable in Figure 4-17 in a combination of change of the angles φ and ψ.

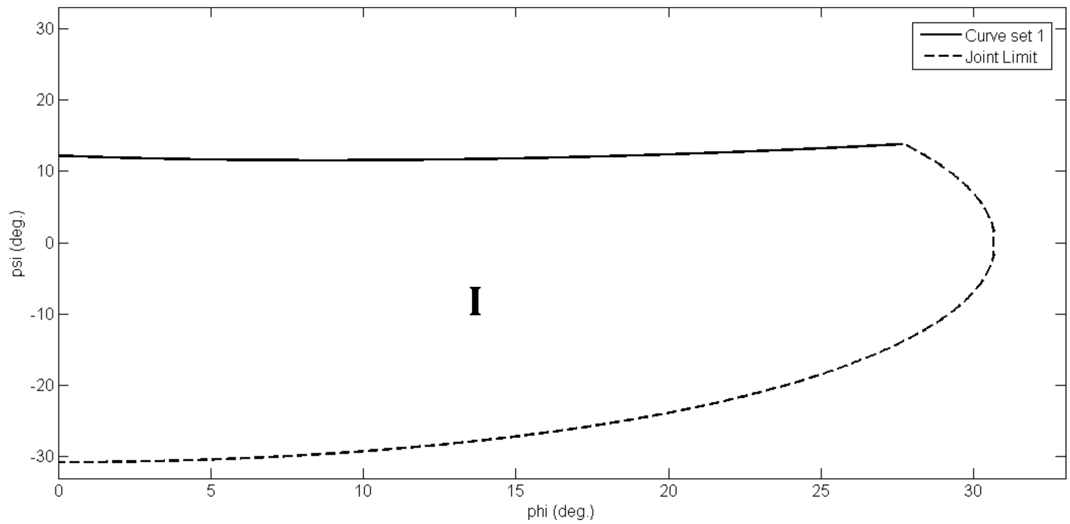

Figure 4-17. Tensionable workspace in φ-ψ plane

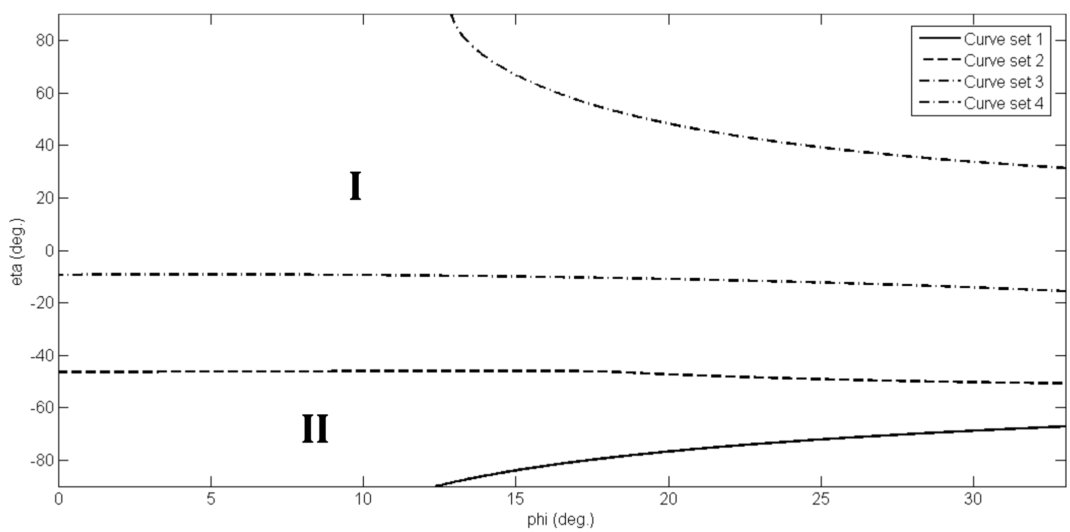

Figure 4-18. Tensionable workspace in φ-η plane

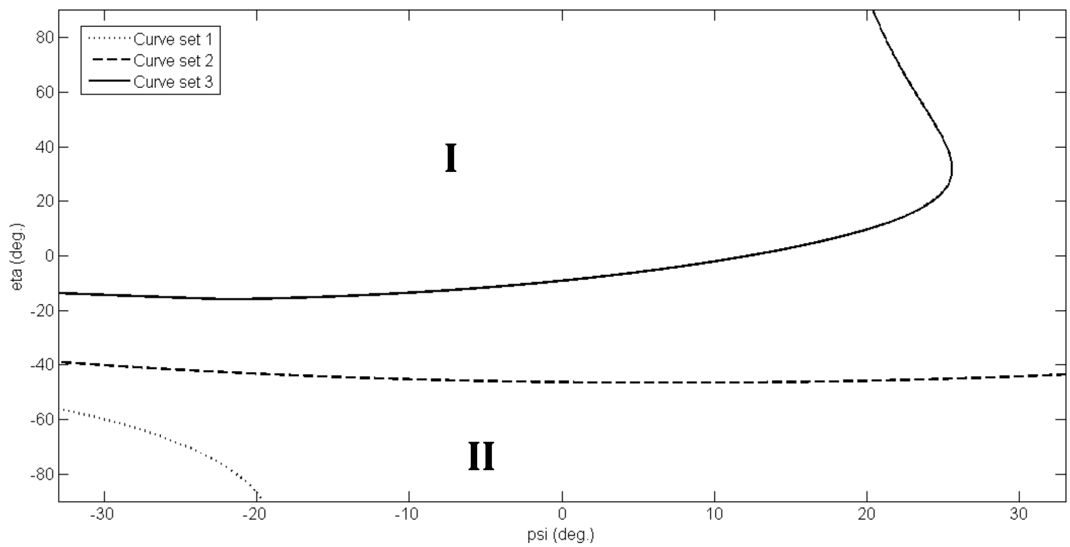

Figure 4-19. Tensionable workspace in ψ-η plane

4.5 Summary

A systematic approach for analytical or numerical determination of the tensionable workspace of the cable-driven multibody systems is presented. The method is based on the Lagrange's formulation in order to eliminate the internal forces of the multibody. As a result, a structure matrix is found for the mechanism whose numbers of rows and columns are degrees of freedom and the number of cables, respectively. This matrix can be used to investigate tensionability. Two methods are detailed to detect the tensionable workspace boundaries: null space and supporting/separating hyperplanes. For one redundant cable, (which is the minimum necessary number of cables for tensionability), it has been shown that both of these methods work. However, the computational cost of the null space approach is less. In the case of multiple redundant cables, applying the null space method is difficult, and thus the hyperplane method is preferred.

Having the boundaries of the tensionable workspace is not only beneficial for investigating the tensionability of the system in different configurations, but also it can be used to improve the tensionable workspace. Since the analytical expression of the boundaries is in hand, one can change, reshape, and/or move them by changing the appropriate parameters of the system, such as the location of the winches. The examples provided, demonstrate the usage of this method in obtaining the workspace, changing it, and comparing the different designs of a system both in the number of the redundant cables and in distribution of the cables among the links of the multibody.

Using this approach the designed multibody cable-driven robotic system was investigated and the analytical boundaries of the tensionable workspace in terms of the generalized coordinates were determined. This analysis proves that the system with the cable distribution suggested in chapter 3 is indeed tensionable in a region around the origin and thus can be controlled in that region. In the next chapter, the control design and implementation on the proposed system will be studied.

Chapter 5 Control of the Multibody Cable-Driven Robot

In the previous chapter the boundaries of the tensionable workspace were obtained. Since outside of them there is no guarantee for equilibrium of the multibody cable-driven mechanism against an arbitrary external load, these boundaries set the limit for the motion range of the robot. Having this range, the last step of this project is to control the robot within its tensionable workspace. In this chapter, the control laws suited for the rehabilitation purpose are discussed and designed, and then the implementation of the proposed control logics and the experimental results are presented.

5.1 Control of Rehabilitation Robotic Systems

Along with the extensive research on proposing novel designs for rehabilitation robots, a lot of efforts have been put into developing new strategies for control of these systems. In fact, one can perceive that what makes a robot like MIT-MANUS a rehabilitation robot is essentially the control algorithm. Hence design of appropriate control strategies is one of the most crucial steps in the development of rehabilitation robots.

In their review of the control strategies suggested for the robotic systems used for neurologic injuries, Marchal-Crespo and Reinkensmeyer divide the control approaches into four groups: assisting, challenge-based, simulating normal tasks, and non-contact coaching [57].

In the assisting control paradigm, the robot moves the patient's injured limb in a predefined direction (trajectory) to stretch the limb's muscle [58-61], to induce brain plasticity [62,63], and to help the motor system rebuild the unassisted motor skills [64,65]. The first and most common method for this approach is impedance control [57]. Impedance control (which will be discussed in more detail later in this chapter) allows following the specified trajectory with some deviation, depending on the impedance gains. Other methods include assistance by passive and/or active counterbalancing to support the patient's motion [66-68], and

EMG-based assistance, for supporting the desired motion detected by the EMG signals read from the muscles [69,70].

The challenge-based controllers are those that provide resistance against the movements of the patient in order to strengthen the muscles. The most common types of these controllers are "resistive controllers" [71,72] which apply forces to oppose the movement of the patient, and "error-amplification controllers" which tend to increase the error of following a specified trajectory [57]. One can see that this is the exact opposite of assisting controllers which tend to help the patient to minimize the error.

The third approach is based on simulating the every-day activities of real-life using haptic interfaces to provide a safer training tool before doing them in real-life [73,74]. And finally, the fourth approach uses the robot for directing and encouraging the exercises performed by the patients. The reason for using a robot instead of a simple computerized system is that the research has proved that patients respond better to a "physical embodiment" of the intelligence [75].

Another problem in control of rehabilitation robots that Marchal-Crespo and Reinkensmeyer reviewed is trajectory planning [57]. Defining the desired trajectory is important in that it is required in most of the rehabilitation control paradigms mentioned above. In fact, among the methods of the first two paradigms (which are more relevant to the present research), only the resistive controller algorithm does not require a defined desired trajectory. Various methods have been suggested for determining the desired trajectory, including the use of pre-recorded trajectories from healthy subjects [76,77], using pre-recorded trajectories from therapist's teaching [74,78], mathematical model of human movements using minimum-jerk algorithm [79], and several other algorithms reviewed in [57].

Marchal-Crespo and Reinkensmeyer have based their review on high-level concept of robot control; i.e. on how the control algorithm can assists in motor therapy. However, these high-level control approaches are always implemented by using low-level control of the robotic systems, i.e. position control, force control, etc.

As mentioned earlier, among the four control paradigms mentioned above, the proposed robotic system is more related to the first and second paradigms. From the above review one can immediately conclude that for trajectory following methods two low-level control approaches which are necessary to investigate are position control and impedance control. For resistive control which is a non-trajectory-based controller, it will be shown that it can be derived as a special case of impedance control.

These low-level control methods are investigated in the following sections.

5.2 Control of Cable-Driven Robotic Systems

For a simplified model of cables, assuming they are rigid elements, the control design of cable-driven robots is essentially the same as conventional robots, and almost all control methods of conventional robots reported in literature can be applied to the cable robots. With this simplified model, the only problem is resolving the redundancy, or in other words, distributing the tensions among the cables to achieve a specified resultant force requested by control logic.

Early researches by Agrawal et. al. [80,81] are examples of this basic approach. In [80] they investigated two standard robotic controllers, namely Lyapunov-based controller and feedback linearization controller, for position control of cable robots. Further, in [82] they extended their Lyapunov-based method to incorporate the tension limits.

Another step in control of cable robots is to consider the robot stiffness. This is especially necessary for implementation of compliance and force control methods. In [83], Khosravi and Taghirad considered the elasticity of cables as part of the model used for their proposed Lyapunov-based control design. However, as Behzadipour and Khajepour showed [84], cable elasticity contributes only one part of the total stiffness of the cable-driven robots. A more sophisticated model was proposed by Yu et. al. [85] for the purpose of simultaneous position and stiffness control of the robot. In their work, the position controller was designed using the abovementioned methods and then they took advantage of the redundancy such that by changing the antagonistic force in the cables through an optimization algorithm, it achieving a desired stiffness became possible.

For the rehabilitation application, as discussed earlier, impedance control is one of the most important control approaches. However, almost no impedance control logic proposed specifically for cable-driven robotic systems (considering stiffness, etc.) has been reported in literature. In the following sections of this chapter, the stiffness of multibody cable robots is formulated, and then position control and impedance control are designed and implemented.

5.3 Stiffness of Multibody Cable-Driven Robots

The formulation of the stiffness of multibody cable-driven robots is based on Behzadipour and Khajepour's method for obtaining stiffness of rigid-body cable robots [84]. Rewriting Eq. (4.12):

$$\mathbf{A}_{\mathrm{L}}\boldsymbol{\tau}_{\mathrm{L}} = \mathbf{b}_{\mathrm{L}} \tag{5.1}$$

for a set of generalized coordinates $\boldsymbol{\alpha}$, the stiffness matrix $\mathbf{K}$ can be obtained by taking derivative of the external wrench with respect to $\boldsymbol{\alpha}$:

$$\mathbf{K} = \frac{\mathrm{d}\mathbf{b}_{\mathrm{L}}}{\mathrm{d}\boldsymbol{\alpha}} = \mathbf{A}_{\mathrm{L}} \frac{\mathrm{d}\boldsymbol{\tau}_{\mathrm{L}}}{\mathrm{d}\boldsymbol{\alpha}} + \frac{\mathrm{d}\mathbf{A}_{\mathrm{L}}}{\mathrm{d}\boldsymbol{\alpha}} \boldsymbol{\tau}_{\mathrm{L}} \tag{5.2}$$

But since

$$\frac{\mathrm{d}\boldsymbol{\tau}_{\mathrm{L}}}{\mathrm{d}\boldsymbol{\alpha}} = \frac{\mathrm{d}\boldsymbol{\tau}_{\mathrm{L}}}{\mathrm{d}\mathbf{l}} \frac{\mathrm{d}\mathbf{l}}{\mathrm{d}\boldsymbol{\alpha}} = \frac{\mathrm{d}\boldsymbol{\tau}_{\mathrm{L}}}{\mathrm{d}\mathbf{l}} \mathbf{A}_{\mathrm{L}}{}^{\mathrm{T}} \tag{5.3}$$

in which $\mathbf{l} = [l_1, \dots, l_{\bar{m}}]^{\mathrm{T}}$ is the vector of cable lengths, we have:

$$\mathbf{K} = \mathbf{A}_{\mathrm{L}} \frac{\mathrm{d}\mathbf{T}_{\mathrm{L}}}{\mathrm{d}\mathbf{l}} \mathbf{A}_{\mathrm{L}}{}^{\mathrm{T}} + \frac{\mathrm{d}\mathbf{A}_{\mathrm{L}}}{\mathrm{d}\boldsymbol{\alpha}} \boldsymbol{\tau}_{\mathrm{L}} \tag{5.4}$$

The term $\frac{\mathrm{d}\boldsymbol{\tau}_{\mathrm{L}}}{\mathrm{d}\mathbf{l}}$ can be substituted by:

$$\frac{\mathrm{d}\boldsymbol{\tau}_{\mathrm{L}}}{\mathrm{d}\mathbf{l}} = \boldsymbol{\Omega} = \mathrm{diag}(k_1, \dots, k_{\bar{m}}) \tag{5.5}$$

where k_i's represent the total stiffness along the cable resulted from cable elasticity in series with the closed-loop control.

Finally, $\mathbf{K}$ can be expressed as:

$$\mathbf{K} = \mathbf{A}_{\mathrm{L}} \boldsymbol{\Omega} \mathbf{A}_{\mathrm{L}}{}^{\mathrm{T}} + \frac{\mathrm{d}\mathbf{A}_{\mathrm{L}}}{\mathrm{d}\boldsymbol{\alpha}} \boldsymbol{\tau}_{\mathrm{L}} \tag{5.6}$$

Indeed, due to the dependence of $\mathbf{A}_{\mathrm{L}}$ on position, the stiffness matrix is not constant and it changes with the generalized coordinates, as well as with the cable forces set by control algorithm.

The extra term in right hand side of Eq. (5.6) compared to the renowned formulation of stiffness proposed by Salisbury for the purpose of stiffness control [86] is what Li et. al. called "the changes in geometry through the differential Jacobian matrix, and externally applied forces" [87]. In other words, the stiffness matrix cannot be transformed from one space to another (in this case from actuator space to generalized coordinate space) merely by Jacobian multiplication, and a second term (which depends on forces) is required.

5.4 Position Control

5.4.1 Actuator Model

The first step for position control design is to obtain a dynamic model of the actuators. The electrical motors used for the robot are DC brushless motors. Neglecting the dynamics of the electrical part (due to the fact that it is much faster compared to the mechanical part), a first order linear model can be used:

$$m_{\mathrm{m}}\dot{v}_{\mathrm{m}} + b_{\mathrm{m}}v_{\mathrm{m}} + f_{\mathrm{m}}sign(v_{\mathrm{m}}) = u_{\mathrm{m}} \tag{5.7}$$

where m_{m} and b_{m} are the equivalent mass and linear damping coefficient, f_{m} is Coulomb friction force, and u_{m} and v_{m} (i.e. input and output) are the motor torque and velocity, respectively.

The parameters m_{m}, b_{m}, and f_{m} are unknown and are to be determined. For this purpose, a parameter estimation procedure using least squares has been performed. Pulses with different amplitudes were chosen as inputs in order to identify the nonlinearity of the system more accurately. The input signal is depicted in Figure 5-1 and the estimated parameters are listed in Table 5-1. Note that the parameters are converted from rotational to the equivalent translational values.

Figure 5-2 shows the measured output (velocity) together with the response of the estimated system. As seen from the figure, the error in transient response of the model is very small, whereas the steady state error in some cases is relatively large. This can be explained by the fact that the transient response is resulted from the linear part of the dynamics, i.e. from the linear damping. On the other hand, the steady state response of the system is heavily dependent on the Coulomb friction, which has been considered constant here, but the experiments have proven that due to different mechanical effects it changes considerably. The other source of error is that the motors selected, their inertia (Table 5-1), and their gear ratio of 10:1 (which causes the motor-side shaft inertia multiplied by 100) are all significantly larger than what is suitable for this application. In other words, the motors are for heavy-duty purposes, not for the tasks demanding high precision.

Table 5-1. The estimated parameters of the actuators

Parameter	Estimated Value	Unit
m_m	25.23	kg
b_m	175.56	Ns/m
f_m	11.13	N

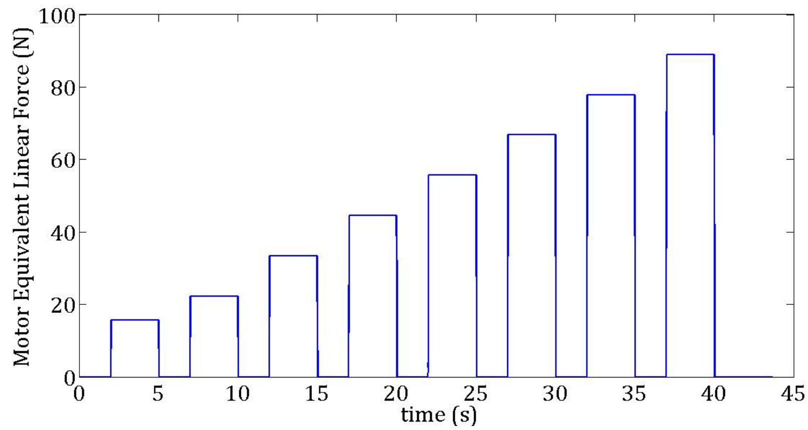

Figure 5-1 Input waveform used for parameter estimation of the actuator

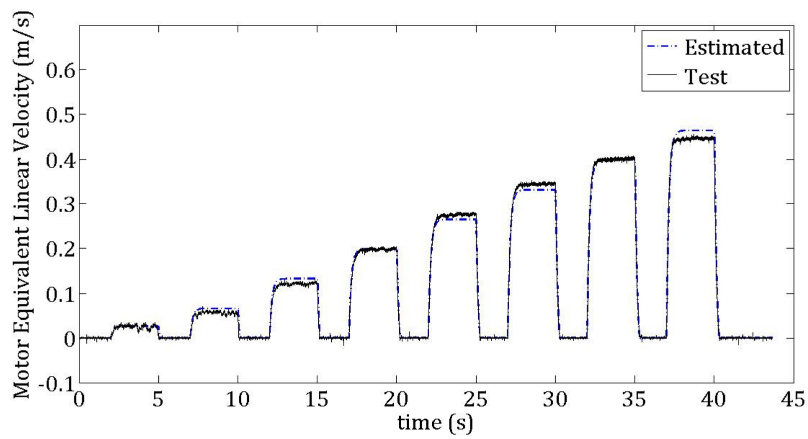

Figure 5-2 Comparison of measured data and output of the estimated model of the actuator

5.4.2 Dynamics

The Lagrangian dynamics of the arm (Eq. (5.1)) can be reformulated as:

$$\mathbf{H}_{\mathrm{a}}(\boldsymbol{\alpha})\ddot{\boldsymbol{\alpha}} + \mathbf{C}_{\mathrm{a}}(\boldsymbol{\alpha}, \dot{\boldsymbol{\alpha}}) = \mathbf{A}_{\mathrm{L}}\boldsymbol{\tau}_{\mathrm{L}} \tag{5.8}$$

where $\mathbf{H}_{\mathrm{a}}$ is the inertia matrix and $\mathbf{C}_{\mathrm{a}}$ includes gravity and other velocity-related terms.

For the i^{th} actuator, using Eq. (5.7) one can write the dynamic equation as:

$$m_{\mathrm{m}}\ddot{l}_i + b_{\mathrm{m}}\dot{l}_i + f_{\mathrm{m}}sign(\dot{l}_i) = u_i - t_i \tag{5.9}$$

where we used $v_{\mathrm{m}} = \dot{l}_i$.

Now using duality:

$$\mathbf{A}_{\mathrm{L}}^{\mathrm{T}}\dot{\boldsymbol{\alpha}} = \dot{\mathbf{l}} \tag{5.10}$$

Substituting Eq. (5.10) in Eq. (5.9) and writing in matrix form:

$$m_{\mathrm{m}}\mathbf{A}_{\mathrm{L}}^{\mathrm{T}}\ddot{\boldsymbol{\alpha}} + \left[m_{\mathrm{m}}\dot{\mathbf{A}}_{\mathrm{L}}^{\mathrm{T}}\dot{\boldsymbol{\alpha}} + b_{\mathrm{m}}\mathbf{A}_{\mathrm{L}}^{\mathrm{T}}\dot{\boldsymbol{\alpha}} + f_{\mathrm{m}}sign\left(\mathbf{A}_{\mathrm{L}}^{\mathrm{T}}\dot{\boldsymbol{\alpha}}\right)\right] = \mathbf{u} - \boldsymbol{\tau}_{\mathrm{L}} \tag{5.11}$$

Substituting $\boldsymbol{\tau}_{\mathrm{L}}$ in Eq. (5.8):

$$\left[\mathbf{H}_{\mathrm{a}}(\boldsymbol{\alpha}) + m_{\mathrm{m}}\mathbf{A}_{\mathrm{L}}\mathbf{A}_{\mathrm{L}}^{\mathrm{T}}\right]\ddot{\boldsymbol{\alpha}} + \left[\mathbf{C}_{\mathrm{a}}(\boldsymbol{\alpha},\dot{\boldsymbol{\alpha}}) + m_{\mathrm{m}}\mathbf{A}_{\mathrm{L}}\dot{\mathbf{A}}_{\mathrm{L}}^{\mathrm{T}}\dot{\boldsymbol{\alpha}} + b_{\mathrm{m}}\mathbf{A}_{\mathrm{L}}\mathbf{A}_{\mathrm{L}}^{\mathrm{T}}\dot{\boldsymbol{\alpha}} + f_{\mathrm{m}}\mathbf{A}_{\mathrm{L}}sign\left(\mathbf{A}_{\mathrm{L}}^{\mathrm{T}}\dot{\boldsymbol{\alpha}}\right)\right] = \mathbf{A}_{\mathrm{L}}\mathbf{u} \tag{5.12}$$

By taking

$$\mathbf{H} = \mathbf{H}_{\mathrm{a}}(\boldsymbol{\alpha}) + m_{\mathrm{m}}\mathbf{A}_{\mathrm{L}}\mathbf{A}_{\mathrm{L}}^{\mathrm{T}} \tag{5.13}$$

and

$$\mathbf{C} = \mathbf{C}_{\mathrm{a}}(\boldsymbol{\alpha},\dot{\boldsymbol{\alpha}}) + m_{\mathrm{m}}\mathbf{A}_{\mathrm{L}}\dot{\mathbf{A}}_{\mathrm{L}}^{\mathrm{T}}\dot{\boldsymbol{\alpha}} + b_{\mathrm{m}}\mathbf{A}_{\mathrm{L}}\mathbf{A}_{\mathrm{L}}^{\mathrm{T}}\dot{\boldsymbol{\alpha}} + f_{\mathrm{m}}\mathbf{A}_{\mathrm{L}}sign\left(\mathbf{A}_{\mathrm{L}}^{\mathrm{T}}\dot{\boldsymbol{\alpha}}\right) \tag{5.14}$$

the Eq. (5.8) becomes:

$$\mathbf{H}(\boldsymbol{\alpha})\ddot{\boldsymbol{\alpha}} + \mathbf{C}(\boldsymbol{\alpha},\dot{\boldsymbol{\alpha}}) = \mathbf{u}_{\mathrm{L}} \tag{5.15}$$

Eq. (5.15) is in the standard form of robotic system dynamics for the control design. In the following section, this equation is used to propose a control law for the position control task. Henceforth $\mathbf{u}_{\mathrm{L}} = \mathbf{A}_{\mathrm{L}}\mathbf{u}$ is referred to as the resultant control input.

5.4.3 Control Design

The control design problem for position control is essentially the problem of tracking a desired trajectory in the generalized coordinate space, $\boldsymbol{\alpha}_{\mathrm{d}}$. Although they are nonlinear, the special from of the dynamic equations of the robotic systems (Eq. (5.15)) enables us to use feedback linearization method [88] to design control for a globally linearized system and apply it to the nonlinear system. In this method (which is a classic approach for control of robotic systems [89], and has also been used for control of cable robots [80]), a nonlinear feedback is used to globally linearize the system dynamics. For this aim, first we write the resultant control input, $\mathbf{u}_{\mathrm{L}}$, as a function of the states of the system:

$$\mathbf{u}_{\mathrm{L}} = \mathbf{A}_{\mathrm{L}}\mathbf{u} = \mathbf{H}(\boldsymbol{\alpha})\boldsymbol{\xi} + \mathbf{C}(\boldsymbol{\alpha},\dot{\boldsymbol{\alpha}}) \tag{5.16}$$

Assuming an exact model, one can conclude that:

$$\ddot{\boldsymbol{\alpha}} = \boldsymbol{\xi} \tag{5.17}$$

which is the linearized dynamics of the system. The control law usually used for Eq. (5.17) is a simple PD control:

$$\boldsymbol{\xi} = \ddot{\boldsymbol{\alpha}}_{\mathrm{d}} + \mathbf{K}_{\mathrm{P}}(\boldsymbol{\alpha}_{\mathrm{d}} - \boldsymbol{\alpha}) + \mathbf{K}_{\mathrm{D}}(\dot{\boldsymbol{\alpha}}_{\mathrm{d}} - \dot{\boldsymbol{\alpha}}) \tag{5.18}$$

Substituting in Eq. (5.17):

$$(\ddot{\boldsymbol{\alpha}}_{\mathrm{d}} - \ddot{\boldsymbol{\alpha}}) + \mathbf{K}_{\mathrm{P}}(\boldsymbol{\alpha}_{\mathrm{d}} - \boldsymbol{\alpha}) + \mathbf{K}_{\mathrm{D}}(\dot{\boldsymbol{\alpha}}_{\mathrm{d}} - \dot{\boldsymbol{\alpha}}) = \mathbf{0} \tag{5.19}$$

From the form of Eq. (5.18) it is evident that taking $\mathbf{K}_{\mathrm{P}}$ and $\mathbf{K}_{\mathrm{D}}$ as diagonal matrices with positive entries, n_{DoF} decoupled equations are obtained, each of which asymptotically stable.

For the present application, the tests have proved that an integral term is also required to compensate the steady state error resulting from parameter uncertainties and unmodeled dynamics. In this case, Eq. (5.18) is extended to the following form:

$$\boldsymbol{\xi} = \ddot{\boldsymbol{\alpha}}_{\mathrm{d}} + \mathbf{K}_{\mathrm{P}}(\boldsymbol{\alpha}_{\mathrm{d}} - \boldsymbol{\alpha}) + \mathbf{K}_{\mathrm{D}}(\dot{\boldsymbol{\alpha}}_{\mathrm{d}} - \dot{\boldsymbol{\alpha}}) + \mathbf{K}_{\mathrm{I}} \int (\boldsymbol{\alpha}_{\mathrm{d}} - \boldsymbol{\alpha}) dt \tag{5.20}$$

Note that in Eq. (5.20), choosing positive-definite matrix coefficients is not sufficient to guarantee stability. However, by taking $\mathbf{K}_{\mathrm{P}}$, $\mathbf{K}_{\mathrm{D}}$, and $\mathbf{K}_{\mathrm{I}}$ to be diagonal matrices, one can obtain decoupled third-order equations, and then choose the matrix components such that each equation becomes stable.

From Eqs. (5.16) and (5.20) the resultant control input is obtained as:

$$\mathbf{u}_{\mathrm{L}} = \mathbf{H}(\boldsymbol{\alpha})[\ddot{\boldsymbol{\alpha}}_{\mathrm{d}} + \mathbf{K}_{\mathrm{P}}(\boldsymbol{\alpha}_{\mathrm{d}} - \boldsymbol{\alpha}) + \mathbf{K}_{\mathrm{D}}(\dot{\boldsymbol{\alpha}}_{\mathrm{d}} - \dot{\boldsymbol{\alpha}}) + \mathbf{K}_{\mathrm{I}} \int (\boldsymbol{\alpha}_{\mathrm{d}} - \boldsymbol{\alpha}) dt] + \mathbf{C}(\boldsymbol{\alpha}, \dot{\boldsymbol{\alpha}}) \tag{5.21}$$

The last step is to obtain the control input of the actuators, $\mathbf{u}$. Since $\mathbf{u}_{\mathrm{L}} = \mathbf{A}_{\mathrm{L}}\mathbf{u}$:

$$\mathbf{u} = \mathbf{A}_{\mathrm{L}}^{+}\mathbf{u}_{\mathrm{L}} + \kappa \mathbf{n}_{\mathbf{A}} \tag{5.22}$$

where κ should be selected such that the tensions in all of the cables be in a desired range. (If the tension is too high there will be risk of snapping, and if the tension is too low, the cables might become slack).

Due to the existence of antagonistic forces, normally the total forces in the cables are much larger than the dynamic forces. Therefore, the desired range for u_i's can be approximated by the range given for t_i's, $[t_{\min}, t_{\max}]$. As a result, for each actuator there will be a $\kappa_{\max,i}$ that results in $u_i = t_{\max}$ and a $\kappa_{\min,i}$ that gives $u_i = t_{\min}$:

$$\kappa_{\min,i} = \frac{t_{\min} - \mathbf{A}_{\mathrm{L},i}^{+}\mathbf{u}_{\mathrm{L}}}{n_{A,i}}, \quad i = 1, \dots, n_{\mathrm{DoF}} \tag{5.23}$$

$$\kappa_{\max,i} = \frac{t_{\max} - \mathbf{A}_{\mathrm{L},i}^{+}\mathbf{u}_{\mathrm{L}}}{n_{A,i}}, \quad i = 1, \dots, n_{\mathrm{DoF}} \tag{5.24}$$

where $\mathbf{A}_{\mathrm{L},i}^{+}$ represents the i'th row of $\mathbf{A}_{\mathrm{L}}^{+}$.

The selected κ must satisfy two sets of conditions: $\kappa > \kappa_{\min,i}$ and $\kappa < \kappa_{\max,i}$. In this work, we select κ according to the following equation:

$$\kappa = \frac{\max_i(\kappa_{\min,i}) + \min_i(\kappa_{\max,i})}{2} \tag{5.25}$$

When the system is within the tensionable workspace boundaries, but there is no κ that can satisfy the above set of conditions, the robot is stopped. This occurs when the system has gone too close to the boundaries, and the risk of instability is high.

The block diagram of the proposed control law is depicted in Figure 5-3.

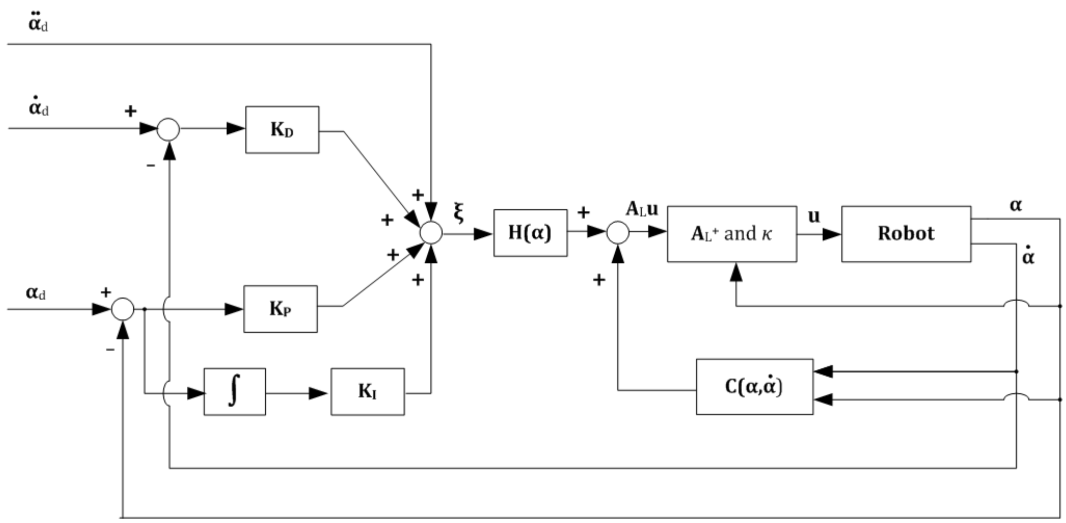

Figure 5-3 Block diagram of the proposed position control logic

5.5 Impedance Control

5.5.1 History and Formulation

In many robotic tasks the end-effector is required to physically interact with its environment. This interaction can be in the form of kinematic constraints that the environment imposes on the robot motion, or in the form of dynamic contact between robot and environment. To apply position control for such tasks, a very accurate model of the interaction is required, which in turn demands an accurate modeling of the physical environment. It is not hard to conclude that this approach is not practical.

To solve this problem, *interaction control* methods have been introduced. The goal of these methods is to provide some compliance in the interaction between the robot and the environment. One way to achieve this compliance is to use flexible materials in the structure of the robot by designing soft robot links and elastic joints. This method is called *passive interaction control*, and since there is no need for force and torque sensors, they are considered economical. However, as compliance is not being controlled in this method and the mechanical behavior of the manipulator is fixed, this approach suits only a limited class of applications. Indeed, when a specific compliant behavior is expected from the robot, controlling the compliance becomes inevitable. This approach is called *active interaction control* and it usually requires the measurement of the interaction force with the environment to modify/generate the desired trajectory of the robot.

Impedance control is a type of interaction controllers proposed by Hogan [90] as a generalization of stiffness control method developed by Salisbury [86]. In stiffness control the static response of the robot to its interaction with the environment is controlled such that the robot acts similar to a mechanical spring, while in impedance control the dynamics of the robot is controlled such that its response to the interaction simulates a mass-spring-damper system. In other words in impedance control the control law ensures that the following equation is satisfied:

$$\mathbf{\Lambda}\left(\ddot{\boldsymbol{\alpha}} - \ddot{\overline{\boldsymbol{\alpha}}}\right) + \mathbf{\Psi}\left(\dot{\boldsymbol{\alpha}} - \dot{\overline{\boldsymbol{\alpha}}}\right) + \mathbf{\Gamma}(\boldsymbol{\alpha} - \overline{\boldsymbol{\alpha}}) = \mathbf{f}_{\mathrm{e}} \tag{5.26}$$

where $\overline{\boldsymbol{\alpha}}$ is the "equilibrium" trajectory, $\mathbf{f}_{\mathrm{e}}$ is the environment generalized force applied to the robot, and $\mathbf{\Lambda}$, $\mathbf{\Psi}$, and $\mathbf{\Gamma}$ are inertia, damping, and stiffness matrices, respectively.

The simplest way to achieve this formulation is to take the control input as:

$$\mathbf{u} = -\mathbf{f}_{\mathrm{e}} = \mathbf{\Lambda}(\ddot{\boldsymbol{\alpha}}_{\mathrm{d}} - \ddot{\boldsymbol{\alpha}}) + \mathbf{\Psi}(\dot{\boldsymbol{\alpha}}_{\mathrm{d}} - \dot{\boldsymbol{\alpha}}) + \mathbf{\Gamma}(\boldsymbol{\alpha}_{\mathrm{d}} - \boldsymbol{\alpha}) \tag{5.27}$$

in which the equilibrium trajectory has been taken the same as the desired trajectory. In practice, usually $\mathbf{\Lambda}$ is taken to be zero [91], and the resulted controller (spring-damper) will be very similar to a PD controller.

Note that for the control law of Eq. (5.27) there is no need for environment force measurement. Although the control law is very simple, it works with acceptable performance in a large class of applications, where the robot inherent impedance and the friction are negligible compared to the desired impedance and the interaction forces.

In human-robot interaction problems, usually the desired impedance is preferred to be low. One way to achieve this is to design low-impedance robots with backdrivable actuators. However, development of such robots involves many problems both in design and in manufacturing. Therefore, it is desirable to improve the control logic such that the conventional robots can be used in such applications.

The first solution for this problem is to use force sensors to take a feedback from the environment forces. Having the exact interaction force applied to the robot's end-effector improves the controller by making the system less sensitive to the robot impedance and frictions. However, as shown in [91], using force feedback tends to make the system non-passive which leads to instability in interaction with some environments.

A method proposed for solving the problem of loss of passivity in using of force feedback is *position-based impedance control* or *admittance control* [92]. The main idea in this method is that the position control loop, in the normal way used in robotic control, is utilized here, but with the difference that the input trajectory to the position control loop is not the desired trajectory. Instead, the input trajectory of the position control loop is set by an outer control loop. The outer loop determines the "new" trajectory that the position control loop is to follow using the desired impedance and feedback of the force sensor. Hence the outer loop can be named "impedance loop". A schematic of this control scheme is depicted in Figure 5-4.

In this figure, $\boldsymbol{\alpha}_e$ is the new desired position set by impedance loop and is obtained from Eq. (5-26) by setting $\bar{\boldsymbol{\alpha}} = \boldsymbol{\alpha}_d$ and $\boldsymbol{\alpha} = \boldsymbol{\alpha}_e$.

Due to benefits of admittance control, this is the approach taken in this work for interaction control of the robot with humans.

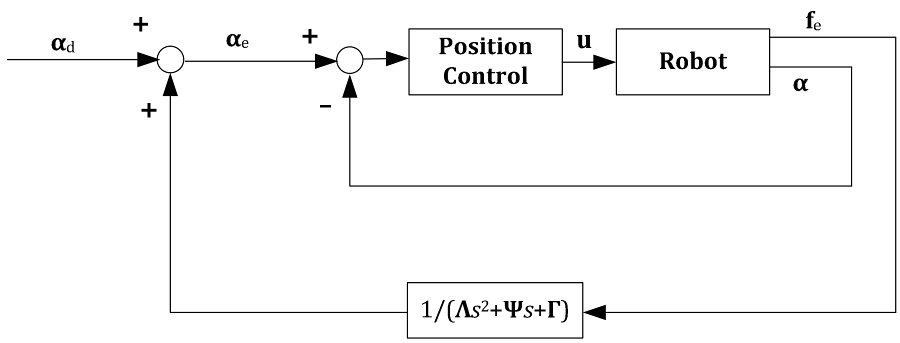

Figure 5-4 Admittance control scheme

5.5.2 Impedance Control of the Multibody Cable-Driven Robot

At this point, we are able to combine what was discussed in the previous sections to design an impedance control for the robot. The impedance control proposed for this application is essentially the two-loop control logic of Figure 5-4, where the position control loop is embedded from the diagram of Figure 5-3. Naturally, in the case of cable robots, there are two specific problems (compared to the general scheme of Figure 5-4) that should be addressed. The first problem is ensuring positive cable tensions and resolving redundancy which has already been considered in the position control law proposed. The second problem, as mentioned before, is the inherent stiffness of the structure of the cable robot which may interfere with the stiffness controlled by the impedance control loop. This is due to the fact that the position feedback for the position control loop is taken from the outlet points of the winches, and not from the end-effector. In other words, even if the cable spools of the winches are fixed (or equivalently: the position control loop responses instantly) the position of end-effector can be changed by applying external forces. This displacement is due to finite stiffness of the robot, which was obtained in Eq. (5.6):

$$\delta\boldsymbol{\alpha} = \mathbf{K}^{-1}\delta\mathbf{f}_{\mathrm{e}} \tag{5.28}$$

This stiffness is in series with the stiffness of impedance control. Thus the total stiffness $\boldsymbol{\Gamma}_{\mathrm{t}}$ the user feels will be:

$$\boldsymbol{\Gamma}_{\mathrm{t}}^{-1} = \mathbf{K}^{-1} + \boldsymbol{\Gamma}^{-1} \tag{5.29}$$

Therefore, from Eq. (5.29) one can conclude that by taking:

$$\boldsymbol{\Gamma}^{-1} = \boldsymbol{\Gamma}_{\mathrm{des}}^{-1} - \mathbf{K}^{-1} \tag{5.29}$$

the effect of the inherent stiffness of the cable robot can be eliminated. Note that normally the stiffness of the robot is larger than the desired stiffness of impedance control and thus $\boldsymbol{\Gamma}$ will be positive.

The final variable required for impedance control is the environment force $\mathbf{f}_{\mathrm{e}}$. The environment force in the case of this application is the patient's or operator's muscle force trying to move the robot in a specific direction. This force can be obtained in generalized coordinates using the dynamic equation of the arm (Eq. (5.8)) and the kinematic formulation of section 4.4. In the presence of an external force Eq. (5.8) becomes:

$$\mathbf{H}_{\mathrm{a}}(\boldsymbol{\alpha})\ddot{\boldsymbol{\alpha}} + \mathbf{C}_{\mathrm{a}}(\boldsymbol{\alpha},\dot{\boldsymbol{\alpha}}) = \mathbf{A}_{\mathrm{L}}\boldsymbol{\tau}_{\mathrm{L}} + \mathbf{f}_{\mathrm{e}} \tag{5.30}$$

Considering that all the other terms in Eq. (5.30) can be measured and calculated, $\mathbf{f}_{\mathrm{e}}$ can be obtained from this equation. Note that since the velocities and accelerations in this application are normally low, in practice the system can be approximated by a quasi-static system. This has the advantage of eliminating the acceleration term (which is usually too noisy to be usable) as well as the arm inertia matrix which varies from one person to the other.

From what was discussed above and in the previous sections, the block diagram of the impedance control logic proposed for the cable robot is depicted in Figure 5-5.

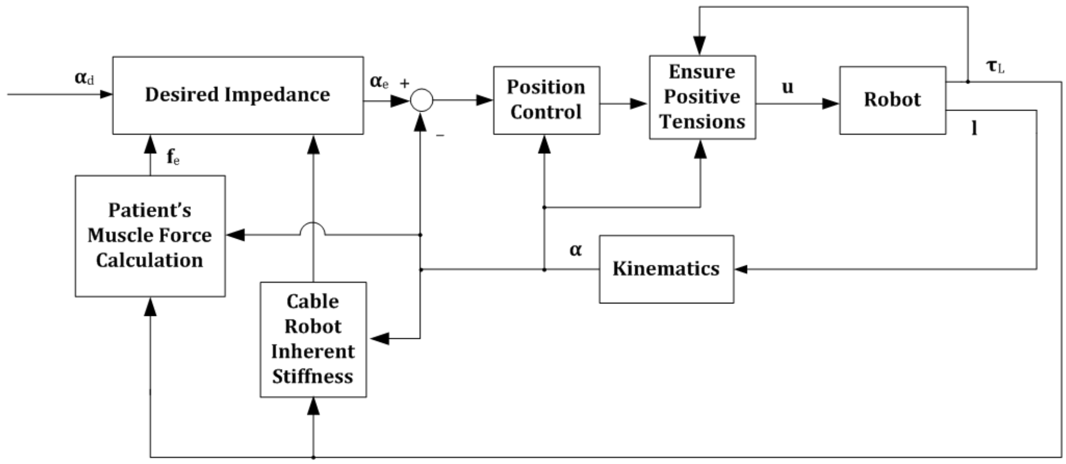

Figure 5-5 Block diagram of implemented impedance control

5.5.3 Teaching-Playback and Resistive Controller Schemes

In many robotic applications it is desirable that the robot can be "taught" by a human operator, and then replicate the learned task. This method is very common for conventional robots and for applications such as spray painting where the desired trajectory is much easier to be given by a human operator instead of being defined mathematically [93]. It is essential for the robots used in this method to need low guiding force, so that the operator can handle them easily.

In the case of cable robots, the major difference compared to conventional robots is that even in the teaching phase the cables must remain in tension. One way to overcome this issue is to set the cable tensions to be comprised merely of the antagonistic part (i.e. $\boldsymbol{\tau}_{\mathrm{L}} = \kappa \mathbf{n}_{\mathbf{A}}$). In this scheme, the cable forces at any position will cancel out each other and the resultant force on the arm will be the operator's force. However, note that this approach is basically an open-loop control scheme and has the major drawback of being highly sensitive to the measurement errors (in this case position measurement which leads to error in $\mathbf{n}_{\mathbf{A}}$). Furthermore, normally the antagonistic forces tend to be much larger than the operator's force and thus in the presence of error, the difference between the resultant force and the operator's force (due to measurement errors) can be significant.

Another way which will be used in this project and does not have the drawbacks of the previous method is using the admittance control scheme. The main idea is the same: to use the feedback from the operator's force for enforcing a prescribed behavior to the robot. The difference from the general impedance control is that in this case the robot should not have any stiffness and as the operator releases the robot, it does not move back to the equilibrium position. In other words: $\mathbf{\Gamma} = \mathbf{0}$. The essential term here is the damping matrix $\mathbf{\Psi}$, which determines the velocity of the system against a specific external force. The other gain matrix, $\mathbf{\Lambda}$, can also be set to zero, unless feeling a "sense of inertia" of the system for the operator is desirable.

What was discussed above for the teaching phase of the teaching-playback scheme is also applicable to the concept of resistive force controller. As explained before, in the case of resistive force controller, the robot resists against any motion that the patient applies. Similar to the teaching phase, this resistance can be generated by impedance control and specifically the damping term. As the damping coefficients (elements of $\mathbf{\Psi}$) increase, the resistance against the motion of the patient's limb will be amplified. Note that there is no desired trajectory for this scheme.

5.6 Experimental Results

Having designed control logics for position and impedance control of the robot, the next step will be implementation of the control in real-time.

The system is controlled via Labview® Real-Time Module with a host PC (CPU: AMD Athlon™ 64, 2.20 GHz - RAM: 1.00 GB) operating on Windows and a target National Instrument PXI-1042Q computer (CPU: Intel Core™ 2, 2.16 GHz - RAM: 512 MB) running Labview RT operating system. The two computers are connected using a crossover cable. The Labview model is created in the host computer and then uploaded to the target computer to perform data-acquisition and real-time control tasks through its integrated PXI cards. The sampling rate of the system is 50 Hz.

5.6.1 Position Control Experiment

Naturally, for any experiment, the motion of the robot must be kept within the boundaries of the tensionable workspace. As a result, for position control task the desired positions have to be defined considering the boundaries of the tensionable workspace obtained by use of the methods suggested in the previous chapter. Since the tensionable workspaces were presented in 2-D plots, the same approach is taken here and each position control experiment is designed in 2-D within the tensionable workspaces obtained in Chapter 4.

Indeed, maintaining a certain distance from the boundaries of the tensionable workspace is compulsory. As noted in the previous chapter, in the regions close to the boundaries at least one of the components of the null space vector becomes very small. Thus, in order to maintain the positive tensions, the tension of the other cables must be increased. Naturally, the high actuator forces tend to make the system unstable. To improve the stability, the control gains have to be reduced, which in turn affects the transient response of the system. Therefore, there is a trade-off between the transient response and the size of the subspace of the tensionable workspace in which the controller remains stable.

With regard to the above discussion, the position control tests are designed as: 1) starting from the zero position; 2) passing through three via-points which are chosen as close as possible to the boundary; 3) returning to the zero point. The 2-D results are shown in Figures 5-6 to 5-11 and the corresponding 3-D path of the end point of the arm are depicted in Figures 5-12 to 5-17. The controller gains have been chosen as (with $\boldsymbol{\alpha}$ in radians):

$$\mathbf{K}_{\mathrm{p}} = \mathrm{diag}(350{,}500{,}2200{,}800)$$

$$\mathbf{K}_{\mathrm{D}} = \mathrm{diag}(45{,}25{,}50{,}35)$$

$$\mathbf{K}_{\mathrm{I}} = \mathrm{diag}(60{,}45{,}200{,}50)$$

It can be seen in Figures 5-6 to 5-8 that the tracking error is much larger compared to those of Figures 5-9 to 5-11. In all cases of the first set of figures (i.e. Figures 5-6 to 5-8) one of the angles is θ. This leads us to assume that θ is "the most difficult" direction to control. Also, the fact that in each 2-D experiment, θ is the dimension with more tracking error (especially in Figure 5-6 where error of φ is much smaller than θ) supports this assumption. To prove this, we calculate the singular values of the MIMO (Multi-Input Multi-Output) system using Singular Value Decomposition (SVD) method. The dynamic model of the robot (Eq. 5.15)) was linearized and the singular values in different frequencies were obtained and plotted in Figure 5-18. The output directions corresponding to the singular values confirm that the smallest singular value correspond to the θ direction. For example at ω = 1 rad/s:

$$\boldsymbol{\Sigma} = \mathrm{diag}(\sigma_1, \sigma_2, \sigma_3, \sigma_4) = \mathrm{diag}(0.46{,}0.97{,}9.15{,}1.71)$$

$$\mathbf{U}_{\boldsymbol{\Sigma}} = \begin{bmatrix} 0.974 & 0.163 & 0.047 & -0.153 \\ -0.124 & 0.952 & 0.025 & 0.232 \\ -0.036 & -0.038 & 0.997 & 0.037 \\ 0.183 & -0.229 & -0.032 & 0.907 \end{bmatrix}$$

where $\boldsymbol{\Sigma}$ is the matrix of singular values and σ_i is the i'th singular value. $\mathbf{U}_{\boldsymbol{\Sigma}}$ is the matrix of output directions.

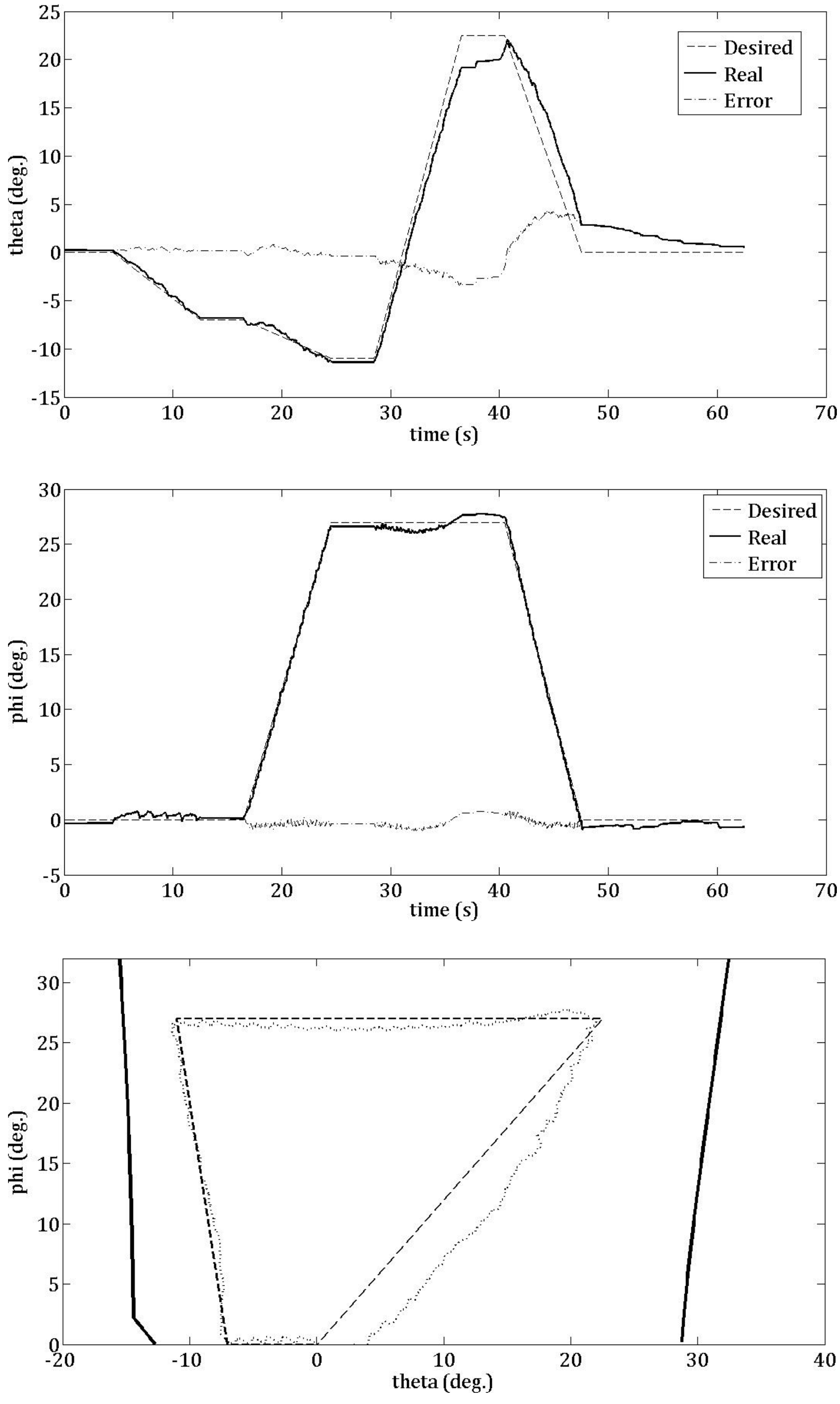

Figure 5-6. Position Control in coordinates θ and φ. Top: θ vs. time, center: φ vs. time,

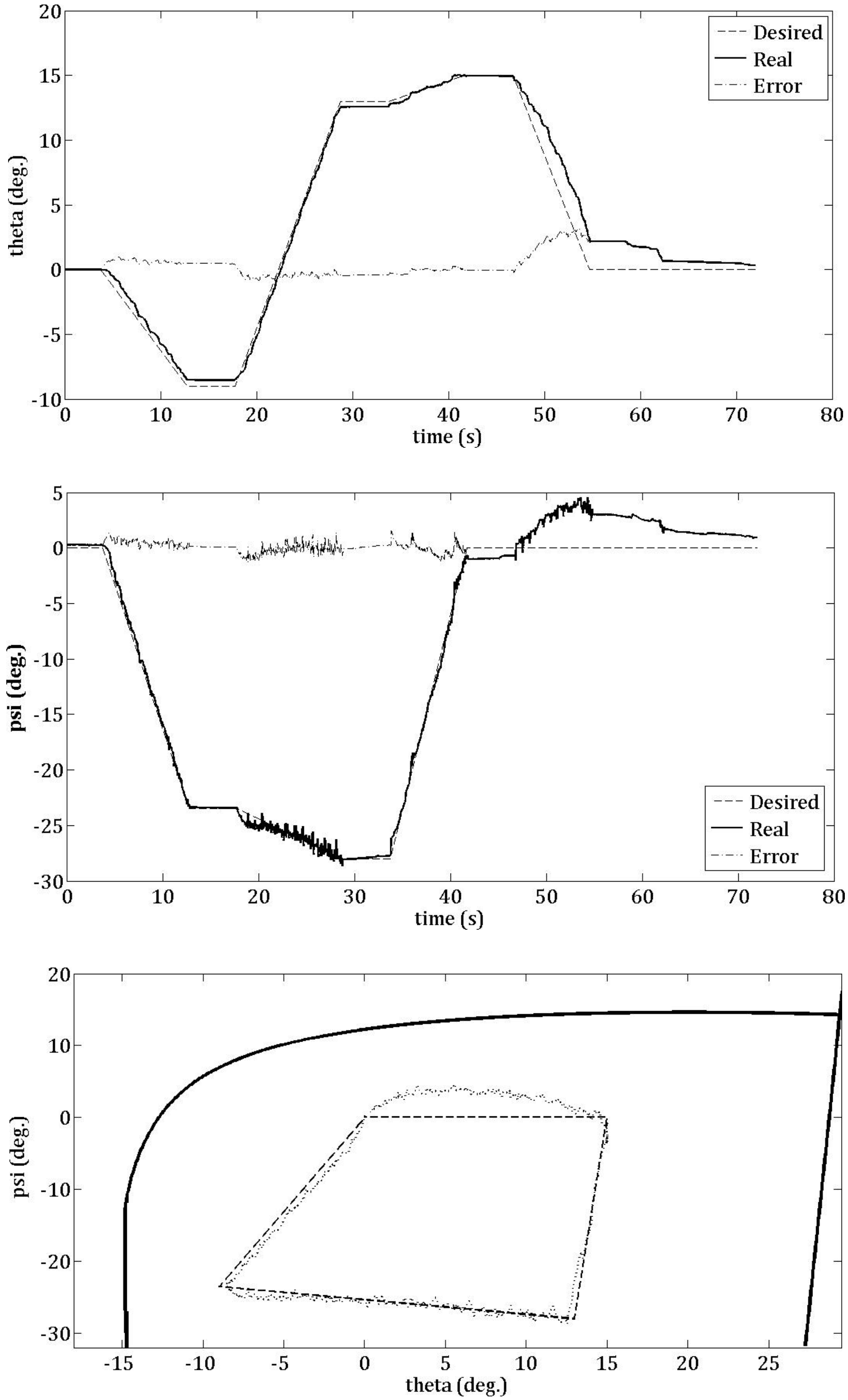

Figure 5-7. Position Control in coordinates θ and ψ. Top: θ vs. time, center: ψ vs. time,

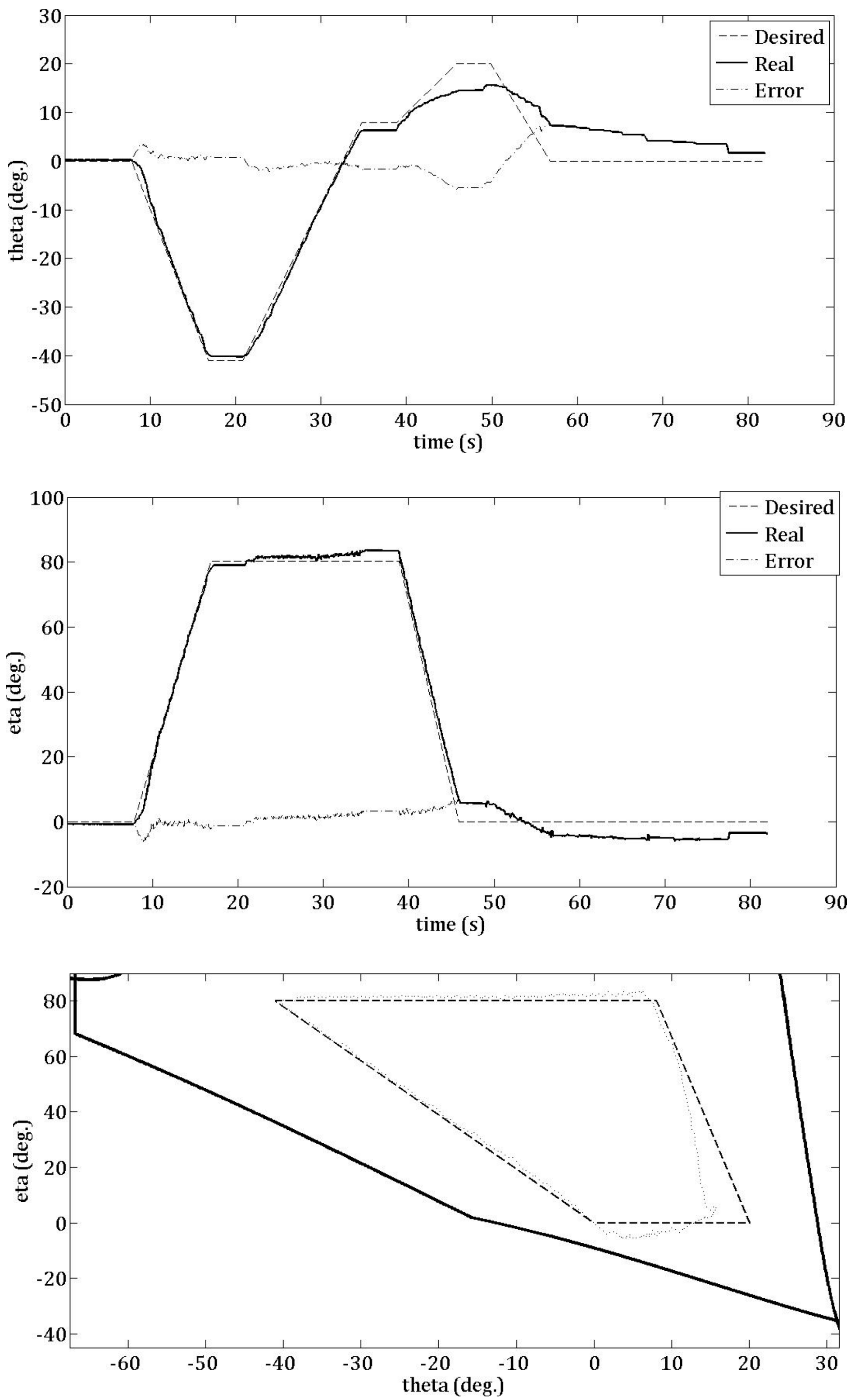

Figure 5-8. Position Control in coordinates θ and η. Top: θ vs. time, center: η vs. time,

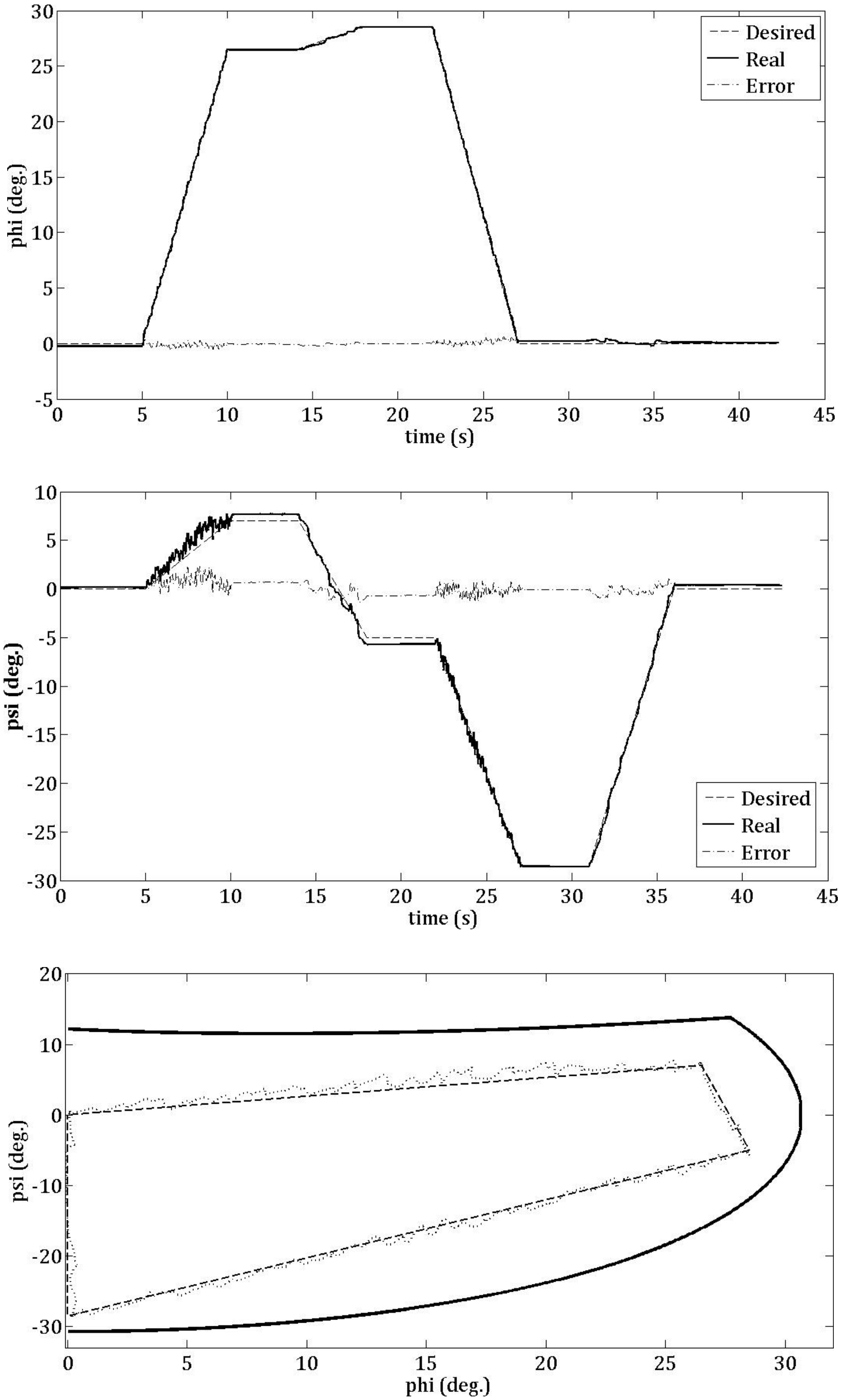

Figure 5-9. Position Control in coordinates φ and ψ. Top: φ vs. time, center: ψ vs. time, bottom: motion in φ -ψ plane: boundaries (solid), desired (dashed), real (dotted)

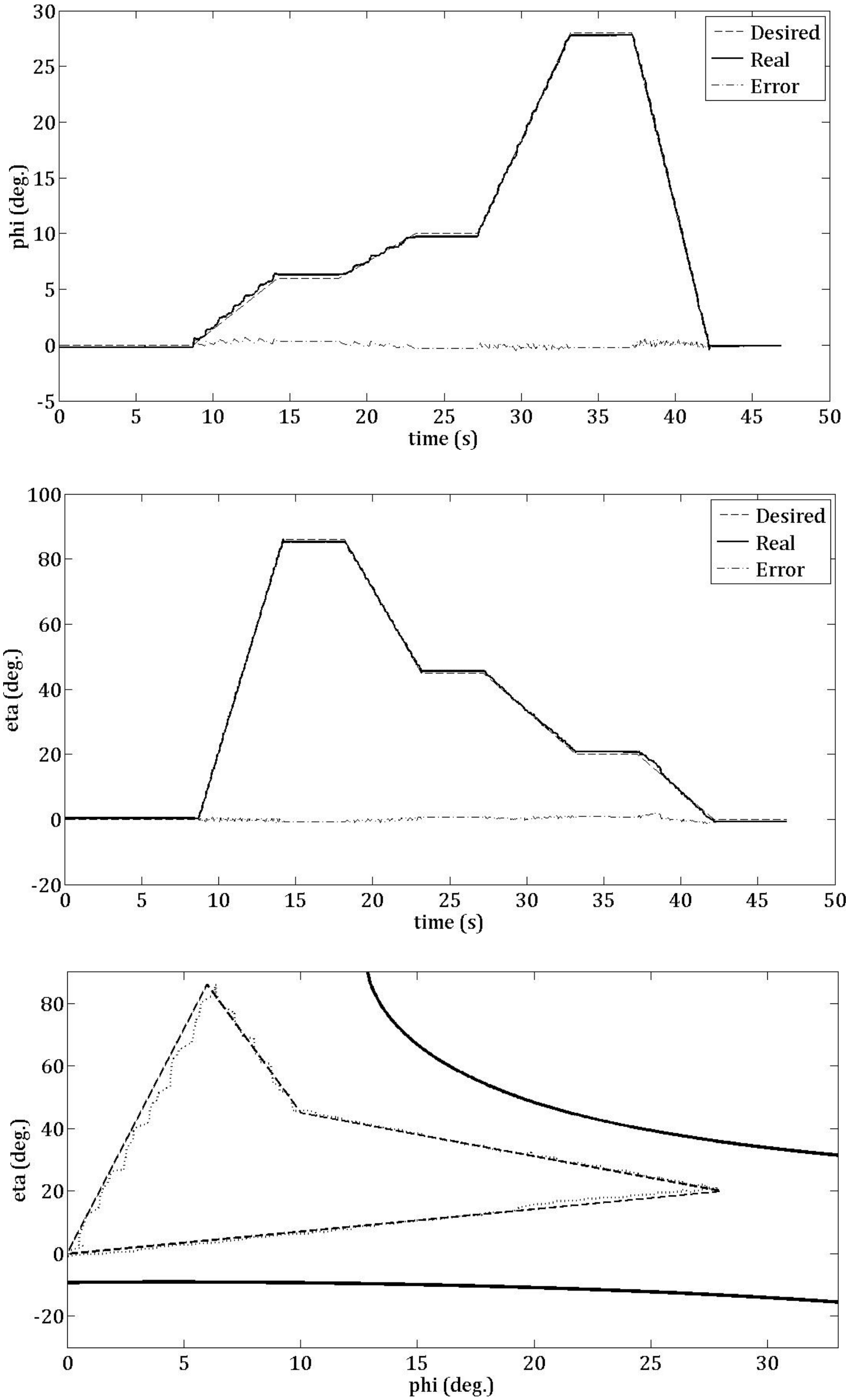

Figure 5-10. Position Control in coordinates φ and η. Top: φ vs. time, center: η vs. time, bottom: motion in φ -η plane: boundaries (solid), desired (dashed), real (dotted)

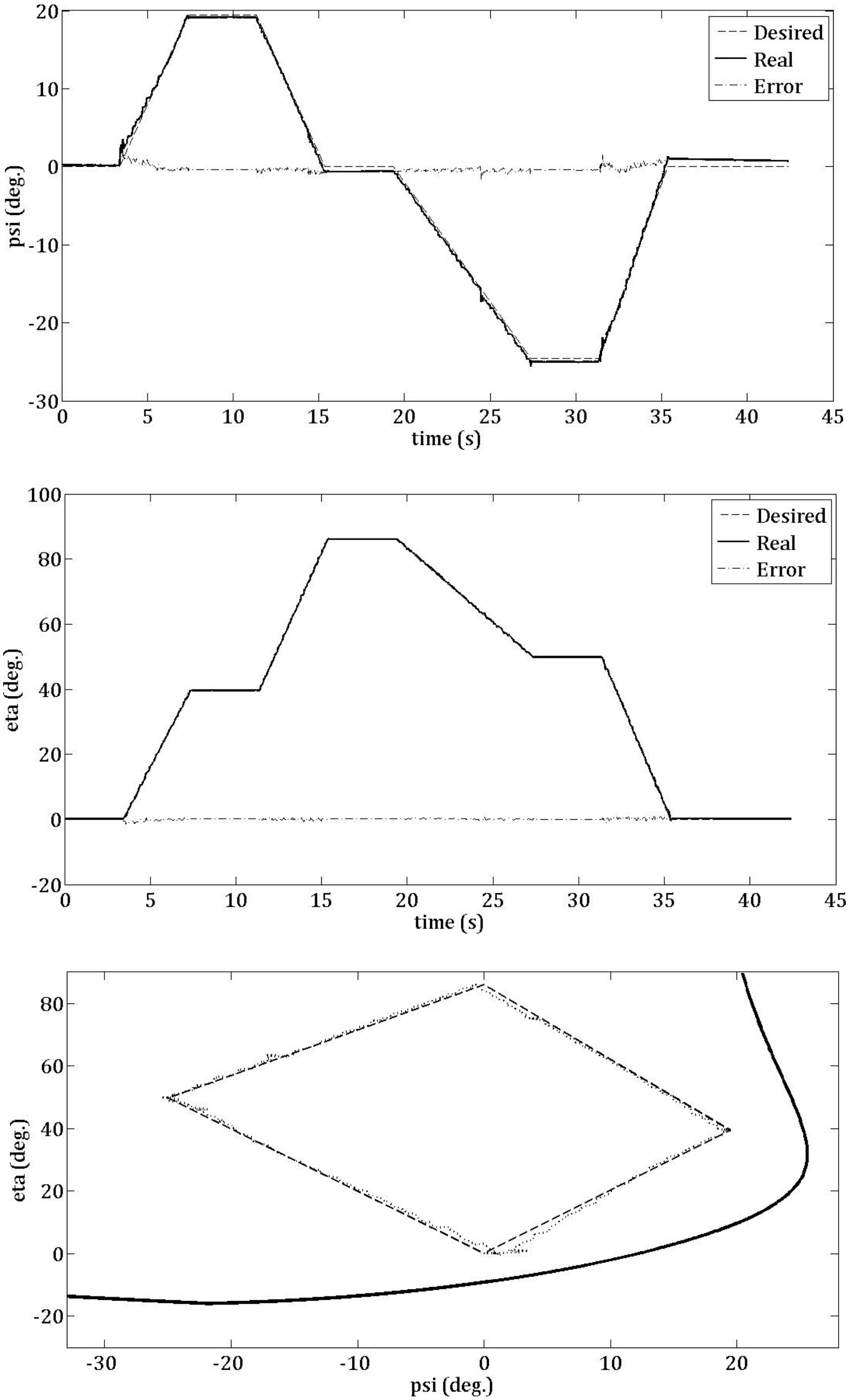

Figure 5-11. Position Control in coordinates ψ and η. Top: ψ vs. time, center: η vs. time, bottom: motion in ψ-η plane: boundaries (solid), desired (dashed), real (dotted)

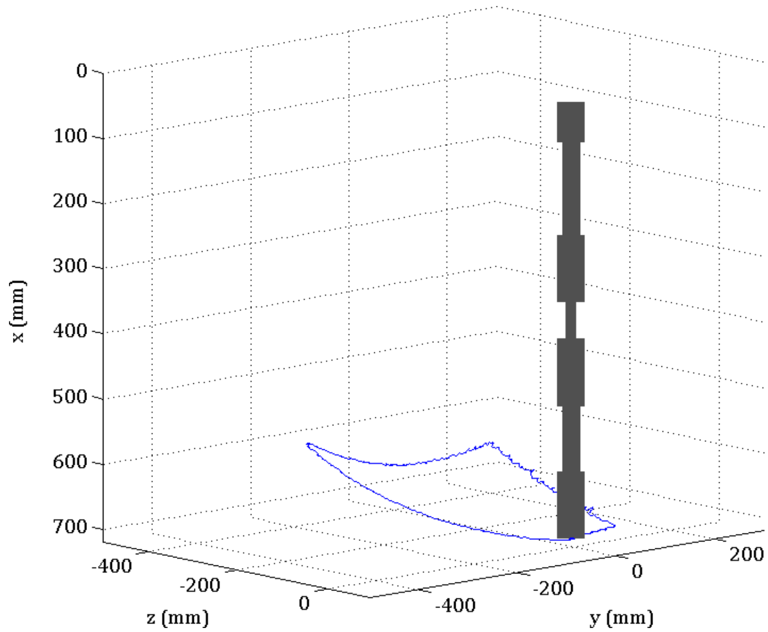

Figure 5-12. 3-D path of the end point of the arm in θ-φ experiment

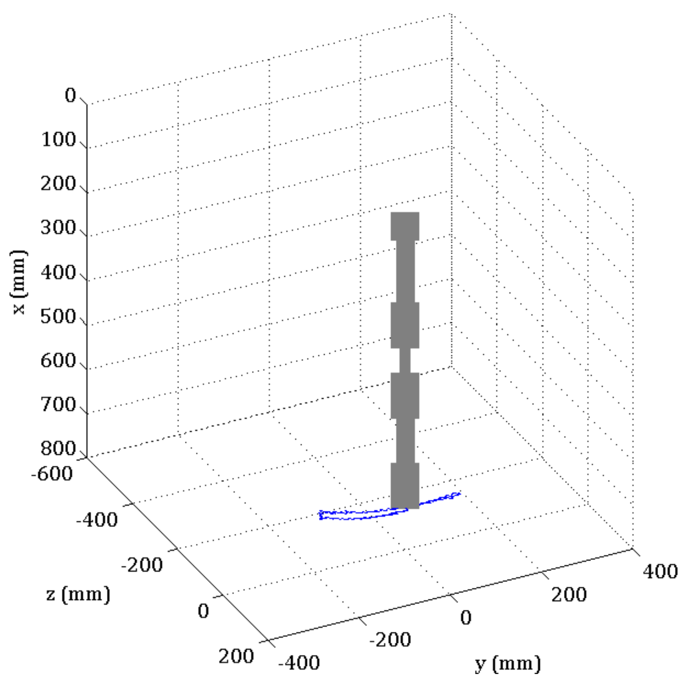

Figure 5-13. 3-D path of the end point of the arm in θ-ψ experiment

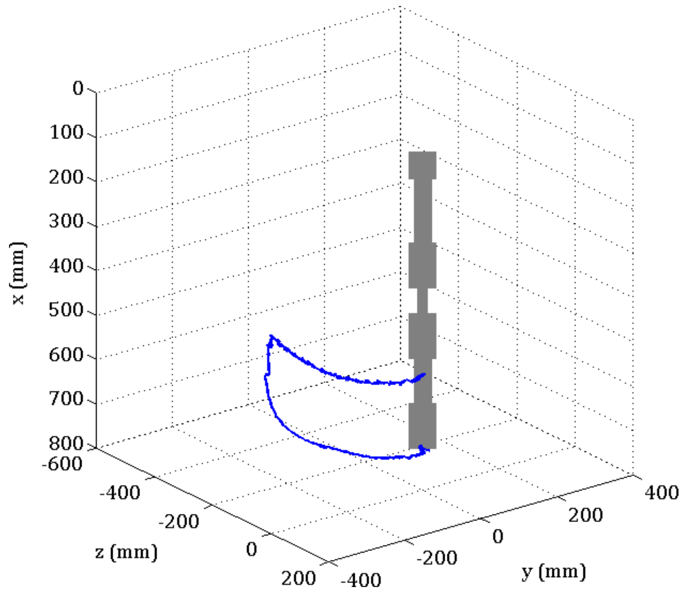

Figure 5-14. 3-D path of the end point of the arm in θ-η experiment

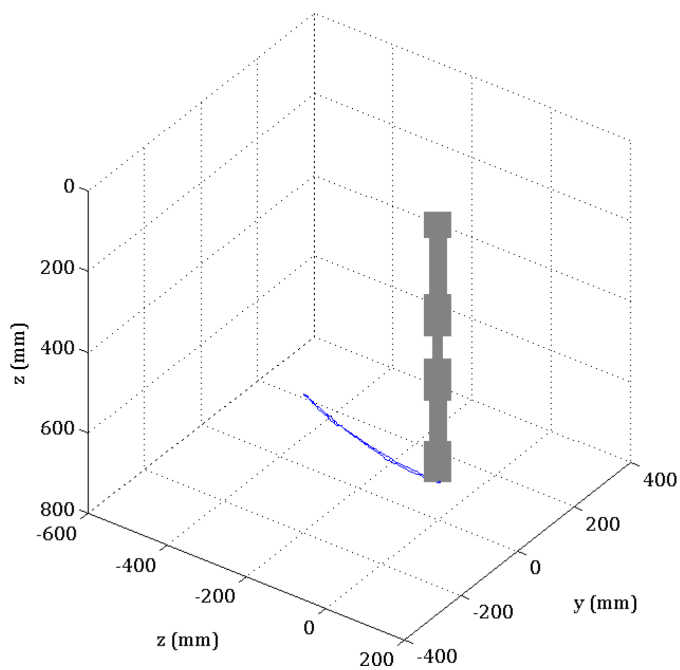

Figure 5-15. 3-D path of the end point of the arm in φ-ψ experiment

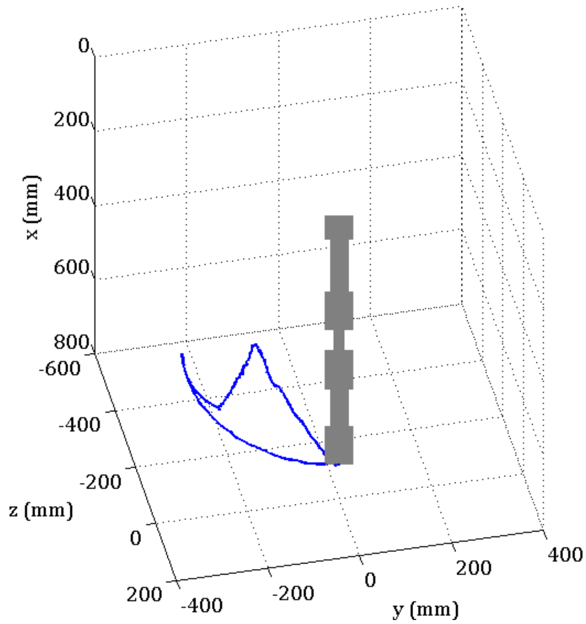

Figure 5-16. 3-D path of the end point of the arm in φ-η experiment

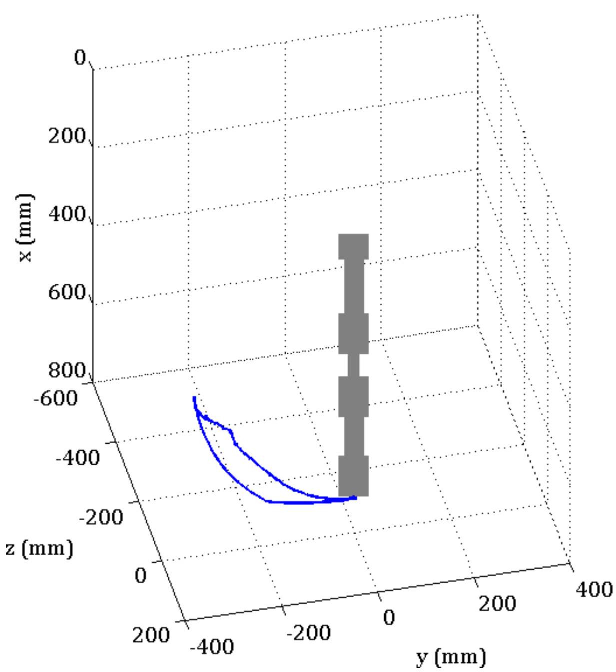

Figure 5-17. 3-D path of the end point of the arm in ψ-η experiment

A useful parameter that is usually used as a measure of controllability of the MIMO system in different directions is called "condition number" and is the ratio of the largest singular value (which in this case is in the ψ direction) to the smallest one (which is in θ direction). Condition number of the present system in terms of frequency has been depicted in Figure 5-19. As can be seen from the figure, the minimum condition number is 19.2, which is considerably large. As a result, the system is ill-conditioned. In order to improve the performance in θ direction, it is suggested to change the locations of the winches.

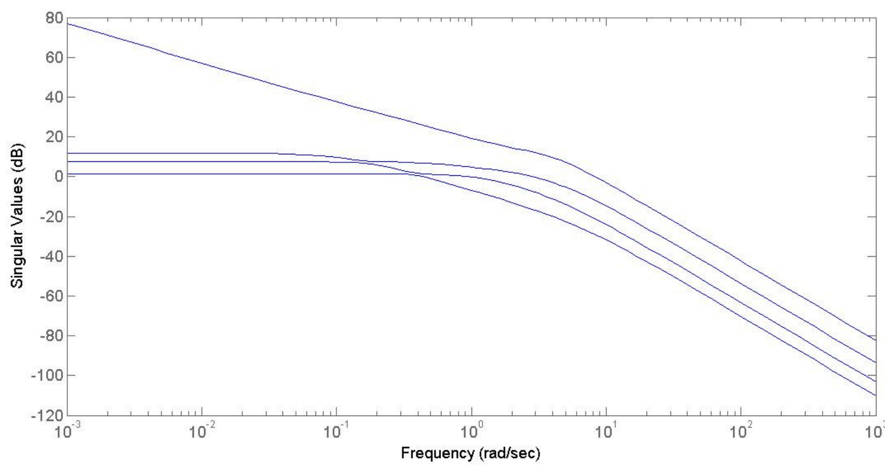

Figure 5-18. Singular values at the starting point of the robot

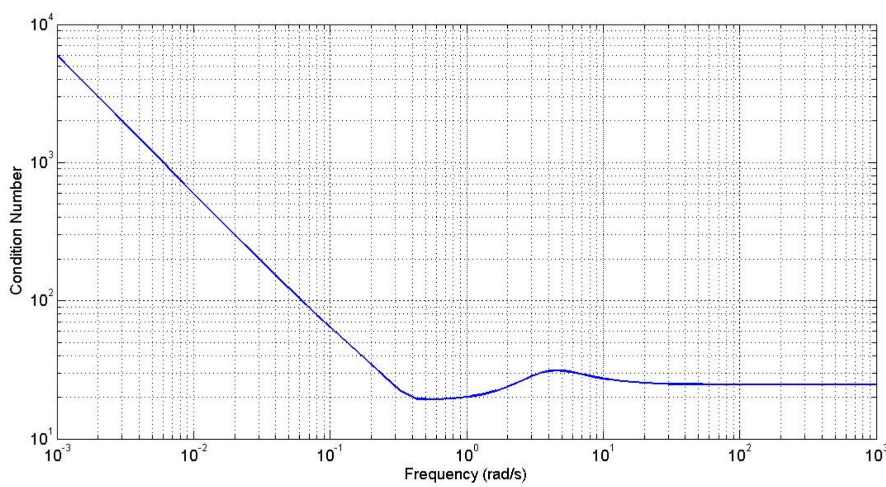

Figure 5-19. Condition number corresponding to the singular values at the starting point of the robot

5.6.2 Impedance Control Experiment

Impedance control law, as proposed in section 5.5, is based on the estimation of the external force and controlling the motion of the robot accordingly. To verify that the motion of the robot against an external force is equal to what is expected from impedance control, a force sensor was attached to the arm and the operator's force was applied through this sensor (Figure 5-20). Using this method, the external force can be measured and compared with the force according to the desired impedance, which is calculated from: $\mathbf{\Lambda}(\ddot{\boldsymbol{\alpha}}_{\mathrm{d}} - \ddot{\boldsymbol{\alpha}}) + \mathbf{\Psi}(\dot{\boldsymbol{\alpha}}_{\mathrm{d}} - \dot{\boldsymbol{\alpha}}) + \mathbf{\Gamma}(\boldsymbol{\alpha}_{\mathrm{d}} - \boldsymbol{\alpha})$.

To perform the experiment, the arm is moved from the starting position by the force applied to the sensor and then is released. The stiffness part of the impedance control (provided that it is large enough to overcome the Coulomb friction) will move the system back to the original position.

Figure 5-20. Impedance control experimental set-up

The impedance gains have been selected as: $\mathbf{\Psi} = \mathbf{\Gamma} = \mathrm{diag}(1200{,}1350{,}600{,}700)$, and $\mathbf{\Lambda} = \mathbf{0}$. (As mentioned before, because of the high level of measurement noise on the acceleration signal, usually the impedance inertia matrix is taken to be zero). The results are shown in Figures 5-21 to 5-23. The experiment was not done for ψ direction, as the moment arm is too small and applying an external force not having projection on any of the three other generalized coordinates is very difficult.

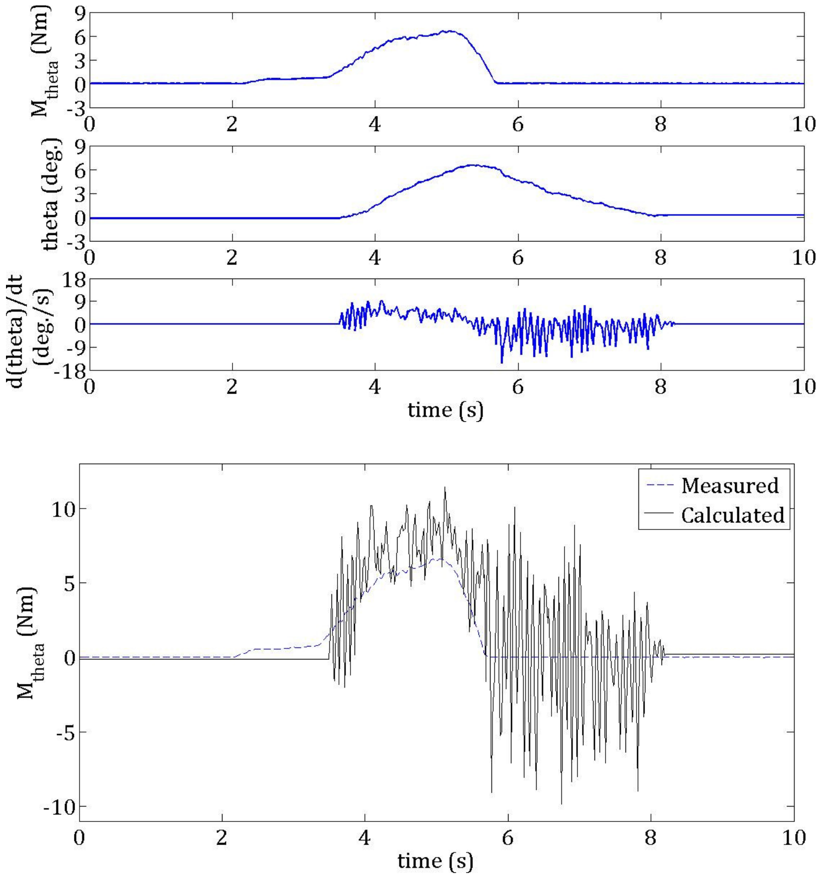

Figure 5-21. Impedance control in θ direction. Top: response of the robot; bottom: comparison of measured applied force and the force calculated from the desired impedance

As can be seen from all three tests, the motion starts after the magnitude of the external forces reaches a certain value. This value is in fact a deadband set to prevent the vibration of the system as a result of presence of noises and errors. As soon as the force is removed, the system goes back to the original position with acceleration and velocity set by $\boldsymbol{\psi}$ and $\boldsymbol{\Gamma}$.

The high level of oscillations in the "calculated" forces is partly due to the velocity measurement noise, and partly (and more significantly) because the beam to which the arm is connected is not completely fixed and can have small rotations. Due to high length of the beam, these small rotations result in rather large deflections in the connecting point of the arm, which in turn appears as the oscillations in position measurements. However, neglecting these inaccuracies, one can see that the measured force and the calculated impedance force have the same trend and close magnitudes. This proves the functionality of the designed impedance control logic.

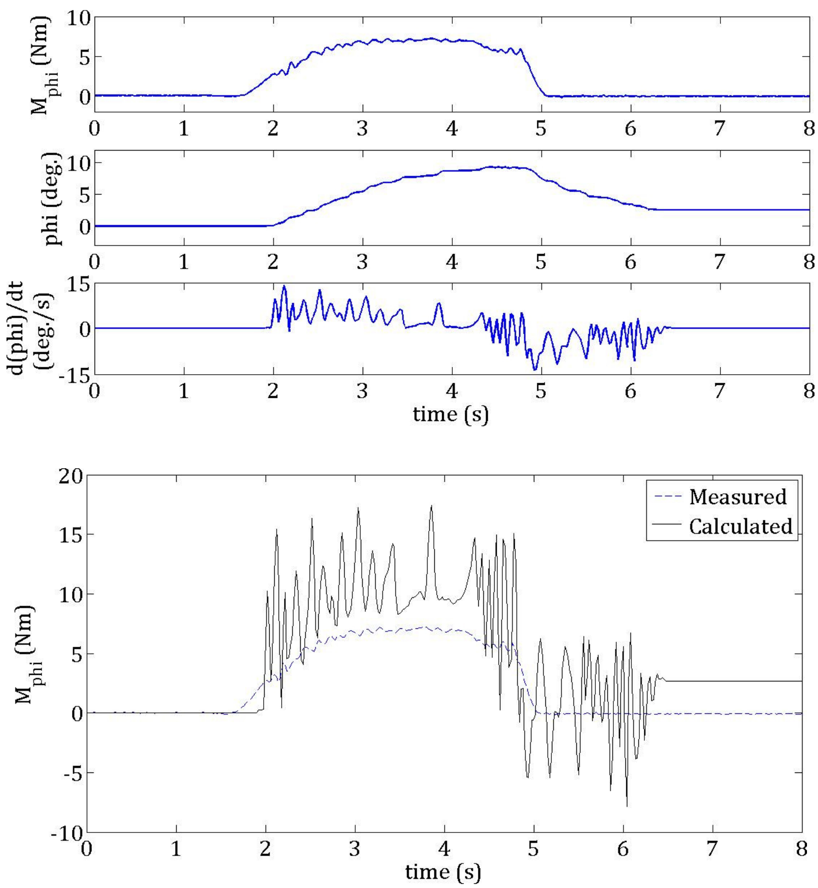

Figure 5-22. Impedance control in φ direction. Top: response of the robot; bottom: comparison of measured applied force and the force calculated from the desired impedance

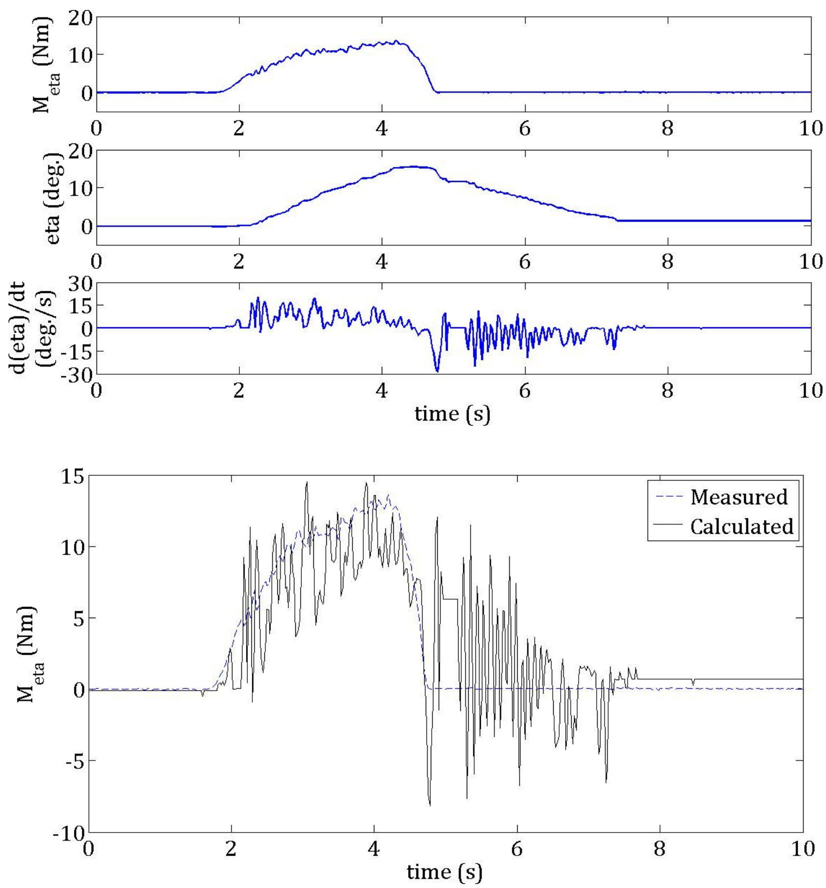

Figure 5-23. Impedance control in η direction. Top: response of the robot; bottom: comparison of measured applied force and the force calculated from the desired impedance

5.6.3 Teaching-Playback Experiment

As discussed before, in teaching-playback scheme, the teaching phase can be considered as a special case of impedance control where $\mathbf{\Gamma} = \mathbf{0}$, and the playback phase is essentially the same as position control.

The teaching-playback experiments were done using the same procedure performed for impedance control. The results are depicted in Figures 5-24 to 5-26. Since in this case the unfiltered calculated force is too noisy to be informative, the filtered signal is plotted as well.

As can be seen from the figures, (except for θ due to the small singular value, as discussed before), the position error (playback vs. teaching) is close to zero, which proves the good performance of the position control loop. As for impedance control, the error in position control of θ also affects the performance of the impedance control, as the difference between measured force and the calculated impedance force is the largest in the case of θ. This is not the only source of error, as in the other two coordinates, although the difference is smaller, it is still significant. The other source of error is that the generalized coordinates are calculated from kinematics and based on the measurement of cable length changes, which in turn are obtained from the motor resolvers. As discussed before, the measurement of the cable lengths using the resolvers has much less accuracy compared to the proposed external encoder mechanism. The inaccuracy in length measurement is amplified by the high sensitivity of the system. The sensitivity to this error can be obtained by calculating $\mathrm{d}\mathbf{l}/\mathrm{d}\boldsymbol{\alpha}$, which are the elements of the transpose of the structure matrix. For example, at the start position:

$$\frac{\mathrm{d}\mathbf{l}}{\mathrm{d}\boldsymbol{\alpha}} = \mathbf{A}^{\mathrm{T}} = \begin{bmatrix} -93.12 & 17.38 & -9.29 & 0 \\ -249.84 & -22.85 & 27.93 & 0 \\ 312.39 & -49.44 & -19.61 & 55.18 \\ 147.97 & 198.94 & 3.21 & 0 \\ -314.89 & -52.68 & -2.36 & -115.67 \end{bmatrix}$$

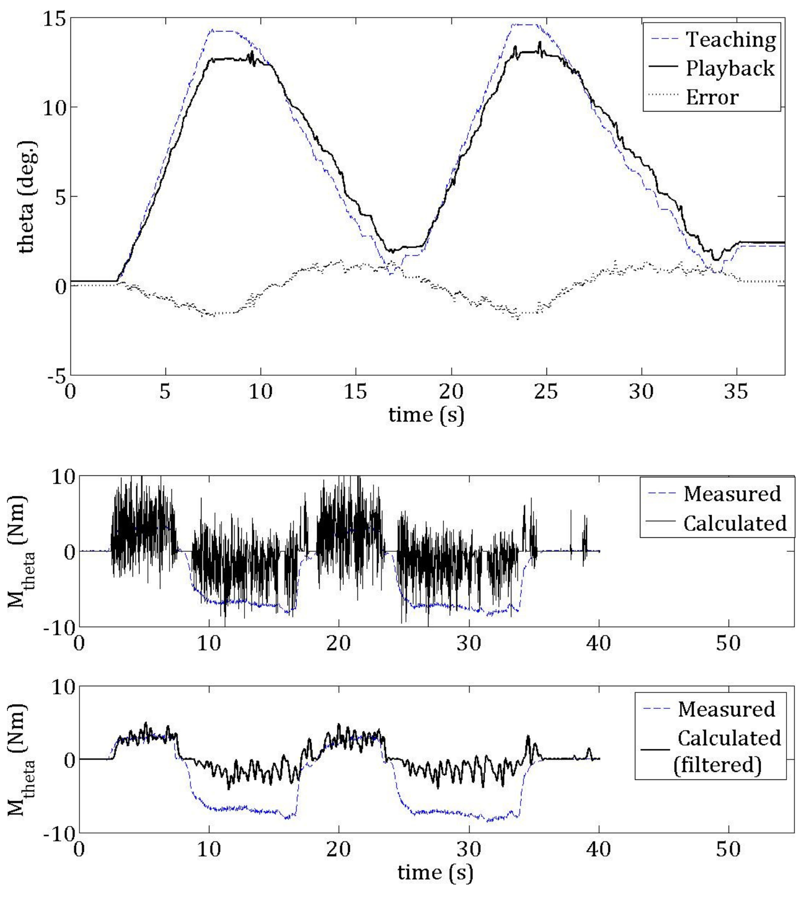

Figure 5-24. Teaching-playback in θ direction. Top: comparison of the positions; bottom: comparison of measured applied force and the force calculated from the desired impedance

As can be seen, the sensitivity in θ direction is small. But in other directions, and especially for ψ, the sensitivity seems large. Numerically, using pseudo-inverse of $\mathbf{A}^{\mathrm{T}}$ for calculation of four angles from five cable length measurements, $\delta l_1 = 1$ cm (i.e. 1 cm of error in l_1) will result in:

$$\begin{bmatrix} \delta\theta \\ \delta\phi \\ \delta\psi \\ \delta\eta \end{bmatrix} = (\mathbf{A}^{\mathrm{T}})^{+} \begin{bmatrix} 10 \\ 0 \\ 0 \\ 0 \\ 0 \end{bmatrix} = \begin{bmatrix} -0.0182 \\ 0.0131 \\ -0.2867 \\ -0.0380 \end{bmatrix}$$

or an error of 16.4° in calculation of ψ. This relatively high sensitivity to the error will cause inaccuracies in the calculation of the generalized coordinates, and as a result to the estimation of the operator's force.

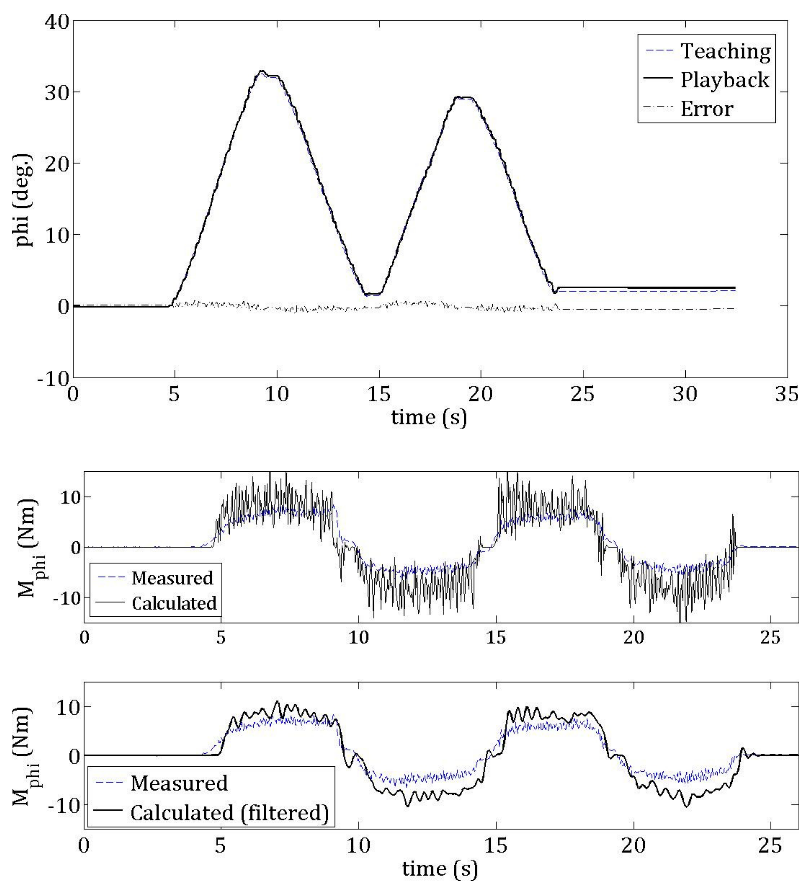

Figure 5-25. Teaching-playback in φ direction. Top: comparison of the positions; bottom: comparison of measured applied force and the force calculated from the desired impedance

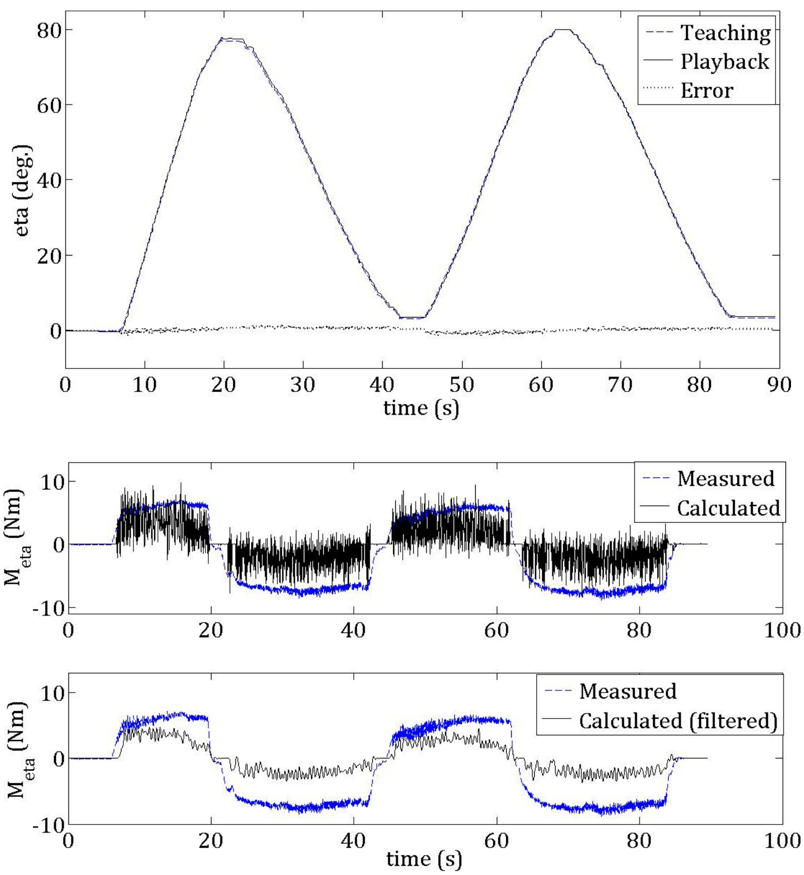

Figure 5-26. Teaching-playback in η direction. Top: comparison of the positions; bottom: comparison of measured applied force and the force calculated from the desired impedance

5.7 Summary

In this chapter, rehabilitation-oriented control algorithms for the designed multibody cable-driven robot were discussed. The first control method was position control in which, using the Lagrangian dynamic formulation proposed in the previous chapter, the standard feedback linearization control for the robotic systems was utilized and applied. Next, because of the importance of compliance in the control of the robots interacting with humans, a position-based impedance control was proposed, in which the inherent stiffness of the multibody cable-driven robots was formulated and considered. The experimental results of the proposed control methods prove the effective functionality of the control laws. The position control, except in one of the four generalized coordinates, is with very low error, and the impedance control, although with some error in magnitude, shows a correct trend in simulating the response to the operator's force by a mechanical impedance. The main source of errors in the results is from the hardware, specifically from the vibrations of the beam connecting the arm to the ground, and from the measurement of the cable lengths from the motor resolvers (instead of the external encoders). Fixing these problems will eliminate most of the associated errors.

Chapter 6 Summary, Discussion, and Future Works

In this thesis, a novel rehabilitation robotic system was proposed and various problems accompanying its development were studied and investigated. The two groups of the therapeutic robots, namely end-effector based robots and exoskeletons, each has specific limitations. The proposed system is an attempt to overcome these drawbacks.

This chapter presents a brief summary of the steps taken to develop the new robotic system. Moreover, the results obtained during this research will be discussed and some guidelines for future works will be suggested.

6.1 Summary

Along with advantages such as reconfigurability and ability of working for multipurpose tasks, one of the main motivations of using cable-driven robots for rehabilitation aids was their ability in driving a mechanism by stationary actuators. Thereby, they can manipulate any DoF without adding any inertia to the driven mechanism. This makes cable robots an ideal choice for the therapy of human limbs.

The major problem of cable-driven mechanism is guaranteeing their tensionability. The conditions of tensionability were well-investigated for the rigid body cable-driven mechanisms; but this has not the case for the multibodies. Since the human limbs are multibodies, the theories of tensionability had to be reviewed and extended. In this way, the necessary conditions for the cable number and distribution of the cables over the links of a general multibody were investigated and a set of conditions that have to be satisfied so that the system can potentially be made tensionable was provided. The sufficiency of these conditions is a much more complex problem, and it was studied for two- and three-link multibodies and the sufficient conditions for these mechanisms were proved. Using this study the necessary number of cables and distribution of them for tensionability of the proposed mechanism was obtained.

Having the number and distribution of the cables, and a suggested design for locations of winches and the cable connection points, the next step was to determine the tensionable workspace of the robot. For this part, again, the theory of the rigid bodies was extended to multibodies. A Lagrangian formulation of the multibody was suggested to minimize the size of the structure matrix. This formulation was used for obtaining the boundaries of the tensionable workspace and thereby, determining the tensionable regions. The study of the proposed design proved that the system is tensionable in a region around the starting point.

The tensionable region determines the "safe region" for motion of the robot. In other words, theoretically the robot can move within this region without risk of collapsing. Having determined this region, the next step was controlling the robot. The first control method applied was position control for which feedback linearization algorithm was used. Another control method which was used due to the rehabilitation application of the robot was impedance control. For better accuracy in impedance control the inherent stiffness of the cable robot was required, and it was formulated by the extension of the rigid body theories. Impedance control was also used for a useful therapy scenario; namely teaching/playback, in which the robot "learns" the motion instructed by the therapist and repeats it.

As the last part of the thesis, the designed controllers were implemented and tested in real-time. The results show effective performance of the controllers in all three scenarios: position control, impedance control, and teaching/playback.

6.2 Discussion and Future Works

In this thesis it was tried to build the theoretical and practical basis for the concept of using a cable robot as a rehabilitation tool. Although much effort was spent on covering all the necessary steps for development of an as-complete-as-possible foundation for the theoretical and practical aspects of the robot, still many topics remained outside of the scope of this thesis. In the following, a brief discussion on what have been accomplished and what can complete this work will be presented.

6.2.1 Design of the Robot

As the first phase of implementation of the project, instead of the human upper extremity, the tests were done on a mechanical arm. Since eventually the robot is expected to work with a human subject, the next step will be defining the concept and designing the interface through which the cables will be driving the patient's limbs. The major issue is that the system must be such that no force is applied in the "constrained" directions of the human's joints. In other words the constraint forces have to be very small or zero. One way to satisfy this condition is considering seven actuators for each link of the multibody and controlling the links as separate rigid bodies. Another way, which seems more practical, is to design an interface which is connected to the ground (possibly through the patient's chair) and thereby the constraint forces are not transmitted to the patient's body.

Another necessary development is design of the chair. Beside the issue discussed above, the importance of the chair is fixing the "zero point" of the mechanism. In other words, in order for the robot to "know" the pose of the mechanism, either the patient's body (or at least the part being exercised) must be fixed to the chair, or the displacement of the patient on the chair sensed and the new location of the limb is fed to the control system.

6.2.2 Safety

According to International Organization for Standardization (ISO) about safety of industrial robots (ISO 10218), industrial robots must be isolated from humans and when for any reason it is not possible, the robot must be turned off [94]. However, in application such as rehabilitation robotics, where the function of the robot is essentially defined for interaction with humans, this safety standard is not applicable. Due to the obvious importance of the consideration of this subject in rehabilitation robots, several approaches for studying safety and reducing the risks of rehabilitation robots have been proposed. Basic methods for increasing safety are designing the robot such that mechanically it is incapable of moving to positions which may injure the user, using redundant sensors for identifying malfunction of other sensors, watchdog timers for checking the controlling computer, and so on [1]. In [95], the authors proposed two "fail-safe components", namely a reflex mechanism and a fail-safe sensor for increasing safety of rehabilitation robots. In [96] a method for measurement of the threshold of human pain was suggested and used in development of a robotic system which can stop the system as necessary. In [97] a risk assessment approach was proposed for defining a safety strategy of the robot. In [98] a quantitative method was proposed to measure the safety of rehabilitation robots.

Since the test of the robot on human subjects was out of the scope of this thesis, the safety issue was not studied and was not considered in the development of the present system. However, for the next stages of development of the robot, defining a safety strategy is essential. As the first step, a portable switch can be added such that in the case of any abnormal function, the user would be able to turn off the system. The cable connection fittings can be selected such that against a certain force they fail and do not apply the force to the user. As briefly reviewed in the above, this subject of safety is new and there is a great potential for new methods and strategies to be proposed, especially for a novel system like the developed cable-driven robot.

6.2.3 Number of Cables and Tensionability Conditions

The study performed in chapter 3 obtained the necessary conditions for a general multibody. However, due to complexity of the problem, the sufficiency was proved only for two- and three-link multibodies. Extension of the sufficiency to multibodies with more links (and possibly the general case) is an interesting topic. The framework suggested which was based on using dependency matrices seems very promising for this purpose.

Also, the cable wrench condition was only considered for planar cases. Considering this condition for spatial case can be another challenge for analysis of tensionability of multibody cable-driven robots.

6.2.4 Workspace Analysis

The formulation developed for analysis of tensionable workspace was general and applicable for all multibodies. The challenge here is in solving the complex parametric equations for obtaining the expressions of tensionable boundaries. As discussed in chapter 4, even for simple multibodies the expressions become so long that they cannot be directly shown and used. For higher-order systems, and as the number of parameters increases, solving the equations will be a problem, too.

Another issue in this subject is the application and representation of the obtained workspace. In this thesis the workspaces were limited to 2-D, as graphical presentation of 3-D workspaces is difficult and more than that is impossible. Limiting the workspace to 2-D is normally what is done in rigid bodies as well (for example see [46] for “constant-orientation workspace”), but motion in more than two DoF especially for the present application is not rare, and thus the boundaries of the workspace for such applications must be determined, too.

Designing the configuration of the robot (i.e. locations of winches and cable connection points) is another interesting problem that can be studied. As mentioned before, the configuration of the robot for this work was based on study of Ghasemalizadeh [29] by use of a numerical method for maximizing the size of the workspace. As shown in chapter 5, another important factor in selection of robot configuration is the singular values and controllability of the robot as a MIMO system. Development of a systematic way for synthesizing cable-driven robots based on various factors affecting their performance can be a very interesting subject of research.

6.2.5 Control

The first issue in control of the robot is its hardware. As shown in chapter 5, the inertia and friction of the motors are considerably high and not suitable for this application. The high inertia and friction, beside making the system heavy and slow-response, increase the effect of parameter uncertainty and unmodeled dynamics, and thereby decrease the accuracy of the system and increase the risk of instability.

Another hardware issue is use of external encoders. In this work, since the high-speed interface of the encoders was not available, the resolvers of the motors were used for position measurement. Use of external encoders is much more beneficial both in terms of the measurement noise and the error caused by cables winding around the spool.

Although the implemented position control is accurate enough in other directions, the motions involving θ were accompanied by relatively high errors. This was proved to occur due to the system being ill-conditioned and required to be redesigned. However, study of other multivariable control methods may result in better performance of the controlled system.

Impedance control is essentially a tool to control the interaction of the robot with the environment. One of the main topics of research in impedance control is study on the passivity of the controlled system, which is an interesting subject for the present robot. Also calibration of impedance control gains for different modes of exercise and different scenarios of therapy can be another subject of future research.

Finally, the estimation of the interaction force was based on quasi-static equilibrium of the robot. A more sophisticated approach can be estimating the force using a state observer. The method proposed in [99] for estimation of force disturbance seems a well-suited approach for this purpose. The Nonlinear Disturbance Observer (NDO) suggested is capable of estimating the disturbance force without measuring the acceleration. However, the formulation in [99] is for a 2-DoF system, and is required to be reformulated for the present robot. This also requires having the dynamic parameters (mass, etc.) of the patient, which vary from one person to another. A solution is using adaptive methods for feedback linearization control of robots, such as the ones suggested in [100-102].

Bibliography

1. Van der Loos, H.F.M. and Reinkensmeyer, D.J., “Rehabilitation and Health Care Robotics”, In *Springer Handbook of Robotics*, Springer-Verlag, 2008.
2. Van der Loos, H.F.M., Mahoney, R., and Ammi, C., “Great Expectations for Rehabilitation Mechatronics in the Coming Decade”, In *Advances in Rehabilitation Robotics*, *Lecture Notes Control and Information Science*, **306**, pp. 427-433, 2004.
3. Tejima, N., “Rehabilitation Robotics: A Review”, Advanced Robotics, **14**, No. 7, pp. 551-564, 2000.
4. Reinkensmeyer, D.J., Schmit, B.D., and Rymer, W.Z., “Can Robots Improve Arm Movement Recovery after Chronic Brain Injury? A Rationale for Their Use Based on Experimentally Identified Motor Impairments”, ICORR’ 99, Stanford, USA, 1999.
5. Mayhew, D., Bachrach, B., Rymer, W.Z., and Beer, R.F., “Development of the MACARM - A Novel Cable Robot for Upper Limb Neurorehabilitation”, IEEE 9th International Conference on Rehabilitation Robotics, Chicago, USA, 2005.
6. Krukowski, R., “BioDex Muscle Exercise and Rehabilitation Apparatus”, US Patent No. 4765315, 1986.
7. Khalili, D., and Zomlefer, M., “An Intelligent Robotic System for Rehabilitation of Joints and Estimation of Body Segment Parameters”, IEEE Transactions on Biomedical Engineering, **35**, No. 2, pp. 138-146, 1988.
8. Dijkers, M.P., deBear, P.C., Erlandson, R.F., Kristi K.A., Geer, D.M., and Nichols, A., “Patient and Staff Acceptance of Robotic Technology in Occupational Therapy: A Pilot Study”, Journal of Rehabilitation Research and Development, **28**, No. 2, pp. 33-44, 1991.
9. Hogan, N., Krebs, H.I., Sharon, A., Charnnarong, J., “Interactive Robotic Therapist”, US Patent No. 5466213, 1994.
10. Krebs, H.I., Ferraro, M., Buerger, S.P., Newbery, M.J., Makiyama, A, Sandman, M., Lynch, D., Volpe, B.T., and Hogan, N., “Rehabilitation Robotics: Pilot Trial of a Spatial Extension for MIT-Manus”, Journal of NeuroEngineering and Rehabilitation, **1**, No. 5, pp. 1-15, 2004.
11. Lum, P.S., Burgar, C.G., Shor, P.C., Majmundar, M., and Van der Loos, H.F.M., “Robot-Assisted Movement Training Compared with Conventional Therapy Techniques for the Rehabilitation of Upper Limb Motor Function Following Stroke”, Archive of Physical Medicine and Rehabilitation, **83**, No. 7, pp. 952-959, 2002.
12. Hesse, S., Werner, C., Pohl, M., Rueckriem, S., Mehrholz, J., Lingnau, M.L., “Computerized Arm Training Improves the Motor Control of the Severely Affected Arm after Stroke: A Single-Blinded Randomized Trial in Two Centers”, Stroke, **36**, No. 9, pp. 1960-1966, 2005.
13. Hesse, S. and Uhlenbrock, D., “A Mechanized Gait Trainer for Restoration of Gait”, Journal of Rehabilitation Research and Development, **37**, No. 6, pp. 701-708, 2000.
14. Colombo, G., Joerg, M., Schreier, R., and Dietz, V., “Treadmill Training of Paraplegic Patients with a Robotic Orthosis”, Journal of Rehabilitation Research and Development, **37**, No. 6, pp. 693-700, 2000.

15. Kathryn, J. and Syranosian, M., “Autoambulator Improves Functionality for Healthsouth's Rehab Patients”, *Online*, Available:
http://www.braintreerehabhospital.com/pdf/autoambulator_MDNews.pdf,
as July 2012.
16. Nef, T., and Riener, R., “ARMin - Design of a Novel Arm Rehabilitation Robot”, IEEE 9th International Conference on Rehabilitation Robotics, Chicago, USA, 2005.
17. http://www.sms.mavt.ethz.ch/, as Dec. 2008.
18. Takahashi, C.D., Der-Yeghiaian, L., Le, V.H., and Cramer, S.C., “A Robotic Device for Hand Motor Therapy after Stroke”, IEEE 9th International Conference on Rehabilitation Robotics, Chicago, USA, 2005.
19. He, J., Koeneman, E.J., Schultz, R.S., Huang, H., Wanberg, J., Herring, D.E., Sugar, T., Herman, R., and Koeneman, J.B., “Design of a Robotic Upper Extremity Repetitive Therapy Device”, IEEE 9th International Conference on Rehabilitation Robotics, Chicago, USA, 2005.
20. Rosati, G., Andreolli, M., Biondi, A., and Gallina, P., “Performance of Cable Suspended Robots for Upper Limb Rehabilitation”, Proceedings of IEEE 10th International Conference on Rehabilitation Robotics, pp. 385-392, Noordwijk, The Netherlands, 2007.
21. http://www.smpp.northwestern.edu/, as July 2012.
22. Mao, Y. and Agrawal, S.K., “Transition from Mechanical Arm to Human Arm with CAREX: a Cable Driven ARm EXoskeleton (CAREX) for Neural Rehabilitation”, IEEE International Conference on Robotics and Automation, RiverCentre, Saint Paul, Minnesota, USA, 2012.
23. Stewart, D., “A platform with six degrees of freedom”, Proceedings of the IMechE, **180**, Pt. 1, No. 15, pp. 371-385, 1965-66.
24. Merlet, J.-P., “Parallel Robots”, Springer, 2006.
25. Albus, J., Bostelman, R., and Dagalakis, N., “The NIST ROBOCRANE”, Journal of Robotic Systems, **10**, No. 5, 709-724, 1993.
26. Campbell, P.D., Swaim, P.L., and Thompson, C.J., “Charlotte Robot Technology for Space and Terrestrial Applications”, SAE Technical Series Paper No. 951520, 1995.
27. Kawamura, S. and Ito, K., “A New Type of Master Robot for Teleoperation Using a Radial Wire Drive System”, Proceedings of the IEEE/RSJ International Conference on Intelligent Robots and Systems, 55-60, Yokohama, Japan, 1993.
28. Dekker, R., Khajepour, A., and Behzadipour, S., “Design and Testing of an Ultra High-Speed Cable Robot”, Journal of Robotics and Automation, **21**, No. 1, 25-34, 2006.
29. Ghasemalizadeh, O., “Synthesis, Kinematic Modeling, Parameter Identification, and Control of a Rehabilitation-Aided Robot”, M.Sc. Thesis, University of Alberta, Canada, 2011.
30. Nguyen, V., “The Synthesis of Stable Grasps in the Plane”, Proceedings of IEEE International Conference on Robotics and Automation, vol. 3, pp. 884-889, 1986.
31. Nguyen, V., “Constructing Force-Closure Grasps in 3D”, Proceedings of IEEE International Conference on Robotics and Automation, vol. 4, 240-245, 1987.
32. Goldman, A.J. and Tucker, A.W., “Polyhedral Convex Cones” In *Linear Inequalities and Related Systems*, Kuhn, H.W. and Tucker, A.W. editors, Princeton Univ. Press, Princeton, 1956.
33. Lee, J.J. and Tsai, L.W., “The Synthesis of Tendon-Driven Manipulators Having a Pseudo Triangular Structure Matrix”, International Journal of Robotics Research, **10**, pp. 255-262, 1991.

34. Kino, H., Yabe, S., and Kawamura, S., “A Force Display System Using Serial-Link Structure Driven by a Parallel-Wire Mechanism”, Advanced Robotics, **19**, No. 1, pp. 21-37, 2005.
35. Mustafa, S.K. and Agrawal S.K., “On the Force-Closure Analysis of n-DOF Cable-Driven Open Chains Based on Reciprocal Screw Theory”, IEEE Transactions on Robotics, **28**, NO. 1, 2012.
36. Gouttefarde, M., “Characterizations of Fully Constrained Poses of Parallel Cable-Driven Robots: A Review”, Proceedings of the ASME International Design Engineering Technical Conferences & Computers and Information in Engineering Conference IDETC/CIE, Brooklyn, NY, USA, 2008.
37. Ming, A. and Higuchi, T., “Study on Multiple Degrees-of-Freedom Positioning Mechanism Using Wires (Part 1)”, International Journal of the Japan Society for Precision Engineering, **28**, No. 2, pp. 131-138, 1994.
38. Roberts, R.G., Graham, T., and Trumpower, J.M., “On the Inverse Kinematics and Statics of Cable-Suspended Robots”, Proceedings of IEEE International Conference on Systems, Man, and Cybernetics, pp. 4291-4296, Orlando, FL, USA, 1997.
39. Rezazadeh, S. and Behzadipour, S., “Tensionability Conditions of a Multibody System Driven by Cables”, Proceedings of ASME International Mechanical Engineering Congress and Exposition, vol. 9, Part B, pp. 1369-1375, Seattle, WA, USA, 2007.
40. Verhoeven, R. and Hiller, M., “Estimating the Controllable Workspace of Tendon-Based Stewart Platforms”, Proceedings of 7th International Symposium on Advances in Robot Kinematics - ARK, Protoroz, Slovenia, pp. 277-284, 2000.
41. Alp, A.B. and Agrawal, S.K., “Cable-Suspended Robots: Design, Planning, and Control”, Proceedings of IEEE Conference on Robotics & Automation, Washington, DC, USA, 2002.
42. Pusey, J., Fattah, A., Agrawal, S., Messina, E., and Jacoff, A., “Design and Workspace Analysis of a 6-6 Cable-Suspended Parallel Robot”, IEEE International Conference on Intelligent Robots and Systems, Las Vegas, NV, USA, 2003.
43. Bosscher, P., Riechel, A.T., and Ebert-Uphoff, I., “Wrench-Feasible Workspace Generation for Cable-Driven Robots”, IEEE Transactions on Robotics, **22**, No. 5, pp. 890-902, 2006.
44. Barette, G. and Gosselin, C.M., “Kinematic Analysis and Design of Planar Parallel Mechanisms Actuated with Cables”, DETC’00 – ASME Design Engineering Technical Conferences and Computers and Information in Engineering Conference, Baltimore, MD, USA, 2000.
45. Gouttefarde, M. and Gosselin, C.M., “On the Properties and the Determination of the Wrench-Closure Workspace of Planar Parallel Cable-Driven Mechanisms”, DETC’04 – ASME Design Engineering Technical Conferences and Computers and Information in Engineering Conference, Salt Lake City, UT, USA, 2004.
46. Gouttefarde, M. and Gosselin, C.M., “Analysis of the Wrench-Closure Workspace of Planar Parallel Cable-Driven Mechanisms”, IEEE Transactions on Robotics, **22**, No. 3, pp. 434-445, 2006.
47. Williams II, R.L., Albus, J.S., and Bostelman, R.V., “3D Cable-Based Cartesian Metrology System”, Journal of Robotic Systems, **21**, No. 5, pp. 237-257, 2004.
48. Pham, C.B., Yeo, S.H., Yang, G., Kurbanhusen, M.S., and Chen, I.-M., “Force-Closure Workspace Analysis of Cable-Driven Parallel Mechanisms”, Mechanism and Machine Theory, **41**, No. 1, pp. 53-69, 2006.
49. Diao, X. and Ma, O., “Workspace Determination of General 6-d.o.f. Cable Manipulators”, Advanced Robotics, **22**, No. 2-3, pp. 261-278, 2008.

50. Ghasemi, A., Eghtesad, M., and Farid, M., "Workspace Analysis for Planar and Spatial Redundant Cable Robots", ASME Journal of Mechanisms and Robotics, **1**, No. 4, pp. 044502.1-044502.6, 2009.
51. Bruckmann, T., Mikelsons, L., Hiller, M., and Schramm, D., "Continuous Workspace Analysis, Synthesis, and Optimization of Wire Robots", IDETC/CIE – ASME International Design Engineering Technical Conferences and Computers and Information in Engineering Conference, Brooklyn, NY, USA, 2008.
52. Gouttefarde, M., Merlet, J.-P., and Daney, D., "Wrench-Feasible Workspace of Parallel Cable-Driven Mechanisms", IEEE International Conference on Robotics and Automation, Roma, Italy, 2007.
53. Stump, E. and Kumar, V., "Workspaces of Cable-Actuated Parallel Manipulators", ASME Journal of Mechanical Design, **128**, No. 1, pp. 159-167, 2006.
54. Behzadipour, S. and Khajepour, A., "A New Cable-Based Parallel Manipulator with Three Degrees of Freedom", Journal of Multibody Systems Dynamics, **13**, No. 4, pp. 371-383, 2005.
55. Alikhani, A., Behzadipour, S., Sadough Vanini, S.A., and Alasti, A., "Workspace Analysis of a Three-DOF Cable-Driven Mechanism", ASME Journal of Mechanisms and Robotics, **1**, No. 4, pp. 041005.1-041005.7, 2009.
56. Casey, J. and O'Reilly, O.M., "Geometrical Derivation of Lagrange's Equations for a System of Rigid Bodies", Mathematics and Mechanics of Solids, **11**, pp. 401-422, 2006.
57. Marchal-Crespo, L. and Reinkensmeyer, D.J., "Review of Control Strategies for Robotic Movement Training After Neurologic Injury", Journal of NeuroEngineering and Rehabilitation, **6**, No. 20, doi:10.1186/1743-0003-6-20, 2009.
58. Lotze, M., Braun, C., Birbaumer, N., Anders, S., and Cohen, L.G., "Motor Learning Elicited by Voluntary Drive", Brain, **126**, No. 4, pp. 866-872, 2003.
59. Perez, M.A., Lungholt, B.K., Nyborg, K., and Nielsen, J.B., "Motor Skill Training Induces Changes in the Excitability of the Leg Cortical Area in Healthy Humans", Experimental Brain Research, **159**, No. 2, pp.197-205, 2004.
60. Reinkensmeyer, D.J., Kahn, L.E., Averbuch, M., McKenna-Cole, A.N., Schmit, B.D., and Rymer, W.Z., "Understanding and Treating Arm Movement Impairment After Chronic Brain Injury: Progress with the ARM Guides", Journal of Rehabilitation Research and Development, **37**, No. 6, pp. 653-662, 2000.
61. Hesse, S., Kuhlmann, H., Wilk, J., Tomelleri, C., and Kirker, S., "A New Electromechanical Trainer for Sensorimotor Rehabilitation of Paralysed Fingers: A Case Series in Chronic and Acute Stroke Patients", Journal of NeuroEngineering and Rehabilitation, **5**, No. 21, 2008.
62. Poon, C.S., "Sensorimotor Learning and Information Processing by Bayesian Internal Models", Proceedings of the 26th Annual International Conference of the IEEE Engineering in Medicine and Biology Society - IEMBS, pp. 4481-2, 2004.
63. Rossini. P.M. and Dal Forno, G., "Integrated Technology for Evaluation of Brain Function and Neural Plasticity", Physical Medicine & Rehabilitation Clinics of North America, **15**, No. 1, pp. 263-306, 2004.
64. Harkema, S.J., "Neural Plasticity After Human Spinal Cord Injury: Application of Locomotor Training to the Rehabilitation of Walking", The Neuroscientist, **7**, No. 5, pp. 455-468, 2001.
65. Reinkensmeyer, D.J., "How to Retrain Movement After Neurologic Injury: A Computational Rationale for Incorporating Robot (or Therapist) Assistance",

Proceedings of the 25th Annual International Conference of the IEEE Engineering in Medicine and Biology Society, IEMBS, pp. 1479-1482, 2003.

66. Sanchez, R.J., Liu, J., Rao, S., Shah, P., Smith, R., Cramer, S.C., Bobrow, J.E., and Reinkensmeyer, D.J., "Automating Arm Movement Training Following Severe Stroke: Functional Exercises with Quantitative Feedback in a Gravity-Reduced Environment. IEEE Transactions on Neural and Rehabilitation Engineering, **14**, No. 3, pp. 378-389, 2006.
67. Stienen, A.H.A., Hekman, E.E.G., Van der Helm, F.C.T., Prange, G.B., Jannink, M.J.A, Aalsma, A.M.M., and Van der Kooij, H., "Freebal: Dedicated Gravity Compensation for the Upper Extremities", Proceedings of IEEE 10th International Conference on Rehabilitation Robotics, ICORR, pp. 804-808, 2007.
68. Matjacic, Z., Hesse, S., and Sinkjaer, T., "BalanceReTrainer: A New Standing-Balance Training Apparatus and Methods Applied to a Chronic Hemiparetic Subject with a Neglect Syndrome", NeuroRehabilitation, **18**, No. 3, pp. 251-259, 2003.
69. Perry, J.C., Rosen J., and Burns, S., "Upper-Limb Powered Exoskeleton Design", IEEE/ASME Transactions on Mechatronics, **12**, No. 4, pp. 408-417, 2007.
70. Krebs, H., Volpe, B., Williams, D., Celestino, J., Charles, S., Lynch, D., and Hogan, N., "Robot-Aided Neurorehabilitation: A Robot for Wrist Rehabilitation", IEEE Transactions on Neural Systems and Rehabilitation Engineering, **15**, No. 3, pp. 327-335, 2007.
71. Voss, D.E., Ionta, M.K., and Meyers, B.J., "Proprioceptive Neurofacilitation: Patterns & Techniques", Harper & Rowe, 1985.
72. Patterson, L.A. and Spivey, W.E., "Validity and Reliability of the LIDO Active Isokinetic System", Journal of Orthopaedic Sports Physical Therapy, **15**, No. 1, pp.32-36, 1992.
73. Schmidt, H., Hesse, S., Bernhardt, R., and Krüueger, J., "HapticWalker **-** A Novel Haptic Foot Device", ACM Transactions on Applied Perception (TAP), **2**, No. 2, pp. 166-180, 2005.
74. Nef, T., Mihelj, M., and Riener, R., "ARMin: A Robot for Patient-Cooperative Arm Therapy", Medical and Biological Engineering and Computing, **45**, No. 9, pp. 887-900, 2007.
75. Reeves, B. and Nass, C., "The Media Equation: How People Treat Computers, Television, and New Media Like Real People and Places", Cambridge University Press, 1998.
76. Banala, S.K., Agrawal, S.K., and Scholz, J.P., "Active Leg Exoskeleton (ALEX) for Gait Rehabilitation of Motor-Impaired Patients", Proceedings of IEEE 10th International Conference on Rehabilitation Robotics, ICORR, pp. 401-407, 2007.
77. Riener, R., Lunenburger, L., Jezernik, S., Anderschitz, J.M., Colombo, G., and Dietz, V., "Patient-Cooperative Strategies for Robot-Aided Treadmill Training: First Experimental Results", IEEE Transactions on Neural System and Rehabilitation Engineering, **13**, No. 3, pp. 380-394, 2005.
78. Kousidou, S., Tsagarakis, N.G., Smith, C., and Caldwell, D.G., "Task-Orientated Biofeedback System for the Rehabilitation of the Upper Limb", Proceedings of IEEE 10th International Conference on Rehabilitation Robotics, ICORR, pp. 376-384, 2007.
79. Wisneski, K.K. and Johnson, M.J., "Quantifying Kinematics of Purposeful Movements to Real, Imagined, or Absent Functional Objects: Implications for Modelling Trajectories for Robot-Assisted ADL Tasks", Journal of NeuroEngineering and Rehabilitation, **4**, No. 7, 2007.

80. Alp, A.B. and Agrawal, S.K., “Cable Suspended Robots: Feedback Controllers with Positive Inputs”, Proceedings of the American Control Conference, Anchorage, AK, USA, 2002.
81. Oh, S. R. and Agrawal, S. K., “Cable Suspended Planar Robots with Redundant Cables: Controllers with Positive Tensions”, IEEE Transactions on Robotics, **21**, No. 3, pp. 457-464, 2005.
82. Oh, S.R. and Agrawal, S. K., “A Control Lyapunov Approach for Feedback Control of Cable-Suspended Robots”, IEEE International Conference on Robotics and Automation, Roma, Italy, 2007.
83. Khosravi, M.A. and Taghirad, H.D., “Dynamic Analysis and Control of Cable Driven Robots with Elastic Cables”, Transactions of the Canadian Society for Mechanical Engineering, **35**, No. 4, pp. 543-557, 2011.
84. Behzadipour, S. and Khajepour, A., “Stiffness of Cable-Based Parallel Manipulators with Application to Stability Analysis”, ASME Journal of Mechanical Design, **128**, No. 1, pp. 303-310, 2006.
85. Yu, K., Lee, L.F., and Krovi, V.N., “Simultaneous Trajectory Tracking and Stiffness Control of Cable Actuated Parallel Manipulators”, ASME 2009 International Design Engineering Technical Conferences & Computers and Information in Engineering Conference IDETC/CIE, San Diego, CA, USA, 2009.
86. Salisbury, J.K., “Active Stiffness Control of a Manipulator in Cartesian Coordinates”, IEEE 19th Conference on Decision and Control, Albuquerque, USA, 1980.
87. Li, Y., Chen, S.F., and Kao, I., “Stiffness Control and Transformation for Robotic Systems with Coordinate and Non-Coordinate Bases”, IEEE International Conference on Robotics & Automation, Washington, DC, USA, 2002.
88. Slotine, J.J.E. and Li, W., “Applied Nonlinear Control”, Prentice-Hall, 1991.
89. Sciavicco, L. and Siciliano, B., “Modelling and Control of Robot Manipulators”, Springer, 2001.
90. Hogan, N., “Impedance Control: An Approach to Manipulation: Part I - Theory”, ASME Journal of Dynamic Systems, Measurement and Control, **107**, No. 1, pp. 1-24, 1985.
91. Buerger, S.P., “Stable, High-Force, Low-Impedance Robotic Actuators for Human-Interactive Machines”, PhD Thesis, Massachusetts Institute of Technology, USA, 2005.
92. Newman, W.S., “Stability and Performance Limits of Interaction Controllers”, ASME Journal of Dynamic Systems, Measurement, and Control, **114**, No. 4, pp. 563-570, 1992.
93. Nof, S.Y., *Ed.*, “Handbook of Industrial Robotics”, John Wiley & Sons, 1985.
94. ISO 10218-1:2011, “Robots and Robotic Devices – Safety Requirements for Industrial Robots”, 2011.
95. Tejima, N. and Stefanov, D., “Fail-Safe Components for Rehabilitation Robots – A Reflex Mechanism and Fail-Safe Force Sensor”, IEEE 9th International Conference on Rehabilitation Robotics, Chicago, IL, USA, 2005.
96. Yamada, Y., Hirasawa, Y., Huang, S., Umetani, Y., and Suita, K., “Human-Robot Contact in the Safeguarding Space”, IEEE/ASME Transactions on Mechatronics, **2**, No. 4, pp. 230-236, 1997.
97. Nokata, M. and Tejima, N., “A Safety Strategy for Rehabilitation Robots” in: *Advances in Rehabilitation Robotics*, Springer-Verlag, 2004.
98. Nokata, M., Ikuta, K., and Ishii, H., “Safety Evaluation Method of Rehabilitation Robots” in: *Advances in Rehabilitation Robotics*, Springer-Verlag, 2004.

99. Chen, W.-H., Ballance, D.J., Gawthrop, P.J., and O'Reilly, J., "A Nonlinear Disturbance Observer for Robotic Manipulators", IEEE Transactions on Industrial Electronics, **47**, No. 4, pp. 932-938, 2000.
100. Spong, M.W. and Ortega, R., "On Adaptive Inverse Dynamics Control of Rigid Robots", IEEE Transactions on Automatic Control, **35**, No. 1, pp. 92-95, 1990.
101. Dawson, D.M. and Lewis, F.L., "Comments on 'On Adaptive Inverse Dynamics Control of Rigid Robots',", IEEE Transactions on Automatic Control, **36**, No. 10, pp. 1215-1216, 1991.
102. Wang, H. and Xie, Y., "Adaptive Inverse Dynamics Control of Robots with Uncertain Kinematics and Dynamics", Automatica, **45**, No. 9, pp. 2114-2119, 2009.